Disquisition on the Acidity in Fluid Catalytic Cracking Catalysts

Using Pyridine Probe Molecule Spectroscopy

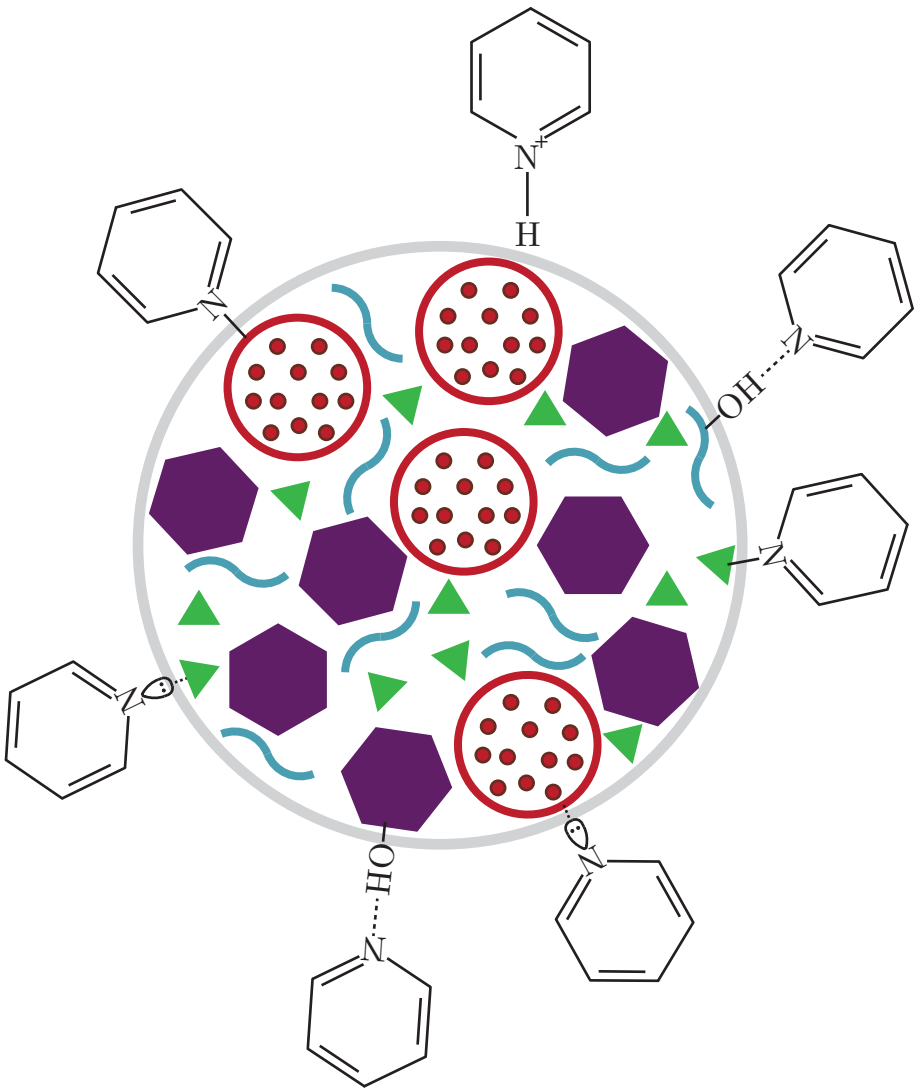

Fréderique Broers

Masterthesis

Disquisition on the Acidity in Fluid Catalytic Cracking Catalysts

Using Pyridine Probe Molecule Spectroscopy

Fréderique T.H. Broers, BSc

Supervisors:
Marjolein E.Z. Velthoen, MSc
Prof. dr. ir. Bert M. Weckhuysen

Inorganic Chemistry and Catalysis
Debye Institute for Nanomaterials Science
Utrecht University

April 14, 2018

Utrecht University

ALBEMARLE®

Abstract

The Fluid Catalytic Cracking (FCC) process has been used for over 75 years to convert crude oil into smaller hydrocarbons like gasoline, propylene and LPG. In this process a FCC catalyst is used composed of zeolite, alumina, silica and clay. Most of the research done on this catalyst focuses on the main active component, zeolite Y. To be able to rationally design the most active, selective and stable FCC catalyst, research on the effect of changes in the binder was done. In the FCC process steam is present, and the effect of steam on the catalysts with different binders is studied. The goal of this work is to make an acidity-activity correlation by studying all of the single components individually as well as combined.

Pyridine was used as a probe molecule to determine the acidity of the samples using FT-IR and UV-Vis spectroscopy. Pyridine FT-IR spectroscopy is an established technique to probe acidity as it distinguishes Lewis acid sites (LAS) from Brønsted acid sites (BAS), as well as determines the strength of the acidic sites. While it also provides information on the pyridine adsorbed in a physisorbed manner and pyridine adsorbed on surface hydroxyl groups, it does not give information on the nature of these hydroxyl groups. Recently, pyridine UV-Vis spectroscopy has shown to provide information on the nature of hydroxyl groups present on the surface of solid acids. In this work, pyridine UV-Vis spectroscopy will be used on a full catalyst set for the first time.

The results showed that Brønsted acid sites were present in the zeolite component and to a very small extent in the clay. The zeolite had two types of LAS and the alumina had one type of LAS. The silica component only showed the presence weakly acidic surface acid sites. Incorporation of the silica in the catalyst showed an increase in the strength of LAS. Catalysts with a binder containing alumina showed an increase in weakly acidic surface sites. The steam treatment of the catalysts caused a decrease in BAS and an increase in amorphous Si-(OH)-Al surface groups. Dealumination took place during the steam treatment and caused migration of LAS from the zeolite to extraframework alumina species. The amount of LAS decreased but their strength increased. In some catalysts, the presence of extraframework alumina caused the formation of superacidic Brønsted sites. Performance tests showed that the FCC catalysts containing more alumina gave better results on vacuum gas oil conversion to gasoline and propylene. As this catalyst showed an increased amount of weakly acidic sites, these sites seem to play a role in the activity of the catalyst.

Contents

Chapter 1

Introduction

The chemical industry strongly contributes to today's society. One of the sectors that relies heavily on chemical products is the transport sector. The amount of fuel, for example gasoline and diesel, that is used for transportation has increased for years. Due to growing economies in developing countries this growth is expected to continue.[1] New technologies are being developed to transit from the use of oil to transport on renewable energy sources, examples being biofuels[2] and solar cars[3]. However, so far no new technologies based on renewable sources are able to reach the demand. Until this is the case, it is necessary to use crude oil or other fossil fuels to meet the demand. Figure 1 shows an analysis done by BP that predicts that the transport energy consumption by oil will only start decreasing from 2035 onwards.[1] Fluid catalytic cracking (FCC) is currently the main technology to produce gasoline from crude oil.[4][5]
In this work, the catalyst used in FCC will be studied with different acid probing methods. The goal is to make an acidity-activity correlation. All loose components as well as total catalysts will be investigated, for a better understanding of the influence of the components on the final catalyst. This could ultimately lead to a more rationally design of the catalyst, resulting in more useful products per barrel of oil processed.

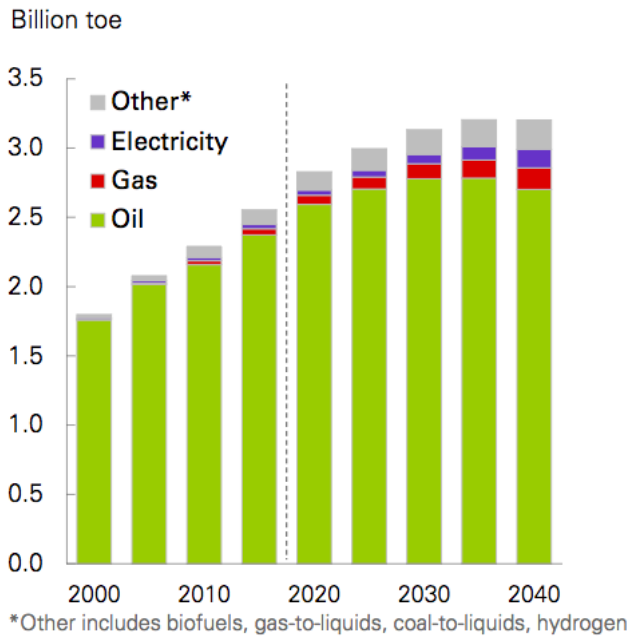

Figure 1: Outlook on transport energy consumption by fuel type in tonnes of oil equivalent (toe). Obtained from BP.[1]

1.1 Fluid Catalytic Cracking

1.1.1 Process

In 1936, catalytic cracking was introduced in petroleum refining and the amount of useful products that could be retrieved from crude oil was increased enormously.[6] In 1942, the first FCC unit was put into use and this process quickly grew out to a worldwide process, with 450 refineries using the technique today.[7][8]

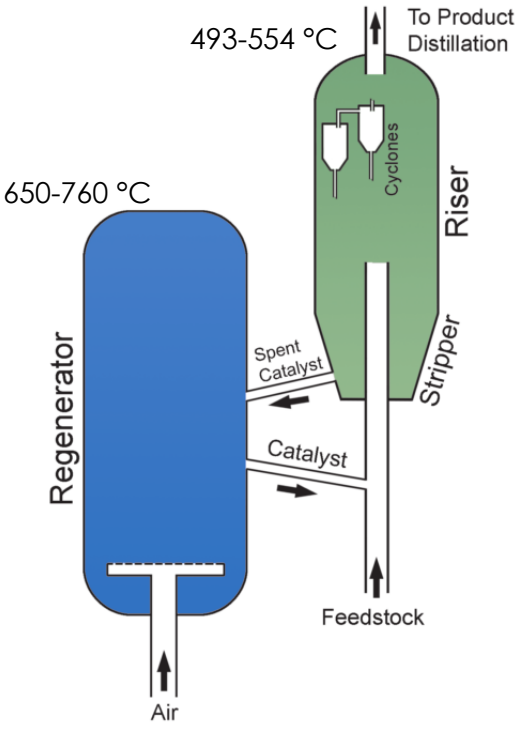

Figure 2: Schematic representation of the main components of the FCC cracking unit. Adapted from Kalirai.[8]

Figure 2 shows the main components of the FCC unit. The FCC process operates at high temperatures and at low pressure. The feedstock that will be cracked is preheated for a more effective process. The vacuum gas oil (VGO) feed enters the riser through a feed nozzler. Smaller particles are easier to crack, because more feed can reach the active sites in the FCC catalyst. Therefore the feedstock is atomized by feed nozzles using atomized steam.[9] Also the catalyst is preheated and added at the bottom of the riser-reactor. The ratio of catalyst to feed at the bottom is high, with an average of 5.5. The riser-reactor has a size of up to 2 meters in diameter and 37 meters or more in height. The temperature at the bottom of the reactor is typically around 550 °C.[5]
The atomized VGO and the FCC catalyst (spheres of about 70 µm)[10] mix and cracking reactions take place. Due to the cracking, reaction gases are formed which increase the volume. The mixture of feedstock and catalyst is pushed towards the top of the riser-reactor with a speed that can reach 40 $\mathrm{m\,s^{-1}}$. Due to this high speed, the mixture will only be in the riser for a few seconds. This short interaction time is also an important reason to make sure the feedstock consist of small particles that can be easily accessed.[9] When the mixture moves through the riser, the temperature drops to around 500 °C due to the

endothermic cracking reactions. At the top of the riser-reactor the catalyst is separated from the products using cyclones. Cyclones use centrifugal force to separate particles based on their size and weight.[11] Residual adsorbed hydrocarbons on the catalyst are removed by steam treatment in the stripper. Finally, the catalyst is brought into the regenerator.

Deactivation

During the cracking, carbonaceous deposits called coke can form on the catalyst. Coke deactivates the catalyst, because they adsorb on active sites or they can block the micropores of the zeolite. In the regenerator, the formed coke is burned off.[12] A temperature as high as 760 ℃ can be reached and a lot of steam is used in this process. After the coke is removed, the FCC catalyst can be reused in the cracking procedure.
During the regeneration, the steam can cause dealumination of the FCC catalyst which also causes deactivation. The steam causes a dehydroxylation reaction of the Brønsted acid sites in the zeolite. This results in a metastable state and alumina can be released from the framework. Al^{3+} migrates from framework alumina to extraframework alumina. This decreases the amount of Brønsted acid sites but creates strong Lewis acid sites in the extra-framework alumina.[12,13] The steam in the stripper also causes dealumination. Another deactivation cause of the FCC catalyst is deposition of metals like Ni and V. These metals can be present in the crude oil and can block the active sites of the catalyst.[12]
Deactivation by dealumination and metal deposition is irreversible. Unfortunately, it is not yet possible to identify the deactivated catalyst particles and selectively remove them from the FCC unit. To account for the deactivated part of the FCC catalyst, a part of the catalyst is periodically removed and fresh catalyst is added to the system. This way, the average lifetime of the catalyst particles in the system is kept constant, called equilibrium catalyst or E-cat. Let's have a closer look at the catalyst used in this process.

1.1.2 Catalyst

Every year about 840,000 metric tons of FCC catalyst is produced to use in industry. On average 0.16 kg of FCC catalyst is used for the conversion of one barrel of feedstock. The amount of catalyst that is necessary is dependent on the heaviness of the feedstock.[5] Figure 3 shows a schematic representation of an FCC catalyst particle. The FCC catalyst is composed of multiple components. Since 1964, the crystalline aluminosilicate zeolite Y is used as the active component of the catalysts.[7] Often the ultra stable zeolite Y (USY) is used and it can be mixed with other zeolites to tune the product preferences.[14] More information on zeolites can be found further on. The other components of the FCC catalyst are clay, alumina and silica.[9] The clay often used for the FCC catalyst is kaolinite. The clay acts as a filler and also provides mechanical strength[11] and higher heat resistance.[5] Alumina and silica act both as active matrix and binder. In the active matrix the long hydrocarbons from the VGO are cracked into smaller species. This is called precracking and takes place in the meso- and macroporous matrix. These smaller hydrocarbons can enter the porous zeolite more easily to reach all active sites for cracking.[8,15]

Zeolites

Zeolites were discovered in 1756 by Axel Cronstedt. He found out that when heating a zeolite mineral, in his case stilbite, it will loose large amounts of water. This is why he

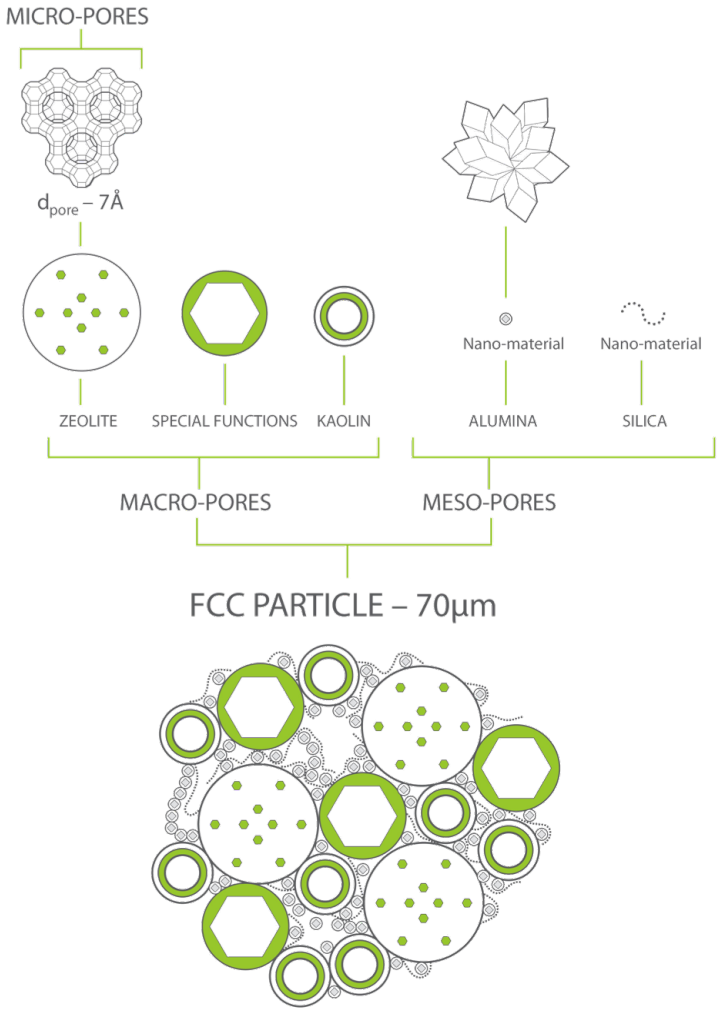

Figure 3: Schematic representation of the structural and chemical composition of FCC catalyst. Obtained from Vogt *et al.*[5]

called it a zeolite - which means "boiling" "stone" in ancient Greek.[16] In the next decades and ages more special characteristics of these zeolites were discovered, such as their great ability of adsorption, their molecular sieve effects and ion exchange capabilities.[10] Zeolites are microporous, crystalline aluminosilicates. Every silicon or aluminum forms a tetrahedral with four oxygen atoms. These tetrahedrals share their oxygen to form a three-dimensional crystalline structure. Because silicon has a 4+ charge and aluminum has a 3+ charge, the compound will become negatively charged due to the presence of aluminum. By adding cations like NH_4^+, Na^+ or H^+ this negative charge can be compensated.[17][18] When protons are used to stabilize the charge, Brønsted acid sites are created that are used during the cracking of hydrocarbons.[19] Rare earth (RE) elements can be added to the zeolite to stabilize the aluminum atoms. They can also increase the zeolite activity.[9]

Figure 4 shows the structure of zeolite Y. Sodalite cages (also called β-cages) are linked by hexagonal prisms. This structure forms larger openings with a twelve membered ring called supercages. Sodalite cages have a diameter of 7.3 Å and the supercages of 13 Å.[20]

The relatively large size of the supercages are very important to transport larger hydrocarbons into the zeolites where they can be cracked. The zeolite accounts for most of the acidic sites in the FCC catalyst.

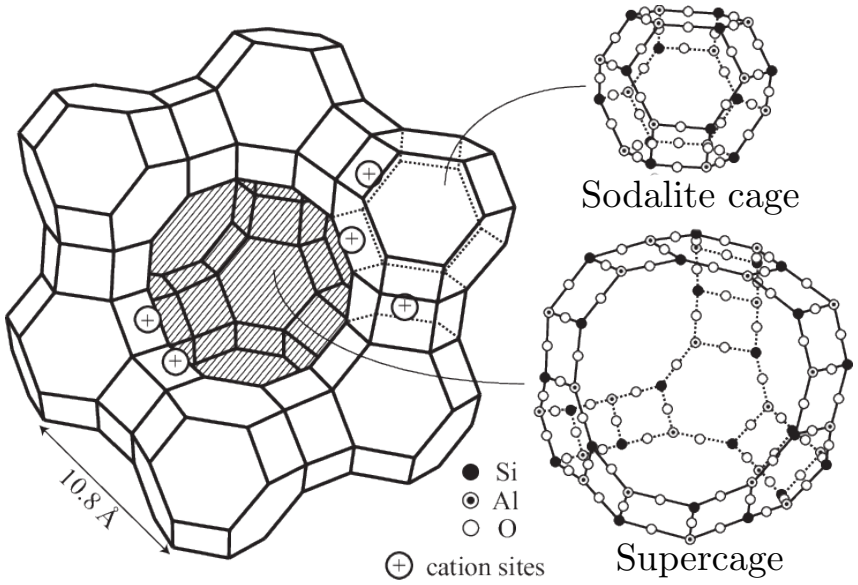

Figure 4: Schematic structure of the framework of zeolite Y. Adapted from Igarashi *et al.*[21]

1.1.3 Lewis and Brønsted acidity

There are two ways to describe acidity. Johannes Brønsted described a compound that can donate a proton as an acid. This is now called a Brønsted type acid and a Brønsted type base can accept a proton.[22,23] The other way of assigning acidity was developed by Gilbert Lewis. In this theory, compounds that can accept an electron pair are called Lewis type acids and compounds that can donate an electron pair are called Lewis type bases.[24] On these acidic sites, the breaking and formation of molecular bonds can take place. Acidity is therefore of great importance in catalysis.
Figure 5 shows a simple representation of Lewis (L) and Brønsted (B) acid sites in zeolites.

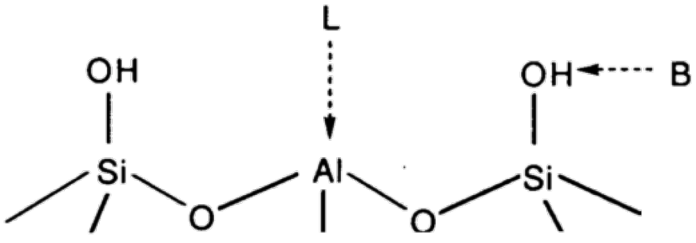

Figure 5: Representation of Lewis (L) and Brønsted (B) acid sites in zeolites. Obtained from Olah.[25]

When the negative formal charge of aluminosilicate zeolites (described in the previous section) is compensated with H^+, Brønsted acid sites (BAS) are created. The Lewis acidity in zeolites is less straight forward. Lewis acid sites (LAS) can be generated by heating the zeolites at high temperatures, causing dehydration. Due to this dehydration

the Brønsted acids are dehydroxylated and structural Lewis acid sites result.[26] Another way to create Lewis acid sites is by performing mild steaming on the zeolites, which forces out a part of the aluminum in the framework. This eliminates Brønsted acid sites but creates new Lewis acid sites.[27,28] The negatively charged aluminosilicates can also be compensated with extra-framework metal cations, causing weak Lewis acid sites. Another possible explanation for the Lewis acid sites in zeolites is that they are located at the extraframework (EF) alumina present at the surface of the zeolites.[29] Both Lewis and Brønsted acid sites can be used for the cracking of oil.

1.1.4 Cracking Reaction

Cracking of long hydrocarbons takes place at high temperatures, and ideally in combination with a catalyst to speed up the process. When a long hydrocarbon is cracked, the products are an alkane and an alkene. Cracking on active sites goes via the formation of an carbenium ion as intermediate.[5]
This carbenium ion can have multiple formation pathways, see Figure 6. The first pathway is via Brønsted acid sites. This Brønsted acid site can donate a proton to an alkane or an alkene (obtained after precracking). When the proton is donated to an alkane, a carbonium ion is formed (penta coordinated ion,[25] see reaction 1 in Figure 6). This carbonium ion is then protolytically cracked, forming an alkane and a carbenium ion.
If the Brønsted acid site donates a proton to an alkene as in Figure 6 reaction 2, a carbenium ion is formed straight away.
A Lewis acid site can take a hydride ion from an alkane, forming a carbenium ion as in reaction 3 from Figure 6. Also a very strong Bønsted site acid can take a hydride ion, forming dihydrogen. The formed carbenium ions are then cracked via β-scission as seen in reaction 4 in Figure 6. This results in a smaller alkene and a smaller carbenium ion.[5]

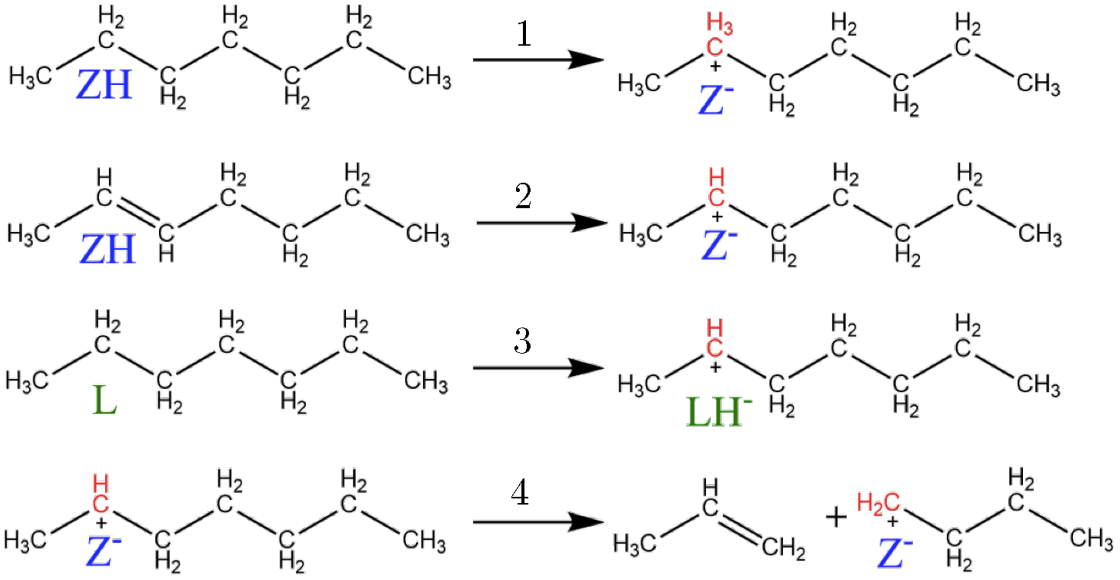

Figure 6: Different reactions that occur during the cracking of hydrocarbons on Lewis or Brønsted acid sites. Reaction 1: formation of carbonium ion by donation of proton from Brønsted acid site (ZH) to alkane. Reaction 2: formation of carbenium ion by proton donation from Brønsted acid site to alkene. Reaction 3: Lewis acid site (L) abstracts hydride from alkane to form a carbenium ion. Reaction 4: carbenium ion is cracked via β-scission to form an alkene and a carbenium ion. Adapted from Vogt *et al.*[5]

1.2 Probe Molecule Spectroscopy

For research on solid acids many different characterization techniques are used.[30] The activity of catalysts mainly takes place at the surface of the catalyst. To study the nature of the surface of a catalyst, probe molecules can be used. Probe molecules are carefully selected molecules that adsorb on specific surface groups of a material.[31] This makes it possible to examine samples with a larger diversity of techniques. Surface sites without the right characteristics for e.g. FT-IR spectroscopy, can now be explored by this technique by studying the interaction of the probe molecule with the surface sites.[13] When using a probe molecule for spectroscopic experiments, information can be obtained from different aspects of the experiment. First of all by the adsorption of the probe molecule on the material: the selected probe molecule interacts with specific surface sites. Information can be obtained by analysis of the order in which the probe molecule is adsorbed on the different surface sites.[17]
Additionally, temperature programmed desorption (TPD) provides information on the order of strength between the different surface sites. In TPD the temperature in the system is gradually increased and the behavior of the probe molecule on the different surface sites is studied. The probe molecule will be desorbed from weaker surface sites at lower temperatures.[30]
The location of the bands of the probe molecule, in the spectrum of the chosen spectroscopy method, provides information on the nature of the surface site on which the probe molecule has adsorbed. A shift in the location of this band with respect to the reference, shows a change in the chemical environment of the surface site. The intensity of the bands provide information on the number of acid sites and the site distribution.[13]

A successful probe molecule has to meet some requirements. The probe molecule has to be site specific at a temperature below the reaction temperature. However, the probe molecule should be able to still selectively reach the surface site with a variation in the electronic structure. It is also important that the probe molecule does not change the surface upon adsorption and that no side reactions occur due to the probe molecule being present.[32,33] There is a wide variety of available probe molecules, for example: CO, NO, CO_2, N_2, NH_3, pyridine, benzene and substituted benzenes.[13]

1.2.1 Pyridine as Probe Molecule

To study the acidic sites of the FCC catalyst, the basic probe molecule pyridine will be used. Pyridine is a very convenient probe molecule to probe acidity as it can both adsorb on Lewis and Brønsted acid sites. On weak Brønsted sites, the pyridine will form an H-bond. An example of this would be a pyridine binding on a silanol group. When the pyridine molecule is adsorbed on a strong Brønsted acid site, the pyridine is protonated and a pyridinium ion is formed. In the case of a Lewis acid site the pyridine will strongly coordinate on the site. Figure 7 shows these different binding modes of pyridine.[33]

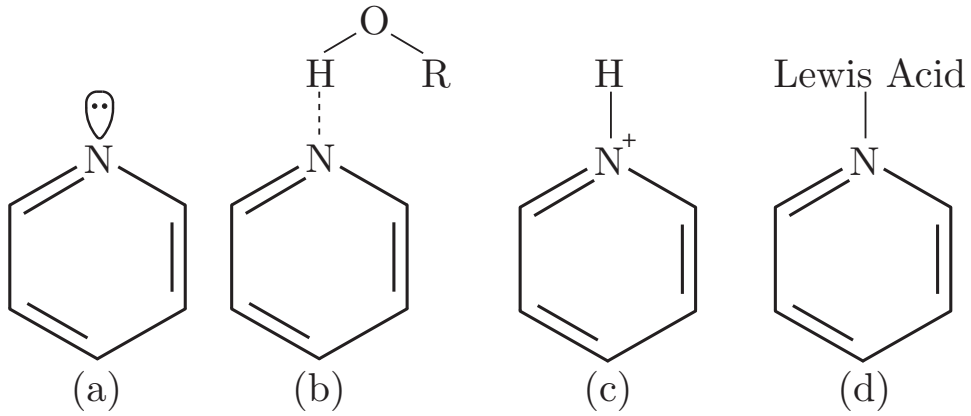

Figure 7: The different binding modes of pyridine, in which (a) shows a pyridine molecule, (b) shows a pyridine molecule bound to a weak acidic site, (c) shows the pyridinium ion that is formed after reaction with a strong Brønsted acid site and (d) shows a pyridine molecule coordinated on a Lewis acid

An additional advantage of pyridine is that it's small enough to enter the 12 membered ring channels of zeolite Y.[34] The location of the bands of adsorbed pyridine give information on the nature of the acid site. The total peak surface can give information on the amount of acid sites. Temperature programmed desorption to define the strength of the acidic sites can be performed as the boiling point of pyridine is 115 ℃.[35] This relatively low temperature can be reached in many setups.

1.2.2 Fourier Transform Infrared Spectroscopy

Infrared spectroscopy is the main characterization technique to explore the surface chemistry of heterogeneous catalysts.[30,36] When using probe molecules the nature and environment of the surface atoms and surface ions can be explored. With infrared (IR) spectroscopy, the frequency of molecular vibrations can be measured. The vibration energies are dependent on the nature and binding of the molecules.[30] The IR radiation can be either absorbed, transmitted or reflected by the surface. Two great advantages of IR spectroscopy are that it's noninvasive and nondestructive. To study acidity in catalysts, it is desirable to create comparable circumstances to the ones in the system in which the catalyst is used. This way of doing measurements is called *in situ*. The FCC process takes place at high temperatures and low pressures. One of the systems in which these circumstances can be recreated is FT-IR spectroscopy in transmission mode using a cell which can be brought under vacuum.[37]
The three main components of an infrared spectrometer are[38]: a light source to emit the desired radiation, a detector to detect the non-absorbed light and a monochromator to separate the radiation into different wavelengths. Modern infrared spectrometers use an interferometer to separate the light instead of a monochromator. This interferometer translates the wave patterns of the different wavelengths into an interferogram. A Fourier transformation (FT) is then performed on this interferogram to convert it into an infrared spectrum.[39]

Pyridine FT-IR spectroscopy

In 1963, Parry introduced the use of pyridine as probe molecule for infrared spectroscopy.[40] In his study he showed the use of pyridine to characterize the surface acidity of solid acids. The frequencies of the vibrational modes of pyridine change when the pyridine molecule is adsorbed on different surface sites. Figure 8 shows an overview of the most sensitive pyridine vibrations.[41] The assignments that are used were introduced by Kline and Turkevich.[42]

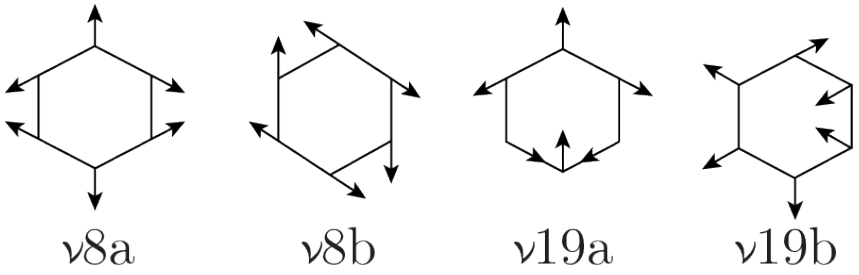

Figure 8: Different vibrations of the pyridine molecule observed in FT-IR spectroscopy. Adapted from Vimont.[33]

The frequencies of these vibrations are different for a pyridine molecule adsorbed on a Lewis acid site or pyridine adsorbed on a Brønsted acid site. Especially the ν8a and ν19b vibrations are used to assign the different acidic sites.[28] When pyridine binds on a Brønsted acid site and a pyridinium ion is formed, a peak at 1541 cm^{-1} is observed for the ν19b vibration. The ν19b vibration for pyridine on a Lewis acid site lies in the region between 1445-1455 cm^{-1}. The exact frequency of this vibration provides information on the strength of the Lewis acid site. A shift of the band to a higher frequency indicates a stronger Lewis acid site. This shift can also be observed for the other binding modes.[40,43] Table 1.2.1 shows the frequencies of the different vibrations of the pyridine molecule adsorbed in a physisorbed manner (liquid pyridine), via a H-bond, coordinated on a Lewis acid site or as pyridinium ion. The fingerprint IR spectra of all these vibrations for the different binding modes can be seen in Figure 10 on the left.

To make sure pyridine can adsorb on all surface sites available, all the H_2O and CO_2 molecules need to be removed from the surface. This can be done by heating the sample *in situ* up to around 550 ℃ under vacuum.

Table 1.2.1: Overview of the frequencies of the bands of the different vibrations of pyridine, adsorbed on different surface sites, in FT-IR spectroscopy. The most characteristic frequencies are shown in bolt. Obtained from Vimont.[33]

	Frequencies (cm^{-1})			
Attribution	Liquid pyridine	H-bond (on silica)	coordinated (on alumina)	pyridinium (on HY zeolite)
ν1 + ν6a	1610-1640		1610-1640	
ν8a	**1579**	**1595(+16)**	**1600-1626(+21-47)**	**1630(+51)**
ν8b	1572	1577 (+5)	1577(+5)	1610(+38)
ν19a	1478	1478(+9)	1488 (+10)	1493(+15)
ν19b	**1439**	**1445(+6)**	**1445-1455(+6-16)**	**1541(+102)**

1.2.3 Ultraviolet Visible Spectroscopy

A new possible technique to study the surface chemistry of FCC catalysts is to use ultraviolet-visible (UV-Vis) spectroscopy in combination with pyridine as probe molecule. In UV-Vis spectroscopy measurements, samples are irradiated with UV-Vis light, which is light with a wavelength between 200 and 800 nm. Near UV light has a wavelength between 200 and 400 nm, or a wavenumber from 50,000 to 20,000 cm^{-1} and visible light has a wavelength between 400 and 800 nm, or a wavenumber between 20,000 to 12,500 cm^{-1}. Electrons can be excited from the highest occupied molecular orbital (HOMO) to the lowest unoccupied molecular orbital (LUMO) upon irradiation of light. The energy of the light has to be equal to the band gap between the two levels. UV-Vis light has enough energy to cause this excitation for a lot of molecules. A UV-Vis spectrometer can measure what part of the light source was absorbed, giving information on the band gap of the excitation.[44]

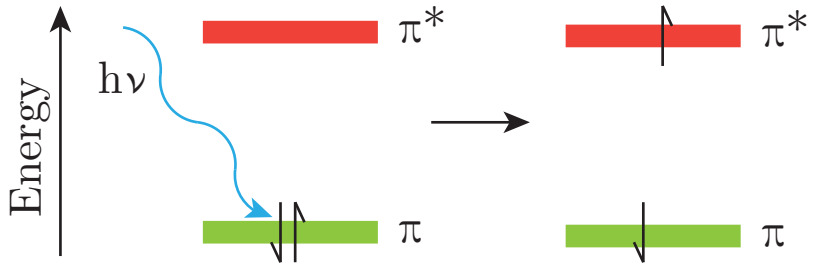

Figure 9: Excitation of an electron from π (bonding) orbital to the π^* (antibonding) orbital by incident light. The energy of the light has to be equal to the energy of the band gap between the ground state and the excited state.

Pyridine UV-Vis spectroscopy

Pyridine is a hetero aromatic molecule. The six atoms that form the aromatic ring all donate one π-electron into the conjugated π-system. UV-Vis light has enough energy to cause a $\pi \rightarrow \pi^*$ transition, with π^* being the excited state. Figure 9 shows a schematic representation of this excitation. Because conjugation lowers the energy of the LUMO and raises the energy of the HOMO, the energy that is necessary for an electronic transition decreases. This explains why the energy of the absorbed radiation of an excitation decreases with increasing conjugation.[45,46,47] Due to the conjugated system of the pyridine molecule, the use of pyridine as probe molecule for Ultraviolet-Visible (UV-Vis) spectroscopy was proposed by Velthoen *et al.*[48] When pyridine was introduced to a solid acid, multiple bands arise in the UV-Vis spectrum. On Brønsted acid sites the pyridine will form a pyridinium ion. Due to the locally positive charge, the π electrons will be more evenly distributed and the system will be more conjugated. Therefore the band from the excitation in a pyridinium ion will be at a lower energy than the one from pyridine.[49,50,51]. First results have shown that by using this technique, one can distinguish different hydroxyl groups on the surface of solid acids. With current characterization techniques used for solid acids, it is difficult to differentiate between these weakly acidic sites and non-acidic sites, and are therefore often not taken into account when addressing the catalytic activity.[48,52] Figure 10 shows on the right the proposed fingerprint spectra of the different binding modes of pyridine observed in UV-Vis spectroscopy.

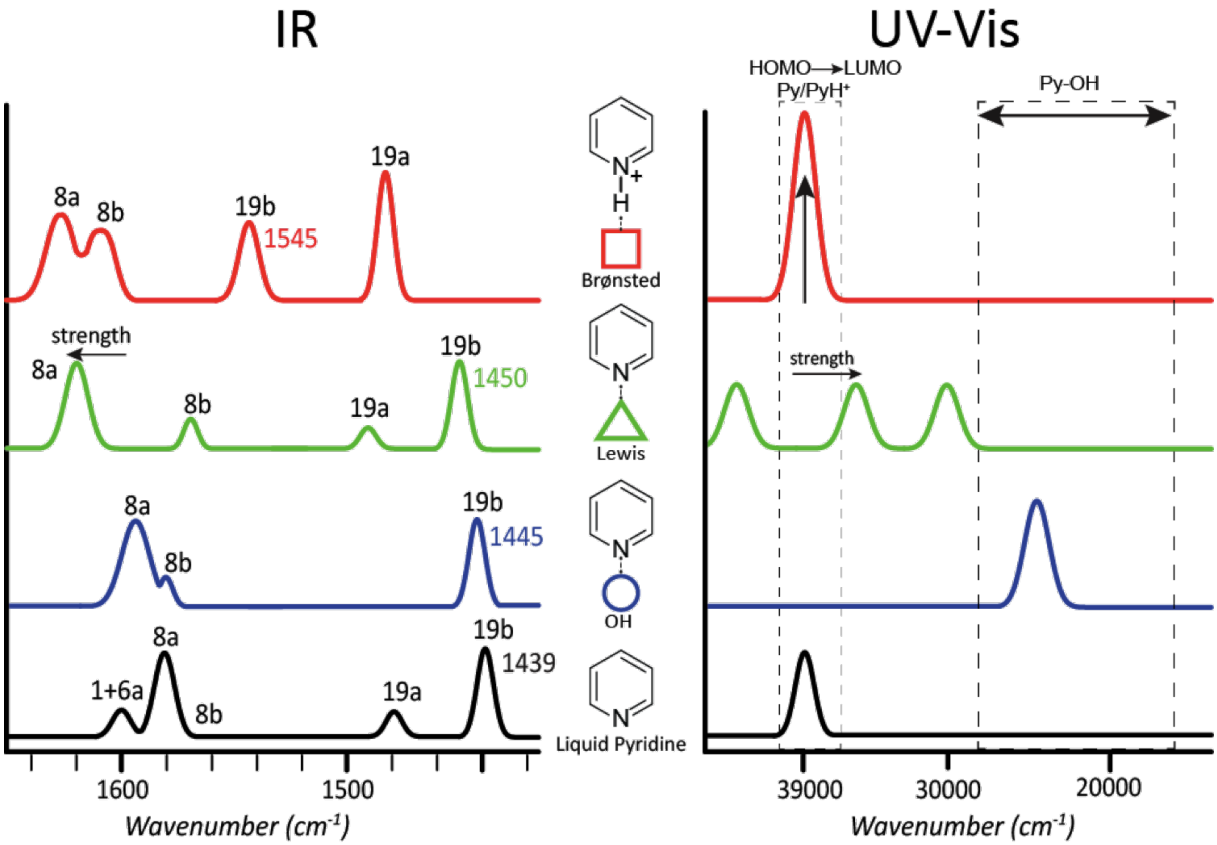

Figure 10: The fingerprint spectra of the different binding modes of pyridine in FT-IR spectroscopy (left) and UV-Vis spectroscopy (right). Pyridinium (pyridine on Brønsted acid site) in red, pyridine coordinated on Lewis acid site in green, pyridine bonded on an OH surface group in blue and physisorbed pyridine in black. Obtained from Velthoen et al.[48]

In the first project in which pyridine UV-Vis spectroscopy was used, a zeolite Y, silica, alumina and different Siral (SiO_2-Al_2O_3 samples with varying silica weight loadings) samples were studied. The bands that were observed in this study and their assignments are summarized in Table 1.2.2. For further information see Velthoen *et al.*[48]

Table 1.2.2: Bands observed in pyridine UV-Vis spectroscopy on solid acids and their assignment. Obtained from the work of Velthoen *et al.*[48]

Band Position	Pyridine Binding Mode	Assignment
38900 cm^{-1}	Physisorbed Py	$\pi \rightarrow \pi^*$ excitation within pyridine
38900 cm^{-1} (very intense)	Pyridinium ion	$\pi \rightarrow \pi^*$ excitation within pyridinium
37700 cm^{-1}	Coordinated on LAS	Interaction between LAS and lone pair on N of Py
44000 cm^{-1}	Coordinated on LAS	Charge transfer within pyridine-LAS complex
31800 cm^{-1}	Coordinated on LAS	Charge transfer within pyridine-LAS complex
28800 cm^{-1}	OH Surface Species	Aluminol (3722 cm^{-1} in IR)
27350 cm^{-1}	OH Surface Species	Isolated silanol group (around 3742 cm^{-1} in IR)
26400 cm^{-1}	OH Surface Species	Isolated aluminol group (around 3742 cm^{-1} in IR)
25500 cm^{-1}	OH Surface Species	Aluminol (3670 cm^{-1} in IR)
24250 cm^{-1}	OH Surface Species	Vicinal silanol group (3670 cm^{-1} in IR)
21250 cm^{-1}	OH Surface Species	Amorphous Si-(OH)-Al groups

1.3 Aim and approach

To maximize the amount of useful products obtained from crude oil with the FCC process, the working mechanism of the FCC catalyst has to be fully understood. Gain in knowledge can lead to a more rationally design of the catalyst. Most research[5,10] focuses mainly on the role of the zeolite component of the FCC catalyst. The zeolite contains Brønsted acid sites (BAS) on which carbenium or carbonium ions can be formed. However, Corma *et al.* discovered that at the same time carbenium ions also can be formed on Lewis acid sites (LAS).[53] These carbocations are used in the cracking reaction. Whether weak acidic sites play a role in the cracking mechanism is not clear.
In this work, the acidic characteristics of silica (weak acid sites), alumina (LAS) and clay (LAS, BAS, weak acid sites) will be studied alongside those of the zeolite. Not only the loose components will be studied, but also a series of FCC catalysts. The binder in the catalyst is varied, it is either a combination of silica and alumina or only alumina or silica. All these different catalysts will be studied with and without zeolite incorporated.
The steam that is present in the stripper and regenerator, is one of the deactivation causes of the FCC catalyst in the FCC process. To study the effect of the steam on the acidity of the different FCC catalysts, the FCC catalysts were subjected to steam treatment. Samples were taken after 5, 10 and 20 hours of steam treatment to study the deactivation rate of the different catalysts.
The single components and the different FCC catalysts will be studied by pyridine FT-IR spectroscopy and pyridine UV-Vis spectroscopy. Pyridine FT-IR spectroscopy, as an established technique, will be used to gain knowledge on the acidic properties of the samples. It will be the first time that pyridine UV-Vis spectroscopy will be used on a full catalyst set. Pyridine UV-Vis spectroscopy will provide information on the LAS and BAS, and additionally, information on the nature of the weak acidic surface sites that cannot be obtained by pyridine FT-IR spectroscopy. These results will help to further develop pyridine UV-Vis spectroscopy as acidity probing technique. XRD measurements will be done to study the effect of the steam treatment on the crystal structure of the FCC catalysts. XRD is a technique often used in catalysis to check the crystal structure of catalysts and other materials.[30] A start will be made on making an acidity-activity correlation by comparing the performance data of the different FCC catalysts.

Chapter 2

Experimental Methods

2.1 Pyridine Fourier Transformation Infrared Spectroscopy

The Fourier-Transform Infrared (FT-IR) spectra were collected with a Thermo Scientific Nicolet iS5 FT-IR instrument in transmission mode using the OMNIC software. The detector was a DTGS detector using 32 scans per spectrum and a resolution of 4 cm^{-1}. Anhydrous pyridine from Sigma-Aldrich (99%) was used.

For the pyridine FT-IR spectroscopy measurements self-supporting wafers of between 10 and 20 mg and a diameter of 12 mm were pressed using a press tool. These wafers were prepared by first grinding the sample with a mortal and pestle. The ground material was divided equally in the pressing tool. The metal cylinder was turned around one time and then the pressing tool was put in the press. Around five ton pressure was applied for about ten seconds. Depending on the ease of making the wafer, the pressure or the time was varied.
The wafer was put in a cell with KBr windows connected to a vacuum system. A drying program of 10 ℃/min up to 550 ℃ was used. The temperature was kept at 550 ℃ for approximately 30 minutes before cooling down to room temperature. Before and after the drying procedure spectra were recorded. During the drying procedure also some spectra were recorded, the number varied per sample. During the drying procedure the system was under vacuum.
A static pyridine atmosphere was created by allowing pyridine to enter the pump system for ten seconds. The pyridine was now introduced to the cell for 30 minutes. During the pyridine adsorption, every five minutes a spectrum was recorded. Afterwards, vacuum desorption was allowed for 45 minutes and a spectrum was recorded after 45 minutes. Temperature programmed desorption followed, with a rate of 5 ℃/min up to 550 ℃. The temperature was kept at 550 ℃ until all the pyridine had desorbed. During the TPD a spectrum was recorded every 25 ℃.

2.2 Ultraviolet Visible Light Spectroscopy

UV-Vis spectra were collected in reflection mode using an AvaSpec 2048L spectrometer connected to a high-temperature UV-Vis optical fiber probe. Per spectrum an integration time of 3 ms and an average of 300 scans was used. The software that was used was

Avasoft 8. A Linkam Scientific temperature controlled cell equipped with a quartz lid was used. The Linkam cell was connected to a Eheim Professional 3 water cooler and a Linkam TMS 93 or 94 heater.

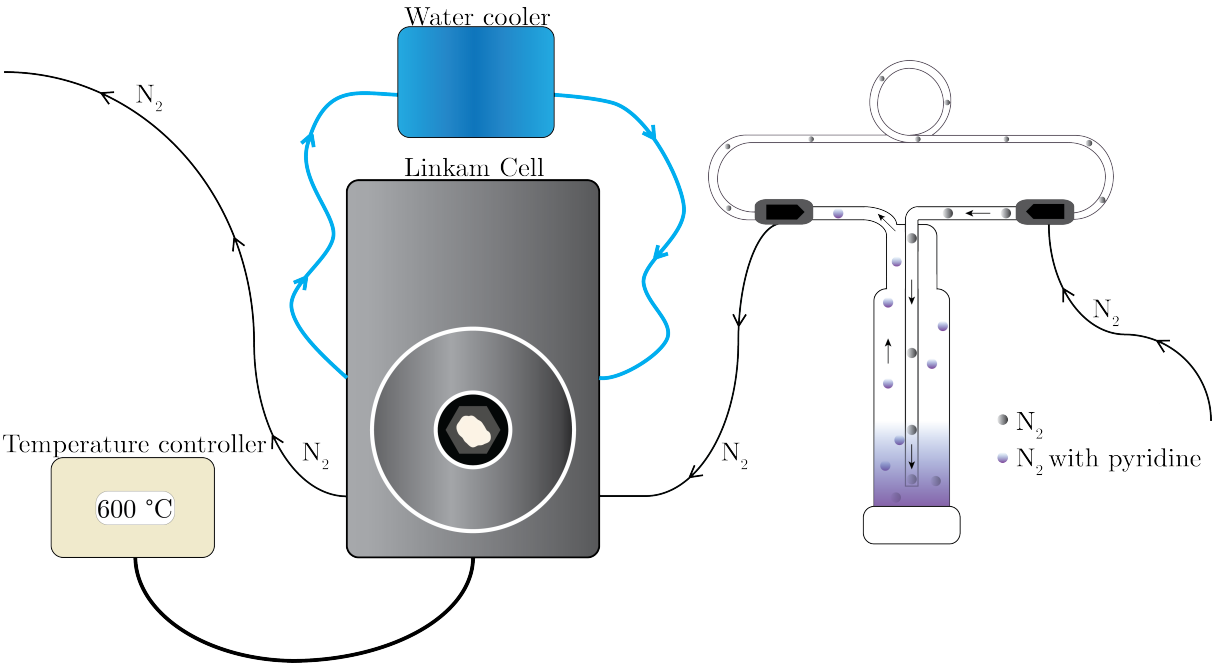

Figure 11: In the bypass/saturater setup in which the saturater is filled with pyridine. Nitrogen flows through the liquid pyridine and is saturated with pyridine. The nitrogen can also be led through the bypass, during drying and desorption. The nitrogen flow is introduced into the Linkam Cell that is connected to a water cooler and a temperature controller. The outlet is led into an extraction pipe.

For the pyridine UV-Vis spectroscopy measurements, the sample was crushed with a pestle and mortar. The sample was then transfered to the Linkam cell. The sample was flattened with the use of a cover glass. The Linkam cell was connected to a nitrogen flow via the set up in Figure 11. The nitrogen can either go via the bypass or through a saturater filled with anhydrous pyridine (Sigma-Aldrich, 99%). This saturater was filled in a N_2 glovebox.

The sample was first dried under a N_2 flow of 15 mL/min with a heating program of 10 °C/min up to 600 °C. The cell was kept at 600 °C for two hours. Because the Linkam Cell cannot be put under vacuum the drying procedure differs from that of the pyridine IR measurements.

For the UV-Vis measurements a background was taken using a reference white. The height of the probe was adjusted until the top op the spectrum reached 50,000 ADC Counts in Scope mode in the Avasoft 8 software. The probe was then directed at the sample. The height of the Linkam cell was adjusted so that the top of the spectrum was just below 50,000 ADC counts. A spectrum was recorded of the sample before introducing pyridine. The N_2 flow was changed to a lower rate between 5 and 15 ml/min. As the flow was different between days, the flow was adjusted to meet the same output. This was evaluated by putting the exit tube into a beaker and observing the bubbles that exited the system. The valves on the saturater/bypass setup were turned and pyridine saturated

nitrogen was allowed to flow into the Linkam cell. A timer was set for 30 seconds from the moment the valves were opened. After 30 seconds, a continuous measurement was started. Every minute a spectrum was saved. Pyridine adsorption was allowed for 45 minutes. Afterwards, the valves were switched to nitrogen and the flow was increased to 20 ml/min. Temperature programmed desorption was employed at a rate of 5 ℃/min up to 600 ℃. Every minute a spectrum was saved.

The temperatures reported in this thesis are the ones displayed on the temperature controller. The actual temperature of the heating plate is lower. The temperature calibration that was performed can be found in Appendix A.1.

2.3 Performance Test

All of the catalysts were tested after 20 hours of steam treatment. The test that was used to acquire performance data was the Fluid-bed Simulation Test (FST).[54 55] Kelamayi vacuum gas oil (KVGO) was used as feed and all tests were performed in duplicate. The ratio between FCC catalyst and feed was 4:1. The test was performed at 537 ℃.[56]

2.4 XRD Measurements

X-ray Diffraction measurements were performed on a Bruker D2 Phaser with Co Kα radiation (λ=1.789 Å). The angle range was from 20° to 80° in 2θ with an increment of 0.03 and a time scale of one second was used. DIFFRAC Eva software was used to analyze the diffractograms. The samples were crushed with a pestle and mortar and transfered into a holder before the measurement.

Chapter 3

Results and Discussion

The first part of this chapter will give an overview of the samples used for this research and their properties.
The second part will describe the acidity of the single components. Also the acidity of a full FCC catalyst with and without zeolite will be discussed. All samples were characterized by pyridine FT-IR spectroscopy, which is an established method to probe acidity. More on this method can be found in section 1.2.2. Additionally, pyridine UV-Vis measurements were done on all samples. More on why this is an promising technique can be found in section 1.2.3.
The third part of this chapter will further investigate the effect of using different combinations of binders (silica, alumina or silica-alumina) on the acidity of the catalyst.
In the fourth part the effect of steam treatment on the different fresh catalysts will be studied.
To study new bands arising during TPD, pyridine UV-Vis experiments at elevated temperatures are performed. The fifth part of this chapter will give the results of these experiments.
The acidity data will then be correlated to the performance data for the steamed catalysts in the sixth part of this chapter. The performance data were provided by Albemarle.
A short overview of the results of XRD measurements on a part of the samples is given in the seventh part.

The ultimate goal is to develop a method to predict the acidity of a total FCC catalyst based upon the acidity of the separate components. Ideally, this would also be applicable to predict the activity of the complete FCC catalyst.

3.1 Samples

The samples that were used for this research were all provided by Albemarle. The first set exists of all the single components, namely clay, silica, zeolite and alumina. These components were all calcined at 600 ℃ for one hour. For all samples the surface area (SA-BET), matrix surface area (MSA), zeolite surface area (ZSA) and micropore volume (MiPV) were determined. For the single components these textural properties can be found in Table 3.1.1.

Table 3.1.1: Overview of the single components of the FCC catalyst and their textural properties provided by Albemarle.

	SA-BET (m^2/g)	MSA (m^2/g)	ZSA (m^2/g)	MiPV (cm^3/g)
Clay	21	17	5	0.00194
Silica	162	157	5	-0.00023
Zeolite	625	51	574	0.26819
Alumina	123	136	-13	-0.0075

The next set exists of fresh catalysts made from the single components. The binder of the catalyst was varied, being either alumina, silica or alumina and silica. Fresh catalysts with and without zeolite were produced. The dry weight rates of the samples before calcination can be found in Appendix B.1.1. The catalysts were made by mixing the single components in an aqueous slurry. This mixture was spray-dried to form porous microspheres.[5] These catalyst were then calcined at 600 ℃ for one hour. The textural properties of these samples can be found in Table 3.1.2. The sample names give information on the condition of the catalyst (F for Fresh and D for Deactivated), the binder type (SiAl: combination of silica and alumina, Si: only silica and Al: only alumina) and on the presence of the zeolite (Z: contains zeolite, NZ: contains no zeolite).

Table 3.1.2: Overview of the calcined fresh FCC catalysts (with different binders) and their textural properties provided by Albemarle.

	SA-BET (m^2/g)	MSA (m^2/g)	ZSA (m^2/g)	MiPV (cm^3/g)
F_Al_NZ	54	52	3	0.00074
F_Al_Z New	230	75	156	0.07284
F_Si_NZ	54	48	7	0.00247
F_Si_Z	231	54	178	0.08191
F_SiAl_NZ	49	42	7	0.00309
F_SiAl_Z	232	59	173	0.0808

The last set consists of these fresh calcined catalysts subjected to steam treatment. Samples were taken after 5, 10 and 20 hours of steam treatment. For the catalysts without zeolite, only samples were taken after 20 hours of steam treatment. Steam treatment was performed at 788 ℃ in 100 % steam for 5, 10 or 20 hours. The textural properties can be found in Table 3.1.3. The steam treatment is performed to reproduce the dealumination that takes place in the FCC process.

Table 3.1.3: Overview of the steamed samples and their textural properties provided by Albemarle.

	SA-BET (m^2/g)	MSA (m^2/g)	ZSA (m^2/g)	MiPV (cm^3/g)
D20_Al_NZ	34	31	3	0.00087
D5_Al_Z New	159	43	116	0.0541
D10_Al_Z New	136	41	95	0.0443
D20_Al_Z New	124	38	85	0.0398
D20_Si_NZ	33	27	6	0.00255
D5_Si_Z	170	39	131	0.06079
D10_Si_Z	158	35	124	0.05763
D20_Si_Z	134	31	104	0.04825
D20_SiAl_NZ	30	26	4	0.00165
D5_SiAl_Z	177	46	131	0.06134
D10_SiAl_Z	154	43	121	0.05651
D20_SiAl_Z	142	41	101	0.0473

Composition ratios and chemical composition as determined with XRF spectroscopy of all samples can be found in Appendices B.1.1-B.2.3.

3.2 Single Components and Fresh FCC Catalyst

First of all the single components will be discussed. In other studies often only the acidic properties of the zeolite Y are investigated as this is considered the main source of activity within the FCC catalyst.[10 12 57] However, for this research we also look at the influence of the alumina, silica and clay.

Pyridine FT-Infrared Spectroscopy

Components

There are several regions of interest in the FT-IR spectrum when using pyridine as probe molecule. The most important region is that between 1300 and 1700 cm^{-1}. In this region different vibrations of the pyridine molecule are observed. The energies of these vibrations change when the pyridine molecule is adsorbed on a different surface site. The location of the peak also gives information on the strength of the acid site on which pyridine is adsorbed. An overview of the different vibrations and their frequencies can be found in section 1.2.2. In Figure 12 the different lines that will be used in the spectra of this thesis to indicate the different binding modes are shown.

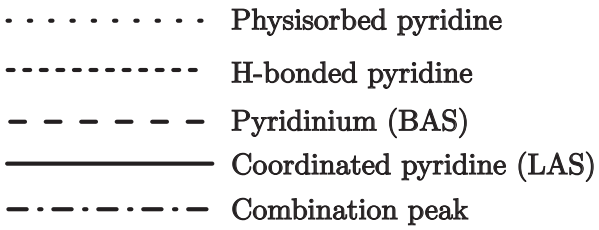

Figure 12: The different types of lines that are used in the pyridine IR and UV-Vis spectra to identify different binding modes of pyridine

Figure 13 shows the absorption peaks of pyridine species adsorbed on the single components zeolite, alumina, silica and clay. For each component the top spectrum is taken after 30 minutes of pyridine adsorption and the bottom spectrum after 200 ℃ of temperature programmed desorption (TPD). When addressing weak and non acidic surface groups we look at the spectrum after 30 minutes of pyridine adsorption. To define stronger acid sites, the spectrum at 200 ℃ is mainly used.

The peak at 1439 cm^{-1} is ascribed to the ν19b vibration of liquid pyridine. This type of adsorption will be called physisorbed pyridine from now on. Due to the very weak bond between the pyridine and the surface this vibration is only visible in the spectrum taken after 30 minutes of pyridine adsorption and not in the spectrum after 200 ℃ of TPD. At this temperature, the physisorbed pyridine has already desorbed from the sample's surface. The physisorbed pyridine peak is observed in the zeolite, alumina and clay. The peak at 1576 cm^{-1} can be ascribed to the ν8a vibration of physisorbed pyridine. However, as the ν8b of H-bonded pyridine and coordinated pyridine are at a frequency very near to this peak (1577 cm^{-1}) the observed peak is seen as a combination of these binding modes. This explains why the peak at 1576 cm^{-1} has decreased a lot after 200 ℃, but has not completely disappeared. The physisorbed pyridine has desorbed but the coordinated

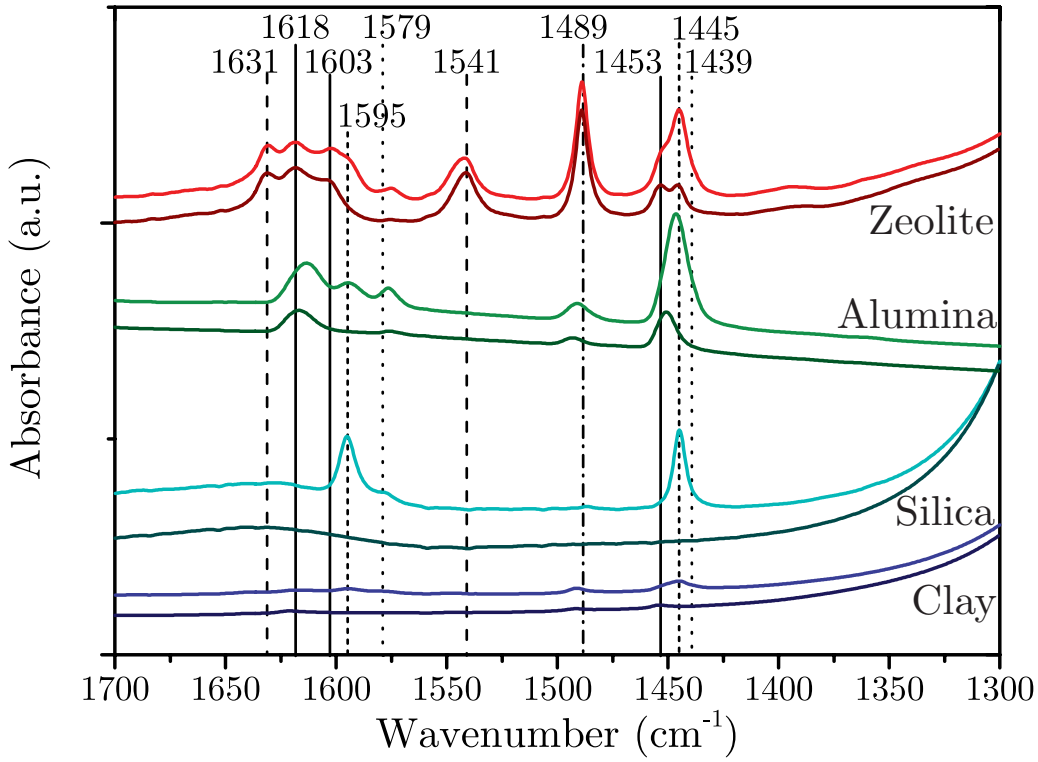

Figure 13: Pyridine absorption peaks in FT-IR spectrum after 30 minutes of pyridine adsorption (top spectra) and after evacuation and temperature programmed desorption up to 200 ℃ (bottom spectra). The zeolite spectra are shown in red, alumina in green, silica in blue and clay in purple. All spectra are corrected for pellet weight. Plotted with y-offset for clarity.

pyridine is still adsorbed.

The peak at 1445 cm^{-1} in Figure 13 (a) is ascribed to the ν19b vibration of pyridine adsorbed on a surface hydroxyl group via a H-bond. The peak at 1595 cm^{-1} indicates the ν8a vibration of pyridine adsorbed on a hydroxyl group. As all components show both these peaks, we can conclude that all components have surface hydroxyl groups. When looking at the spectra after 200 ℃ of TPD, the peak at 1595 cm^{-1} has disappeared. This means that all pyridine has desorbed off the hydroxyl groups at this temperature. For silica, also the peak at 1445 cm^{-1} is gone, showing that silica only has weakly acidic surface hydroxyl groups.

The peak around 1450 cm^{-1} is very characteristic for the ν19b vibration of coordinated pyridine. This shows the presence of Lewis acid sites (LAS) on the surface of the sample. The frequency of this vibration changes with the strength of the LAS. A peak around 1445 cm^{-1} indicates weak LAS and a shift towards 1455 cm^{-1} indicates stronger LAS. Because the peak of H-bonded pyridine and physisorbed pyridine can modify the shape of the LAS peak, the spectrum after 200 ℃ of TPD is used to indicate LAS (Figure 13). The spectrum of zeolite Y shows the presence of two types of Lewis acid sites. The peak at 1453 cm^{-1} indicates strong LAS and the peak at 1445 cm^{-1} weak LAS. The ν19b vibration of coordinated pyridine shows a peak between 1600 and 1626 cm^{-1}, depending on the strength of the LAS. For the zeolite these peaks are seen at 1603 (weak LAS) and 1618 cm^{-1} (strong LAS).
The peaks at 1450 cm^{-1} and 1616 cm^{-1} in the spectrum of alumina shows the presence of one type of LAS.

For the clay it is difficult to see the pyridine peaks in Figure 13. In Appendix C.1 Figure 50, a zoomed in version of the spectra of clay can be found. With peaks at 1452 cm^{-1} and 1618 cm^{-1}, the LAS in the clay are stronger than those in alumina. In Figure 50, we can see that the clay also contains some BAS. As the peak surface gives information on the amount of pyridine adsorbed, we can conclude that clay does not have a lot of acid sites.

The zeolite is the only component containing Brønsted acid sites (BAS). Upon adsorption of pyridine on a Brønsted acid site, a pyridinium ion is formed. The most characteristic peak for pyridinium is the ν19b vibration at 1541 cm^{-1}. The peak at 1630 cm^{-1} indicates the ν8a vibration of pyridinium.
The peak at 1489 cm^{-1} is a combination peak ascribed to the ν19a vibration of pyridine adsorbed on LAS and BAS. The blue-shift of this peak for the alumina spectrum is due to the slightly higher frequency of this vibration for coordinated pyridine (1493 cm^{-1}) than for pyridinium (1488 cm^{-1}).
To summarize, silica contains only weak acidic hydroxyl surface groups. Clay has very little acid sites, but contains Brønsted acid sites, Lewis acid sites and hydroxyl surface groups. Alumina contains Lewis acid sites of medium strength and hydroxyl surface groups. Zeolite Y contains Brønsted acid sites, strong and weak Lewis acid sites and hydroxyl surface groups.

Fluid Catalytic Cracking Catalyst

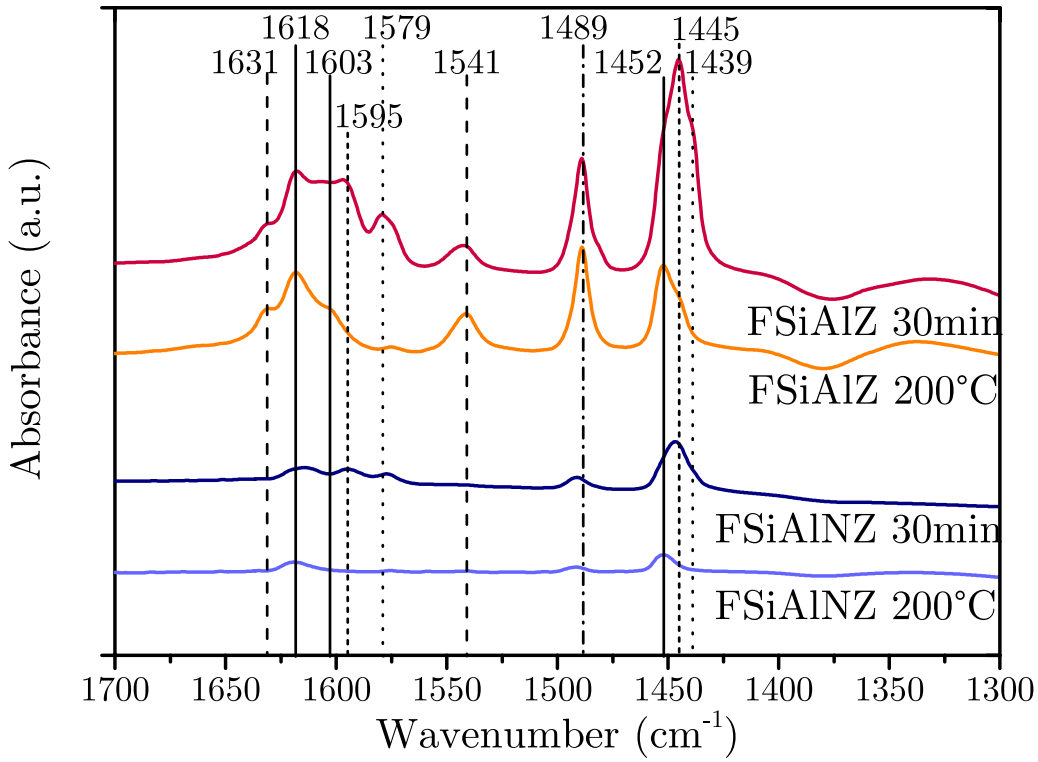

Figure 14: Pyridine FT-IR spectra of the FCC catalyst (SiAl binder) with and without zeolite after 30 minutes op pyridine adsorption and after 200 ℃ of TPD. All spectra are corrected for pellet weight. Plotted with y-offset for clarity.

For the standard FCC catalyst, from here on called FSiAlZ, 30 wt% zeolite, 46 wt% clay, 12 wt% alumina and 12 wt% silica was used. The components are mixed in an aqueous slurry and then spray-dried to form porous microspheres.[5] Textural properties

of the samples can be found in Table 3.1.2. The chemical composition as determined by XRF spectroscopy can be found in Appendix B.2.2.

Figure 14 shows the pyridine FT-IR spectra of FSiAlZ and FSiAlNZ, which is the FCC catalyst without zeolite. For both samples the spectra after 30 minutes of pyridine adsorption and after 200 ℃ of TPD are shown. The spectrum of FSiAlZ resembles that of zeolite Y. Two types of LAS are present: strong LAS (1452 cm^{-1} and 1618 cm^{-1}) and weak LAS (1445 cm^{-1} and 1603 cm^{-1}). FSiAlZ also contains BAS, as can be seen by the presence of the peaks at 1541 cm^{-1} and 1631 cm^{-1}. The peaks at 1445 cm^{-1} and 1595 cm^{-1} in the spectra after 30 minutes of pyridine adsorption show that FSiAlZ has surface hydroxyl groups. These groups are weakly acidic because all pyridine on these groups has desorbed after 200 ℃ of TPD. More physisorbed pyridine is present on the sample surface for FSiAlZ after 30 minute of pyridine adsorption than for the zeolite. This shows that upon incorporation of zeolite and the Si/Al binder, more physisorbed pyridine is adsorbed on the surface of the FCC catalyst.
For FSiAlNZ we see the presence of H-bonded pyridine (1445 cm^{-1} and 1595 cm^{-1}) as well as physisorbed pyridine (1579 cm^{-1}) on the sample surface. The LAS within FSiAlNZ are stronger (1452 cm^{-1} and 1618 cm^{-1}) than those in the single alumina component (1450 cm^{-1} and 1616 cm^{-1}). This agrees with literature that reports an increase in Lewis acid strength upon an increase in Si content.[58] When silica is incorporated, more bridging Si(-OH)-Al are formed. These sites act as Brønsted acid sites, but dehydroxylation of these bridging hydroxyls forms strong LAS. This phenomenon is observed in both zeolites and mesoporous aluminosilicates.[58 59]

Pyridine FT-IR spectroscopy is not able to distinguish different hydroxyl groups. To gain knowledge on the different types of hydroxyl groups we will use the FT-IR spectra taken before introducing pyridine.

FT-IR spectroscopy

The region between 3800-3300 cm^{-1} of the FT-IR spectrum shows the molecular vibrations of surface hydroxyl groups of a species. In Figure 15 the OH regions of all single components and the FCC catalyst with and without zeolite are shown. These spectra were taken at room temperature after heat treatment of the samples at 550 ℃, for 30 minutes under vacuum. This procedure is done to remove any adsorbed species and water from the samples. Water gives rise to a very broad absorbance band in infrared spectroscopy between 3800 and 3300 cm^{-1}. So to use these spectra for surface hydroxyl group identification, all water has to be removed. Stronger acid sites are observed at a lower frequency. Due to the weaker character of the O-H bonds, the vibrations of these bonds have a lower frequency.[58] Due to the differences in strength of the hydroxyl groups, the position of the bands can shift and therefore deviate from the reference positions.

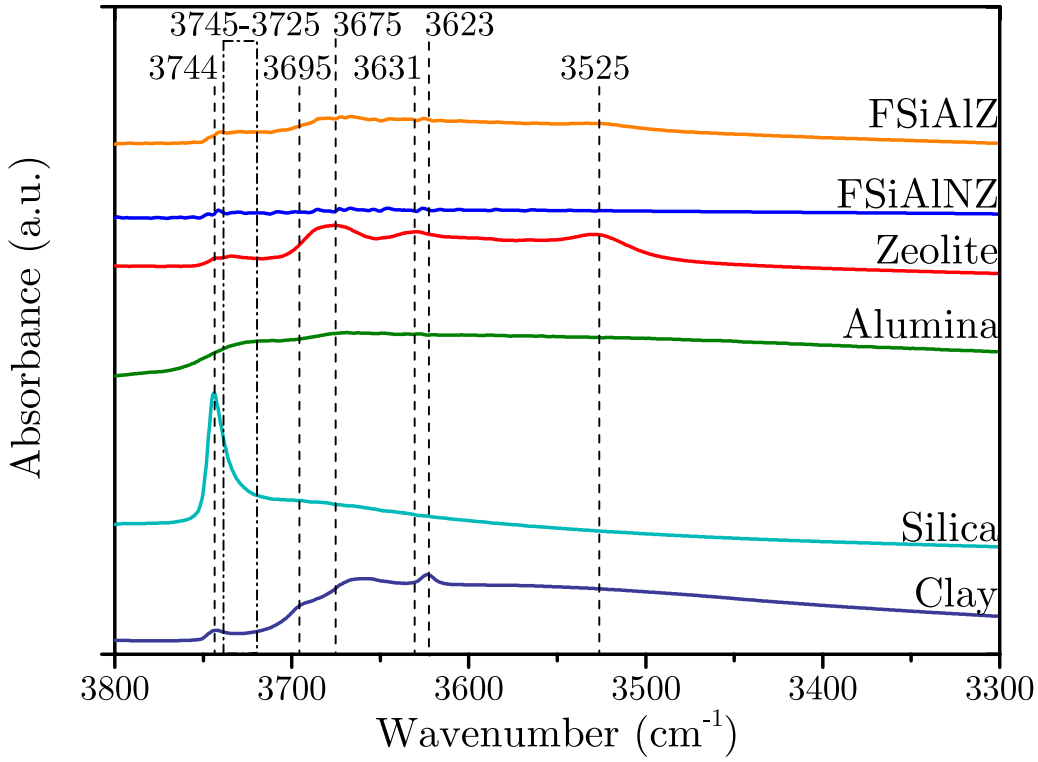

Figure 15: FT-IR spectrum of OH region of all single components and the FCC catalyst with and without zeolite after drying procedure. All spectra are corrected for pellet weight. Plotted with y-offset for clarity.

The band around 3745 cm^{-1} indicates isolated silanol groups.[52] For silica, this is the only surface hydroxyl group present. Isolated silanol groups are also present in the clay, zeolite and the FSiAlZ catalyst. The quality of the spectrum of the FSiAlNZ catalyst is low but a small band is observed around 3743 cm^{-1}. The tail of this peak, to lower frequencies is associated with vicinal silanol groups. These can be created by a vacancy in the silica framework. These vacancies form a hydroxyl nest, which can be formed during steaming upon release of non-framework alumina.[13,52]
The weak band around 3720 cm^{-1} in alumina indicates aluminol groups. The band around 3670 cm^{-1} indicates aluminol groups in extra framework species.[39] This band is clearly observed in the zeolite, and bands with lower intensity are observed for th FSiAlZ and alumina samples.
The 3650-3500 cm^{-1} region indicates isolated Brønsted acid sites. The band at 3631 cm^{-1} indicates a Brønsted acid site in a super cage structure in the zeolite and 3525 cm^{-1} indicates Brønsted acid in the sodalite cage.[39] The 3695 cm^{-1} band in clay is assigned to inner-surface hydroxyl groups and the band at 3623 cm^{-1} is due to bridging hydroxyl groups.[60]

Pyridine UV-Vis spectroscopy

In this work, pyridine UV-Vis spectroscopy is used on a full catalyst set for the first time. As this technique is new, the interpretation is not as straight forward as for an established technique such as pyridine FT-IR spectroscopy. When looking at the results from our pyridine UV-Vis experiments, different information can help us with the interpretation. One can use:

- the location of the band
- the moment the band start arising
- the combinations of bands arising at the same time
- the moment the band start disappearing

The information from the second, third and forth manner can be compared to data obtained by pyridine FT-IR measurements. For all UV-Vis spectra displayed in this thesis the spectrum taken of the sample before the introduction of pyridine was subtracted. Therefore, all bands that arise are due to interaction of pyridine with the species surface. Due to the broad character of the bands in UV-Vis spectroscopy, the resulting spectrum is formed by all the different bands. In Appendix D.3 the results of an attempt to perform deconvolution on the spectra are shown. However, because this did not successfully show bands with the same location and bandwidth for the different samples, it will not be used for the interpretation.

Components

Figure 16 shows the pyridine UV-Vis spectra of the single components after 45 minutes of pyridine adsorption (top) and after 200 ℃ of temperature programmed desorption (bottom).

One of the main differences between the components obtained from the pyridine-IR measurements, is that only the zeolite contains a considerate amount of Brønsted acid sites. Therefor we start the interpretation by looking at what could indicate the presence of Brønsted acid sites in the pyridine UV-Vis spectra. Experimental measurements have shown that pyridinium, which forms when pyridine adsorbs on a Brønsted acid site, gives an absorption band around 39000 cm^{-1} in the electronic spectrum.[49] The absorption band of pure pyridine lies at a slightly lower energy at 38900 cm^{-1}. This band is ascribed to the HOMO to LUMO excitation within the π orbitals of pyridine.[48] In Figure 16, we see that an absorption band around 39000 cm^{-1} is observed for all single components in the spectra taken after 45 minutes of pyridine adsorption. To study the nature of this band we take a look at the spectrum taken after 200 ℃ of TPD. For these spectra we see more distinct differences between the single components. The spectrum of the zeolite shows a broad band at 39000 cm^{-1}, confirming that pyridinium is still adsorbed on the surface of the zeolite. The broad character of the band can be explained by the presence of Lewis acid sites in the zeolite. Due to its electrophilic character, the LAS interacts with the non-bonding lone pair of the nitrogen of the pyridine molecule. This physical shift in electron density causes a decrease in the energy gap between the HOMO and LUMO. The decrease in energy gap shifts the absorption band to a lower energy.[48] Orbital overlap between the LAS and the pyridine cause two charge transfer bands at a lower and higher energy than the HOMO-LUMO excitation band. The band in the spectrum of the zeolite

around 37700 cm^{-1} is ascribed to the π to π^* transition of pyridine on LAS. The shoulder at 44000 cm^{-1} of the broad band around 39000 cm^{-1} is ascribed to one of the charge transfers of this binding mode of pyridine. The shoulder band at 31000 cm^{-1} is ascribed to the other charge transfer.

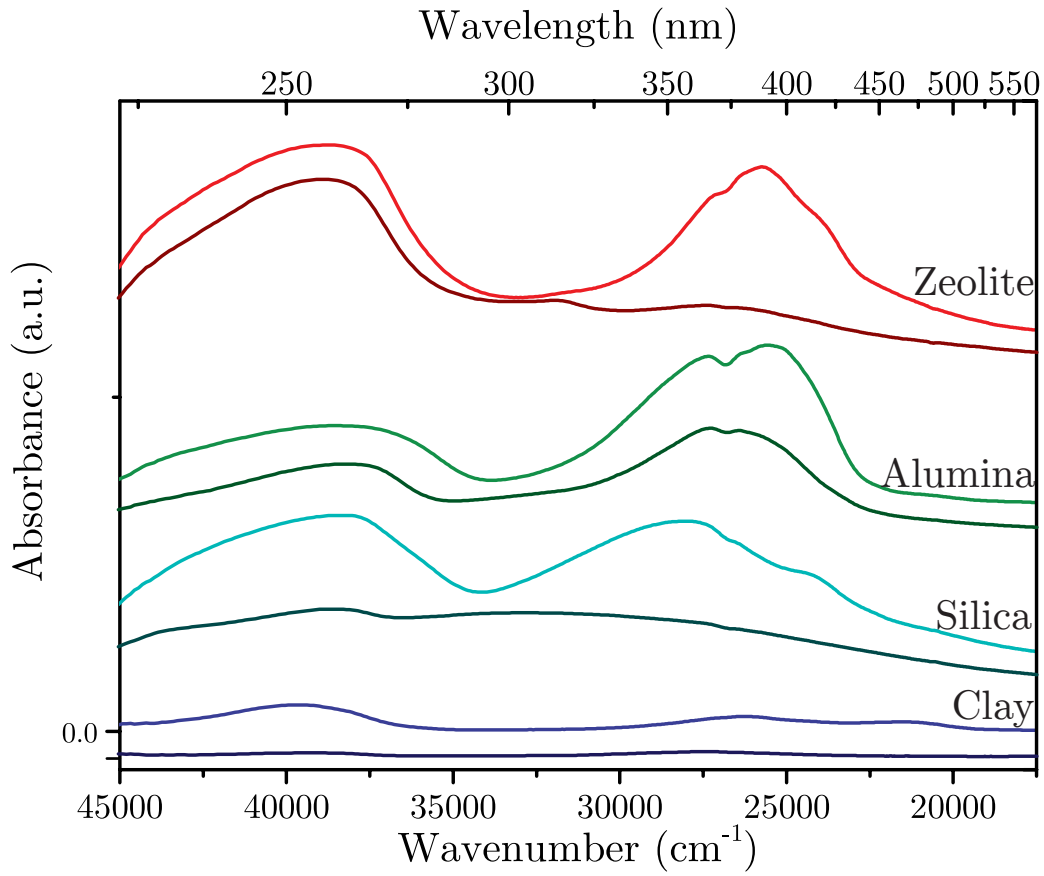

Figure 16: Pyridine UV-Vis spectra of the single components after 45 minutes of pyridine adsorption (top spectra) and after temperature programmed desorption of 200 °C (bottom spectra). Zeolite in red, alumina in green, silica in blue and clay in purple. Plotted with y-offset for clarity.

Bands within the region 30000-20000 cm^{-1} are ascribed to pyridine bonded to different surface hydroxyl groups of the zeolite.[48] These groups have a weakly acidic character and pyridine desorbs quickly during TPD. The band at 27350 cm^{-1} is ascribed to the presence of isolated silanol groups and the shoulder at 24250 cm^{-1} is ascribed to vicinal silanol groups. The pyridine UV-Vis spectrum of zeolite also shows bands arising at 26400 cm^{-1} and 25500 cm^{-1}. The former is ascribed to pyridine adsorbed on isolated aluminol groups and the latter to other aluminol species.[48]

The spectrum of alumina after 45 minutes of pyridine adsorption shows a less intense band at the region around 39000 cm^{-1}, due to the lack of BAS. The band that is still visible after 200 °C of temperature programmed desorption has a maximum around 37000 cm^{-1} and is ascribed to the LAS of the alumina. The hydroxyl region of the UV-Vis spectrum after 45 minutes of pyridine adsorption shows multiple bands. Not only the expected bands at 26400 and 25500 cm^{-1} for aluminol groups are observed, there is also a band at 27350 cm^{-1} visible. As this is assigned to isolated silanol groups this band

is not expected for alumina. However, the chemical compositions determined with XRF spectroscopy shows that the alumina contains 0.16% silica (see Appendix B.2.1). This contamination can explain the presence of the 27350 cm^{-1} band, however the intensity of the band is unexpectedly high.

The UV-Vis spectrum of silica after 45 minutes of pyridine adsorption shows a broad band around 39000 cm^{-1}. As this band has disappeared after 200 ℃ of TPD, we ascribe this band to physisorbed pyridine. In the hydroxyl region we see bands associated with isolated silanol groups (27350 cm^{-1}) and vicinal silanol (24250 cm^{-1}). A very small shoulder at 26400 cm^{-1} indicates a small amount of surface aluminol groups. The chemical composition determined with XRF spectroscopy showed a contamination of alumina of 0.23% (see Appendix B.2.1). Even at lower energy, a new band occurs. This band at 20800 cm^{-1} is ascribed to very weakly acidic amorphous Si-(OH)-Al groups. As all bands have disappeared after 200 ℃ of TPD, we can conclude that all of the pyridine adsorbed on the surface of silica has desorbed at this temperature. This agrees with the pyridine FT-IR spectrum of silica at 200 ℃ of TPD.

The UV-Vis spectrum of clay after 45 minutes of pyridine shows three clear bands. At 39000 cm^{-1}, the combined band of physisorbed pyridine and pyridine on BAS is observed. The band at 26400 cm^{-1} shows the presence of isolated aluminol groups. The band at 21250 cm^{-1} shows the presence of amorphous Si-(OH)-Al groups on the surface of clay. Most pyridine has desorbed after 200 ℃ of TPD.

Figure 17 shows the UV-Vis spectra during 45 minutes of pyridine adsorption on the zeolite and the evolution of the indicated bands. The same was done for alumina (Figure 18), silica (Figure 19) and clay (Figure 20).

Figure 17 shows the gradual arise of the different bands in the region between 45000 and 17500 cm^{-1} for the zeolite component. On the right we see the evolution of the bands indicated in the left graph. The band at 39000 cm^{-1}, which is contributed to the formation of pyridinium, starts arising immediately after pyridine was introduced into the system. The absorbance rises steeply and after 9 minutes it seems as most of the Brønsted acid sites have formed pyridinium and the absorbance has reached an almost linear region. However, after about 24 minutes the absorbance shows another rise. This pattern is characteristic to material containing micro- and mesopores. Between 0 and 7 minutes, pyridinium has formed and filled the micropores of the zeolite. At around 9 minutes the pyridinium species have formed a monolayer on the surface of the solid acid. Between 9 and 24 minutes the pyridinium species form multilayers. Capillary condensation causes pore filling and results in the sudden rise in the adsorption curve at 25 minutes. At the end of this rise, all micro- and mesopores are filled.[30 61 62]
The band at 37700 cm^{-1} starts arising when the pyridine is introduced in the system and the band at 44000 cm^{-1} starts arising a minute into the measurement. The band at 37700 cm^{-1} is ascribed to the HOMO-LUMO excitation of pyridine adsorbed on a Lewis acid site. Although for the pyridine FT-IR measurements we were only able to do a measurement every 5 minutes, we did see the band of the Brønsted acid sites and Lewis acid sites arise as first (see Figure 51 in Appendix C.1).
The very high absorbance of the band at 39000 cm^{-1} is not only due the combination of physisorbed pyridine and Brønsted acid sites, but also because the molecular extinction coefficient of pyridinium is higher than that of physisorbed pyridine.[63] The bands in the region of 20000-30000 cm^{-1} start arising after around 4 minutes. They have not stabilized after 45 minutes of pyridine adsorption. As can be seen in Table 3.1.1, the surface area of

the zeolite is much higher than that of the other components. Apparently, 45 minutes of pyridine introduction is not enough to occupy the whole surface area of the zeolite with pyridine.

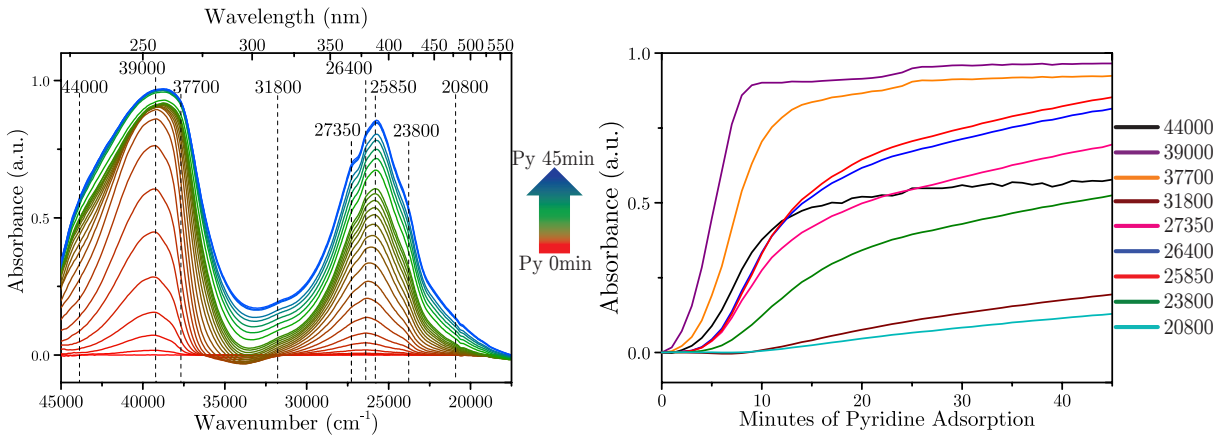

Figure 17: Pyridine UV-Vis spectra of 45 minutes of pyridine adsorption on zeolite (left) and the evolution of the bands marked in the UV-Vis spectrum (right).

Figure 18 shows the 45 minutes of pyridine adsorption on the alumina component. Again the bands at 37700 and 39000 cm^{-1} arise at first. Pyridine FT-IR showed us that the alumina contains one type of Lewis acid site and no Brønsted acid sites. The band at 39000 cm^{-1} is therefore assigned to physisorbed pyridine. Around 10 minutes after the start of introduction of pyridine the absorbance of these two bands is stabilized. There is no sudden rise around 25 minutes as the alumina does not contain any micropores (see Table 3.1.1). The bands at 27350, 26400 and 25850 cm^{-1} start arising after 4 minutes and stabilize after about 25 minutes of pyridine adsorption. The bands at 23800 and 21800 cm^{-1} continue to rise.

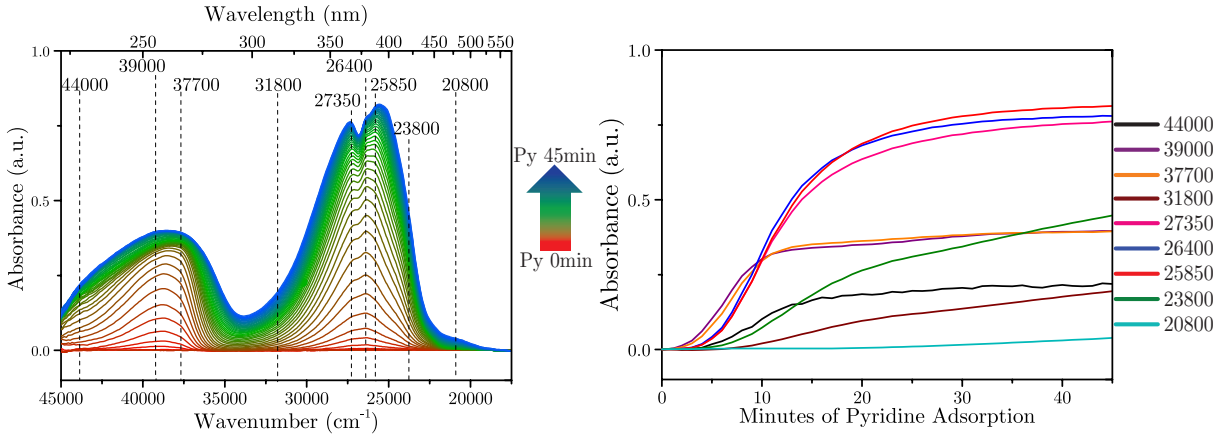

Figure 18: Pyridine UV-Vis spectra of 45 minutes of pyridine adsorption on alumina (left) and the evolution of the bands marked in the UV-Vis spectrum (right).

Figure 19 shows the 45 minutes of pyridine adsorption on the silica component. Looking at the evolution of the bands, we see that all bands except those at 20800 and 23800 cm^{-1} start arising two minutes after introducing pyridine. The fact that the bands around

39000 cm^{-1} do not start arising before those in the region between 20000 and 30000 cm^{-1}, shows that the bands around 39000 cm^{-1} can be assigned to physisorbed pyridine rather than to pyridine adsorbed on acidic sites. The bands in the region between 25000 and 32000 cm^{-1} show and increase for the first 10 to 15 minutes after which they decrease and stabilize. The decrease might be due to migration of the pyridine from isolated silanol groups (around 27350 cm^{-1}) to vicinal silanol groups (23800 cm^{-1}) and amorphous Si-(OH)-Al groups (20800 cm^{-1}). However, as there is a continuous flow of pyridine this would not be expected. Another explanation could be that at the maximum of the absorption, a multilayer of pyridine had formed on the surface hydroxyl groups and the nitrogen flow removes some of the pyridine not directly attached to the surface.

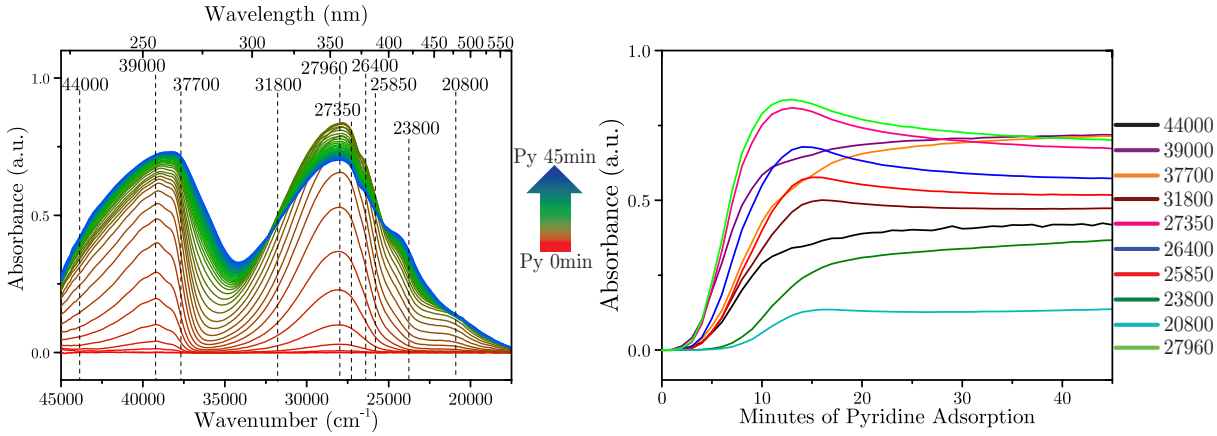

Figure 19: Pyridine UV-Vis spectra of 45 minutes of pyridine adsorption on silica (left) and the evolution of the bands marked in the UV-Vis spectrum (right).

Figure 20 shows the adsorption of pyridine for 45 minutes on the clay component. Notice the very low absorbance units, as also was the case for the pyridine FT-IR measurement for clay (see Figure 13). After 1 minute of pyridine adsorption the bands at 39000 and 37700 cm^{-1} start to arise. After a steep rise during the first 8 minutes the rise in absorbance stabilizes but it keeps increasing. The intensity of the band of pyridine adsorbed on amorphous Si-(OH)-Al groups (20800 cm^{-1}) is larger in comparison to the intensity of bands to different hydroxyl surface groups than for the other components. This is expected as the clay mainly consists of amorphous silica alumina species.

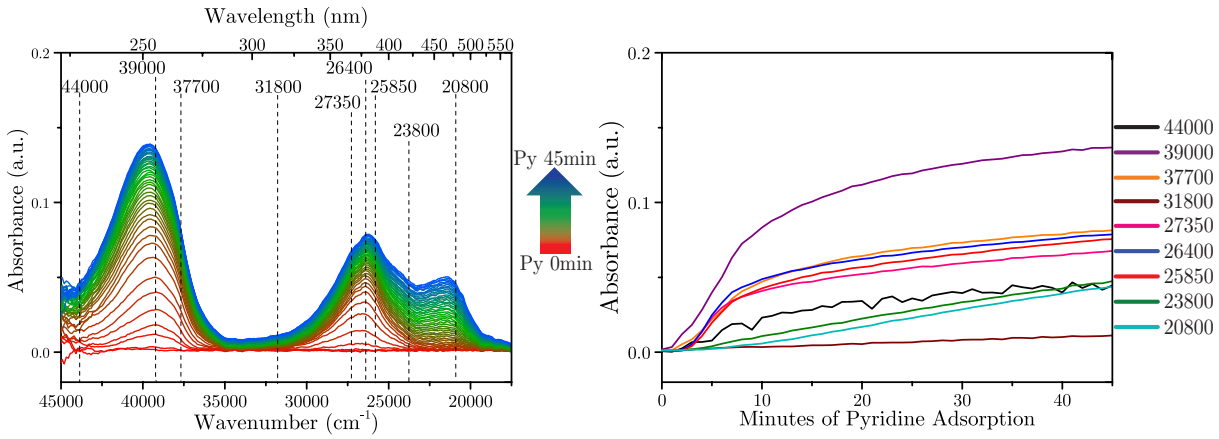

Figure 20: Pyridine UV-Vis spectra of 45 minutes of pyridine adsorption on clay (left) and the evolution of the bands marked in the UV-Vis spectrum (right).

Figure 21 shows the pyridine adsorption during 45 minutes on the full fresh FCC catalyst FSiAlZ. From the evolution of the indicated bands we see that the first band to arise is again the band at 39000 cm^{-1}. From the pyridine IR spectroscopy we know that the FSiAlZ catalyst contains Brønsted acid sites due to the zeolite component. After 7 minutes most the absorbance of the band at 39000 cm^{-1} stabilizes as the micropores are filled and a monolayer of pyridine has formed on the rest of the surface. At 24 minutes, capillary condensation fills the mesopores resulting in a sudden rise of absorbance for pyridinium species. For the evolution of the band at 37700 cm^{-1} we see this shape less clearly. This shows that the Lewis acid sites in the FCC catalyst do not only originate from the zeolite but also from the alumina, as alumina does not have micropores and shows a more continuous adsorption of pyridine.[61]

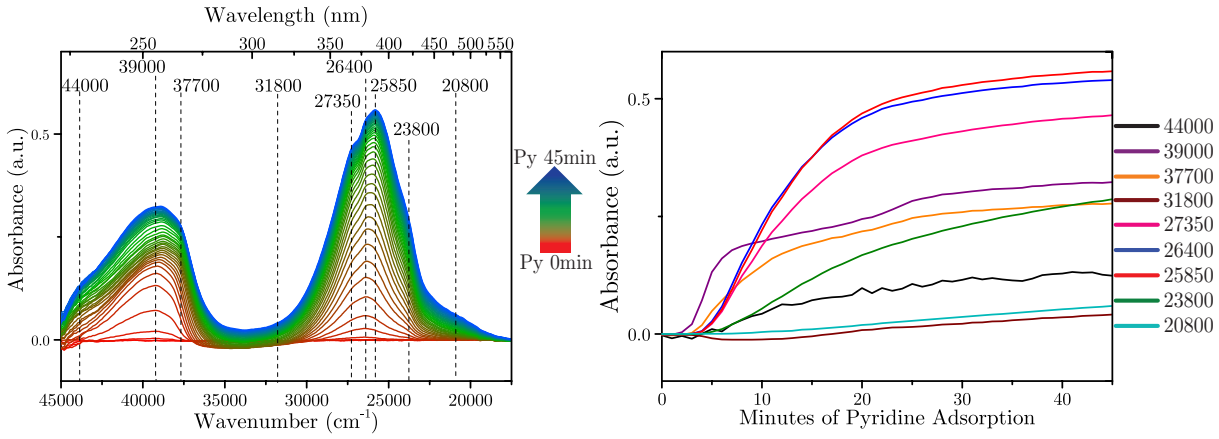

Figure 21: Pyridine UV-Vis spectra of 45 minutes of pyridine adsorption on the FSiAlZ catalyst (left) and the evolution of the bands marked in the UV-Vis spectrum (right).

To compare the rise of bands in the first 5 minutes more easily, in Figure 22 the first five minutes of pyridine adsorption for the zeolite, alumina and FSiAlZ and FSiAlNZ are shown. These spectra show that for the samples which contain Brønsted or Lewis acid sites, the bands around 39000 cm^{-1} arise very fast. The bands around 26000 cm^{-1} also

arise during these first minutes, but much slower. For the FCC catalyst without zeolite, FSiAlNZ, the bands around 26000 arise together with the bands around 39000 cm^{-1}.

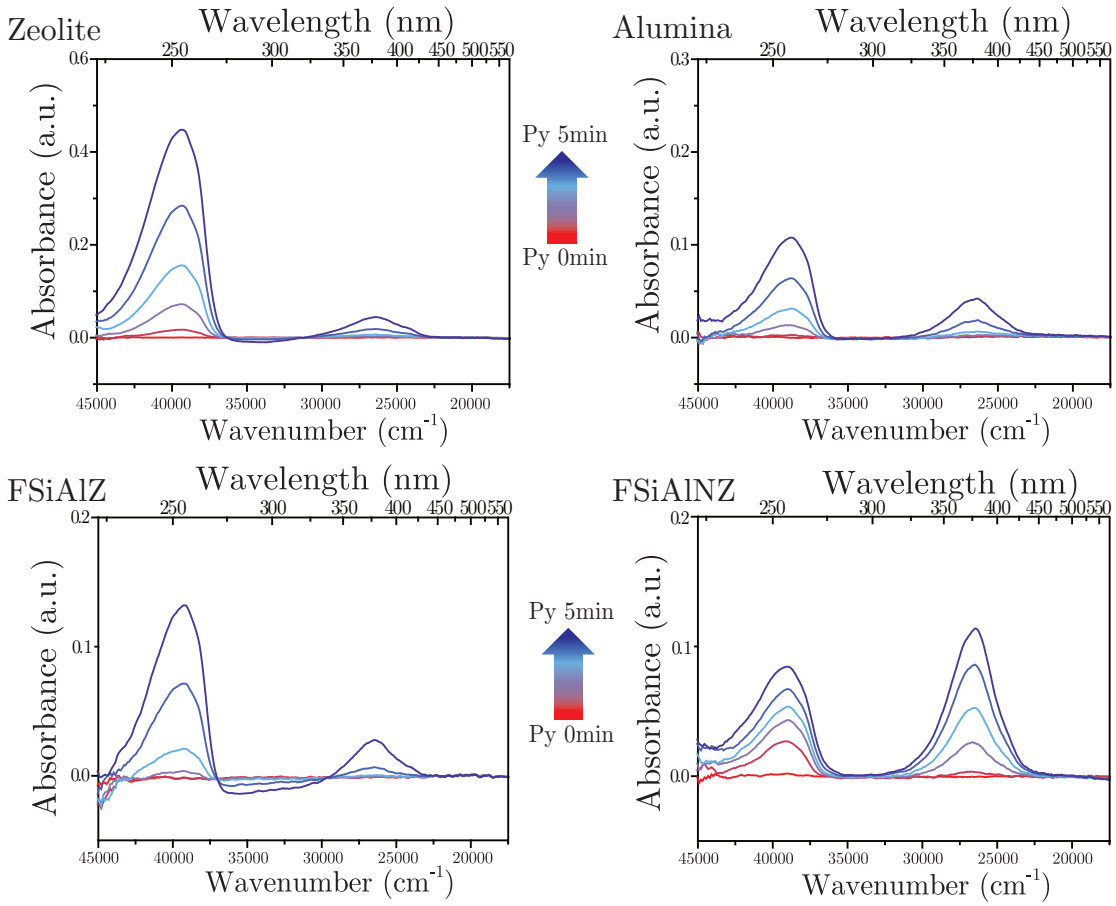

Figure 22: Pyridine UV-Vis spectra of the first five minutes of the pyridine adsorption of zeolite, alumina, FSiAlZ and FSiAlNZ.

Desorption

The desorption of pyridine followed by UV-Vis spectroscopy can give information on the nature and strength of the acidic sites samples. In Figure 23 the temperature programmed desorption for the zeolite component is shown. The increase in temperature leads to an increase in intensity of all the bands up to 75 ℃. Possibly, this increase is due to a higher mobility of the pyridine molecules at a elevated temperature, and all the pyridine in the system that had not yet adsorbed on the surface adsorbs on remaining sites. Another explanation is that the baseline is shifted, which we ascribe to the higher temperature. After 75 ℃ the bands start to disappear. Around 150 ℃ the bands in the region between 20000 and 30000 cm^{-1} have all disappeared. The boiling point of pyridine is 115 ℃ so the disappearance of these bands shows the desorption of pyridine from the weakly acidic surface hydroxyl sites. The bands at 37700, 39000 and 44000 cm^{-1} show a very small decrease. Very little pyridine desorbs during the TPD from the strong acidic sites. A new band rises in the UV-Vis spectrum at 31800 cm^{-1}. The nature of this band will be discussed in section 3.5.

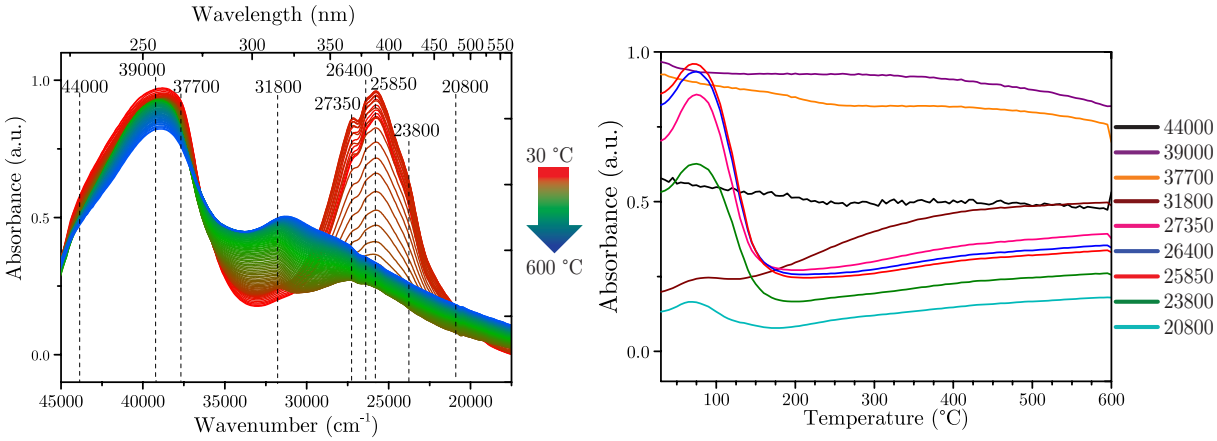

Figure 23: Pyridine UV-Vis spectra of TPD after pyridine adsorption for zeolite from 30 °C to 600 °C (left) and the evolution of the bands marked in the UV-Vis spectrum (right).

In Figure 24, the desorption of pyridine from the alumina component is shown. As for the zeolite, the absorbance of all bands show an increase in intensity up to 75 °C. For the bands between 23000 and 28000 cm^{-1}, the intensity then shows a drop until 100 °C after which the intensity increases again slightly. The boiling point of pyridine is 115 °C, and pyridine from inside the sample leaves the sample. More pyridine species might be at the upper surface of the sample around the boiling point of pyridine. As the UV-Vis spectra are recorded in reflectance mode, this could be an explanation for the increase in absorbance in the spectra. After 150 °C the intensities decrease until all pyridine has desorbed around 275 °C. Again a new band arises during the TPD around 31800 cm^{-1}. However, the bands starts arising at a much lower temperature than for the zeolite and starts decreasing again around the boiling point of pyridine (115 °C). At 600 °C a band around 34000 cm^{-1} is observed. The bands between 37000 and 44000 cm^{-1} show a gradual decrease in intensity. At 600 °C all pyridine has desorbed from the Lewis acid sites of alumina.

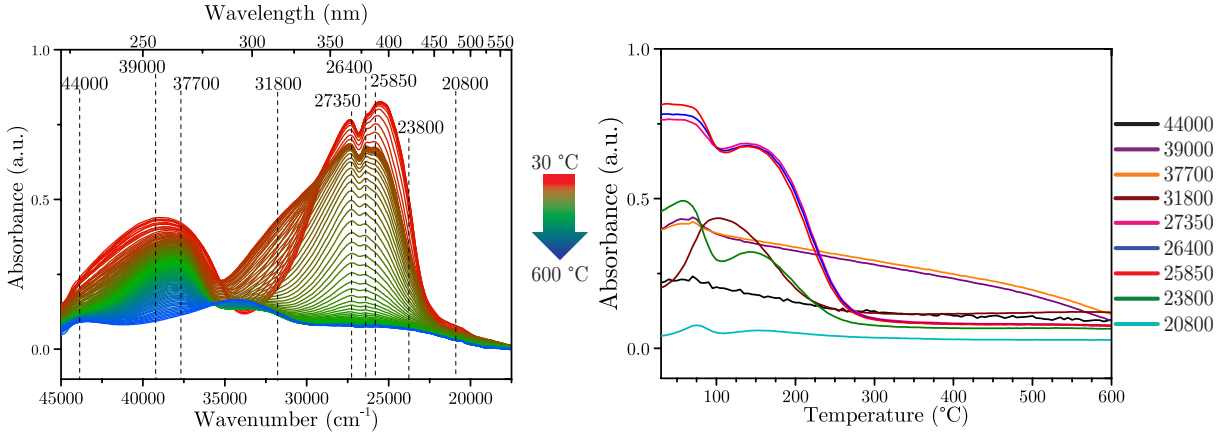

Figure 24: Pyridine UV-Vis spectra of TPD after pyridine adsorption for alumina from 30 °C to 600 °C (left) and the evolution of the bands marked in the UV-Vis spectrum (right).

In Figure 25 the temperature programmed desorption of pyridine on the silica component is shown. Around 250 °C, pyridine has desorbed from all sites. In the pyridine FT-IR

spectroscopy experiment, all pyridine had desorbed at 200 °C. Because the IR setup is under vacuum, a lower temperature is necessary to desorb all pyridine which explains the difference in temperature.

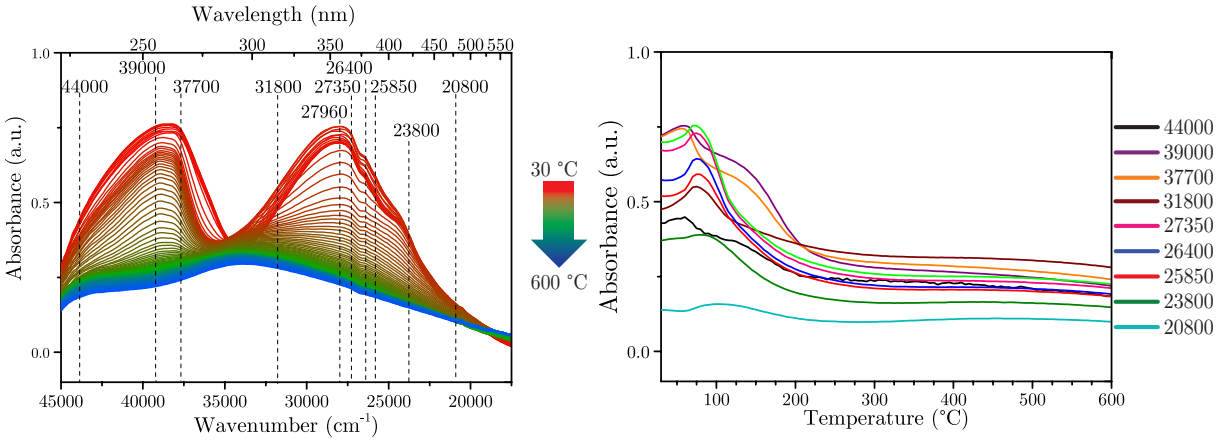

Figure 25: Pyridine UV-Vis spectra of TPD after pyridine adsorption for silica from 30 °C to 600 °C (left) and the evolution of the bands marked in the UV-Vis spectrum (right).

For the clay component the TPD is shown in Figure 26. Around 175 °C pyridine has desorbed from all sites. At higher temperatures a new band seems to arise around 27350 cm^{-1}. However, due to the very low intensity it is uncertain whether this is a new band or an baseline shift caused by the increasing temperature.

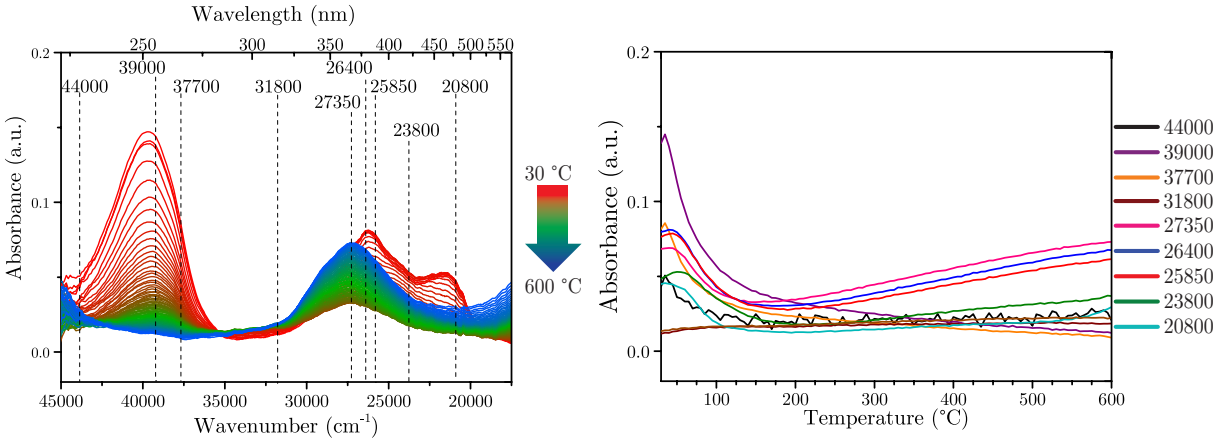

Figure 26: Pyridine UV-Vis spectra of TPD after pyridine adsorption for clay from 30 °C to 600 °C (left) and the evolution of the bands marked in the UV-Vis spectrum (right).

Figure 27 shows the TPD of the FSiAlZ catalyst. The intensity of the bands between 20000 and 30000 cm^{-1} increase up to 75 °C after which they quickly decrease. All pyridine has desorbed off these weakly acidic sites around 150 °C. Pyridine desorbs slower from the Lewis and Brønsted acid sites as can be seen by the gradual decrease of the bands between 37000 and 44000 cm^{-1}. At 600 °C a band around 27350 cm^{-1} is visible.

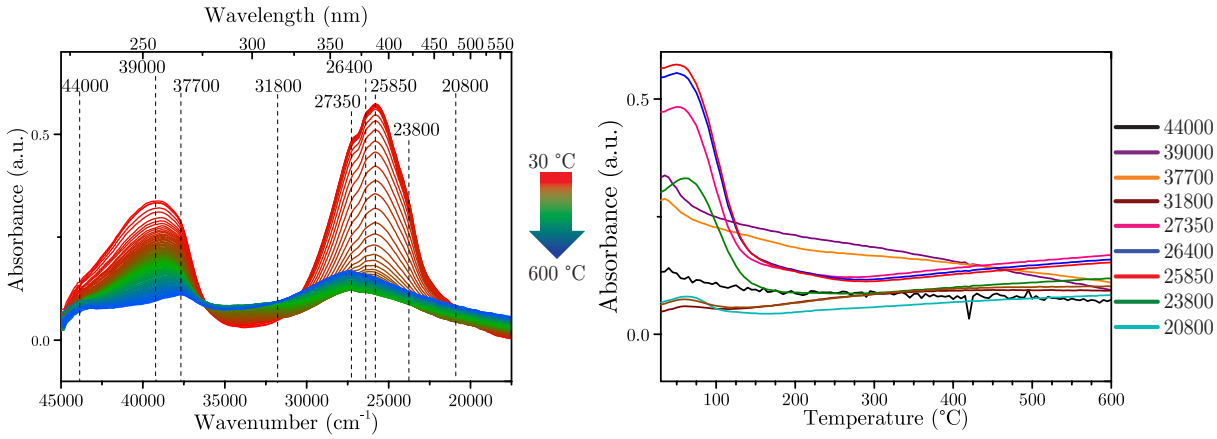

Figure 27: Pyridine UV-Vis spectra of TPD after pyridine adsorption for catalyst FSiAlZ from 30 ℃ to 600 ℃ (left) and the evolution of the bands marked in the UV-Vis spectrum (right).

Figure 28 shows the UV-Vis spectra after 45 minutes of pyridine adsorption and after 200 ℃ of TPD for the FCC catalyst with and without zeolite. It is clear that for the catalyst with zeolite the band around 39000 cm^{-1} is still present at 200 ℃ because pyridine is still adsorbed on Lewis and Brønsted acid sites. For the catalyst without zeolite the physisorbed pyridine, which causes a band at the same location, has desorbed at 200 ℃.

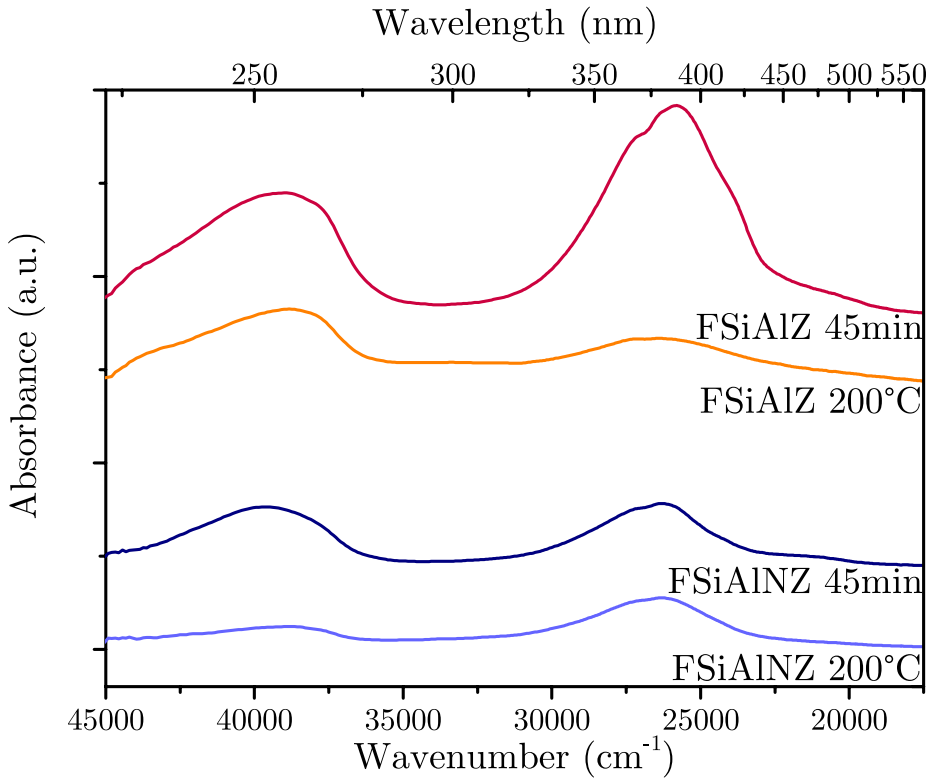

Figure 28: Pyridine UV-Vis spectra of the FSiAlZ and FSiAlNZ, after 45 minute of pyridine adsorption and after 200 ℃ of TPD. Plotted with y-offset for clarity.

3.3 Binder effect

As mentioned before, previous research done on FCC catalyst mainly focused on the role of the zeolite in the catalyst's activity.[10] In this study we were able to investigate the effect of the binder on the acidity and activity of the FCC catalyst by examining FCC catalysts with a binder of only silica, only alumina or a combination of alumina and silica. For all catalysts also samples without zeolite were provided. Further information on the properties of the samples can be found in section 3.1. In this section the FCC catalyst with only alumina as binder will be referred to as FAlZ and the FCC catalyst with only silica as binder will be referred to as FSiZ. For the catalysts without zeolite, Z is substituted for NZ.

Pyridine FT-Infrared Spectroscopy

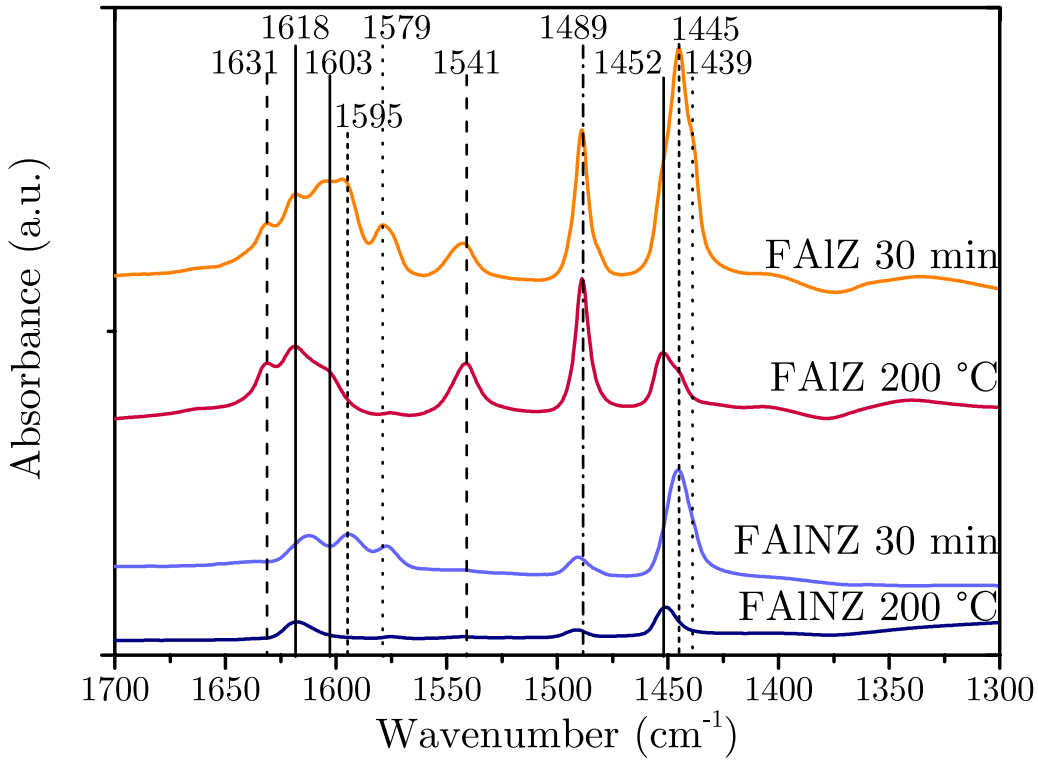

Figure 29: Pyridine FT-IR spectra of the FAlZ and FAlNZ catalysts after 30 minutes op pyridine adsorption and after 200 ℃ of TPD. All spectra are corrected for pellet weight. Plotted with y-offset for clarity.

Figure 29 shows the IR spectra of the FAlZ and FAlNZ after 30 minutes of pyridine adsorption and after 200 ℃ of TPD to study the strong acid sites. For FAlZ we see the peaks for physisorbed pyridine at 1439 and 1579 cm^{-1}, and the peaks for pyridine adsorbed on weak acidic hydroxyl groups are observed at 1445 and 1595 cm^{-1}. When looking at the spectrum taken after 200 ℃ of TPD, we see that physisorbed pyridine and pyridine on hydroxyl groups has desorbed from the surface as the peaks have disappeared. For FAlZ we see the presence of two types of Lewis acid sites. The peaks at 1445 and 1603 cm^{-1} show pyridine adsorbed on weaker Lewis sites and the peaks at 1452 and 1618 cm^{-1} show stronger Lewis acid sites. The peaks at 1541 and 1631 cm^{-1} show the presence of pyridine

adsorbed on Brønsted acid sites.
The spectrum of FAlNZ after 30 minutes of pyridine adsorption shows that less pyridine has adsorbed on the surface in comparison to the FAlZ spectrum after 30 minutes of pyridine adsorption. The peaks for physisorbed pyridine at 1439 and 1579 cm^{-1} are less intense than for the catalyst with zeolite. Also less pyridine has adsorbed on surface hydroxyl groups, as can be seen by the decrease in intensity of the 1445 and 1595 cm^{-1} peaks. When looking at the surface areas of these catalysts in Table 3.1.2, we see that the FAlZ and FAlNZ catalysts have a surface area of 230 m^2/g and 54 m^2/g, respectively. This explains the decrease in weakly adsorbed pyridine, as there is much less surface area on which pyridine can adsorb.
The spectrum of FAlNZ at 200 ℃ of TPD shows that only one type of Lewis acid site is present. This Lewis acid site is slightly weaker than the strong acid site in the FAlZ, with peaks at 1450 and 1616 cm^{-1}. No Brønsted acid sites are present in the FAlNZ catalyst. This also explains the shift of the combination peak at 1489 cm^{-1} to a higher wavenumber, as only the Lewis acid sites contribute to this peak. The frequency of the ν19a vibration of coordinates Lewis is 1493 cm^{-1} (see Table 1.2.1).

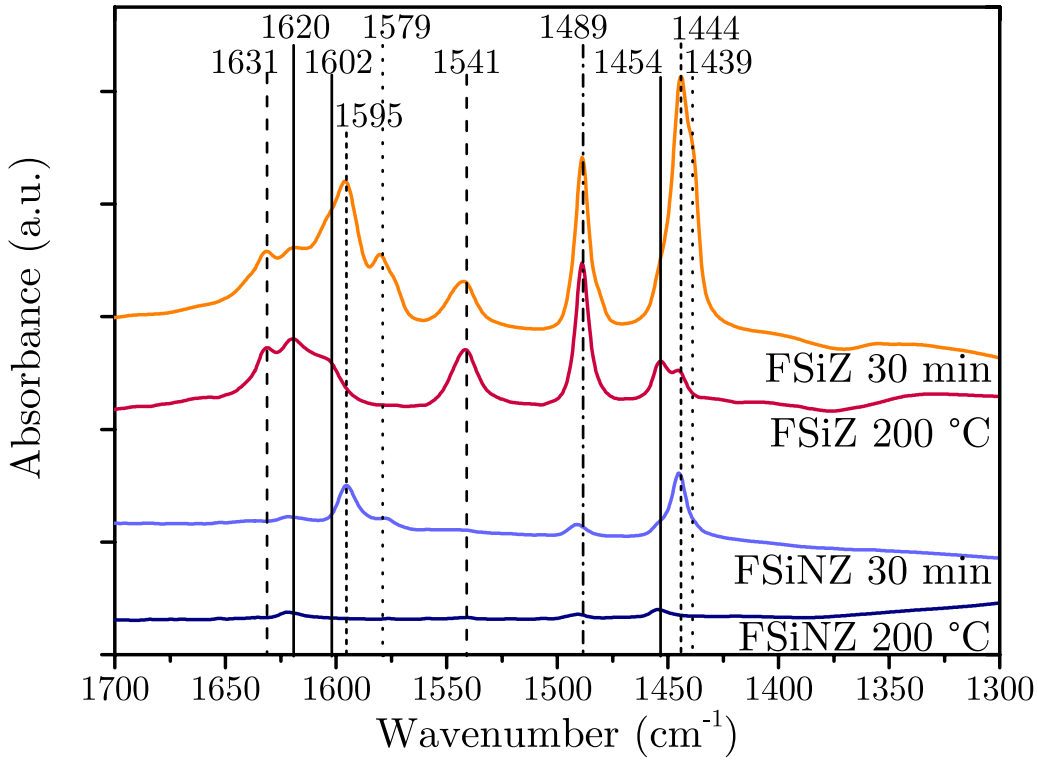

Figure 30: Pyridine FT-IR spectra of the FSiZ and FSiNZ catalysts after 30 minutes op pyridine adsorption and after 200 ℃ of TPD. All spectra are corrected for pellet weight. Plotted with y-offset for clarity.

Figure 30 shows the FT-IR spectra of the FCC catalyst with only silica as binder with (FSiZ) and without (FSiNZ) zeolite. The spectrum of the FSiZ after 30 minutes of pyridine shows adsorption of pyridine in a physisorbed manner by the peaks at 1439 and 1579 cm^{-1}. The peaks at 1445 and 1595 cm^{-1} show pyridine adsorbed on OH surface groups. All these peaks have disappeared after 200 ℃ of TPD. The spectrum after 200 ℃ shows the presence of two types of Lewis acid sites in the FSiZ catalyst. The peaks at

1444 and 1602 cm^{-1} show pyridine adsorbed on weak Lewis acid sites and the peaks 1454 and 1620 cm^{-1} show the presence of strong Lewis acid sites. Also Brønsted acid sites are present in the FSiZ, indicated by the peaks at 1541 and 1631 cm^{-1}.

For the FCC catalyst with silica as binder and without zeolite, much less pyridine has adsorbed on the surface after 30 minutes of pyridine adsorption. The peaks that indicate the presence of physisorbed pyridine are very weak (1439 and 1579 cm^{-1}). The peaks of the pyridine adsorbed on OH surface groups are clearly visible at 1444 and 1595 cm^{-1}, but also for these peaks the intensity is very low compared to the other catalysts. After 200 ℃ of TPD, we see that the peaks indicating stronger acidic sites have very low intensities. Only one type of Lewis acid site is observed with peaks at 1455 and 1621 cm^{-1}. These frequencies indicate that the Lewis acid site has a strong nature. For FSiNZ, only the clay component contributes to the acidity of the catalyst. In section 3.2 we already saw that the clay has very little acid sites in comparison to the other components.

The large differences in total adsorption of pyridine between the catalyst with an without zeolite is due to the very high surface area of the zeolite component. The surface area of FSiZ is 231 m^2/g opposed to only 54 m^2/g for FSiNZ. For the other catalyst, similar trends were observed (see Table 3.1.2).

For both the FSiZ (1454 cm^{-1}) and FSiNZ (1455 cm^{-1}), the peaks of the strong Lewis acid site are at a higher frequency than for the catalyst with alumina (1452 cm^{-1}) or alumina and silica (1452 cm^{-1}) as binder.

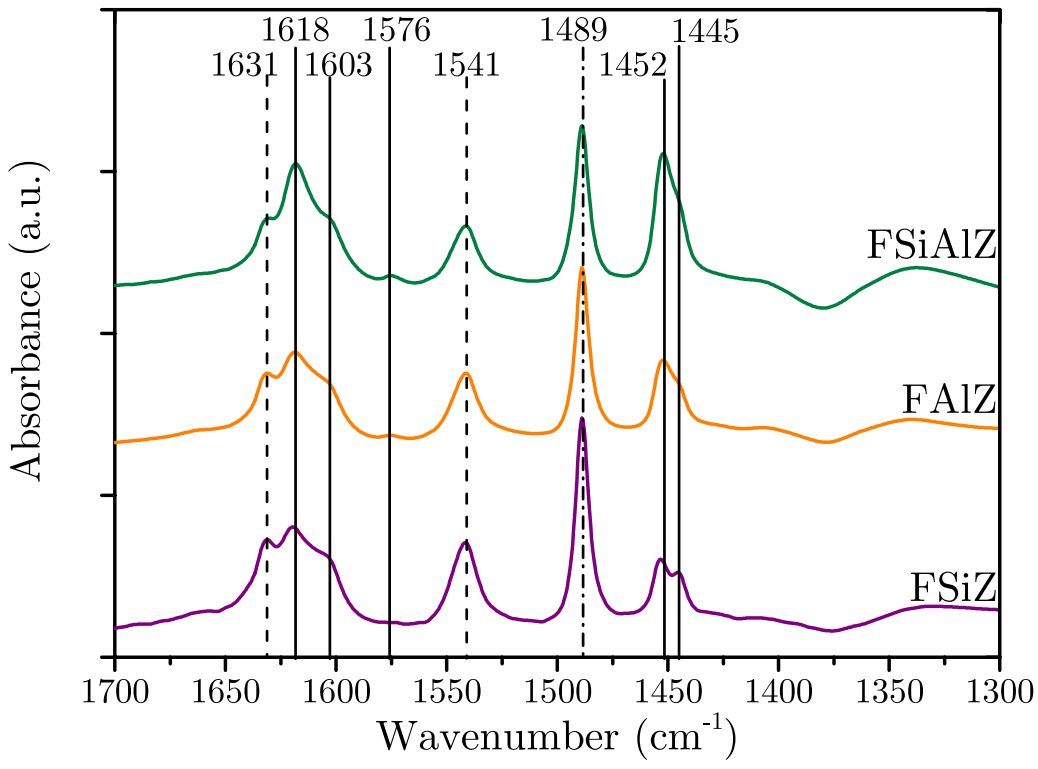

Figure 31: Pyridine FT-IR spectra of the FSiAlZ, FAlZ and FSiZ catalysts after 200 ℃ of TPD. All spectra are corrected for pellet weight. Plotted with y-offset for clarity.

Figure 31 shows the Py-IR spectra of the FSiAlZ, FAlZ and FSiZ catalyst in one graph. All spectra are taken after evacuation and 200 ℃ TPD and have been corrected for the pellet weight. For the best comparison, the spectrum taken before introduction of pyridine was subtracted. The spectra show that FSiZ has less Lewis acidic sites, as

is visible from the weaker intensity of the 1455 cm^{-1} peak and also, though less clear, when looking at the band at 1618 cm^{-1}. This shows that alumina in the binder definitely contributes to the Lewis acidity in the full catalyst.

In this graph the difference in the strength of the strong Lewis acid site is clear by the blue-shift of the Lewis peak from 1452 cm^{-1} (FAlZ) to 1455 cm^{-1} (FSiZ). Lewis acid sites become stronger when the amount of Al in their near crystal structure decreases, as is the case when silica is also part of the binder.[64]

FT-IR Spectroscopy

In Figure 32 the OH region of the different FCC catalysts with and without zeolite are shown.

The band around 3750 cm^{-1} indicates isolated silanol groups.[52] This peak is mainly observed for the catalyst with only silica as binder. The tail of this peak, to lower frequencies, is associated with vicinal silanol groups. This tail is seen for all catalysts.
The weak band around 3720 cm^{-1} in the FAlZ and FAlNZ catalyst indicates aluminol groups. The band around 3670 cm^{-1} indicates aluminol groups in extra framework species.[39] This band is observed for the catalysts containing zeolite.
The region of 3650-3500 cm^{-1} indicates isolated Brønsted acid sites. The band at 3631 cm^{-1} indicates Brønsted acid sites in a super cage structure in the zeolite and 3525 cm^{-1} indicates Brønsted acid sites in the sodalite cage.[39] Only the catalysts containing zeolite show these bands, as expected.

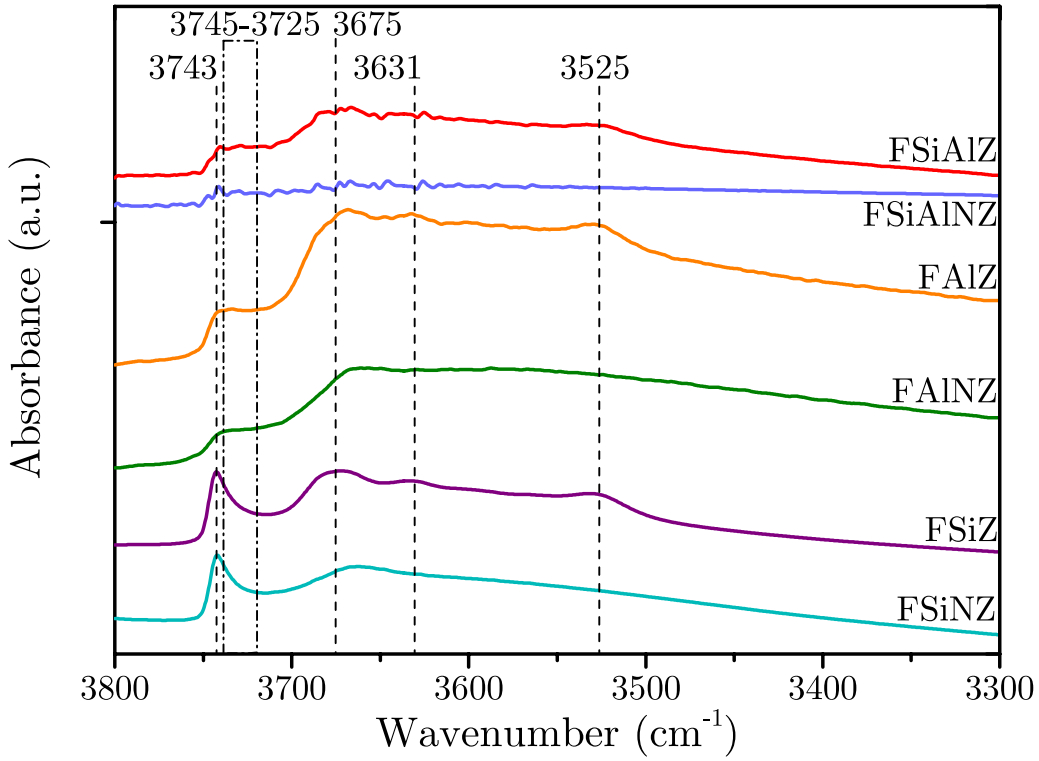

Figure 32: FT-IR spectrum of OH region of all FCC catalysts with and without zeolite after drying procedure. All spectra are corrected for pellet weight. Plotted with y-offset for clarity.

Pyridine UV-Vis Spectroscopy

The shape of the spectra of the pyridine UV-Vis measurements on the FAlZ and FSiZ (see Figures 33 and 34) is very similar to that of the FSiAlZ catalyst (Figure 21). When looking at the evolution of bands, we see that at first the bands around 39000 cm^{-1} arise. For both samples the bands gradually increase up to 15 minutes of pyridine adsorption before a sudden increase in absorbance takes place. This was also observed for the zeolite and FSiAlZ catalyst, due to the presence of both micro and mesopores (see section 3.2). The region between 20000 and 30000 cm^{-1} shows the presence of isolated silanol groups (27350 cm^{-1}), isolated aluminol groups (26400 cm^{-1}), other aluminol species (25850 cm^{-1}), vicinal silanol groups (23800 cm^{-1}) and amorphous Si-(OH)-Al groups (20800 cm^{-1}).[48]

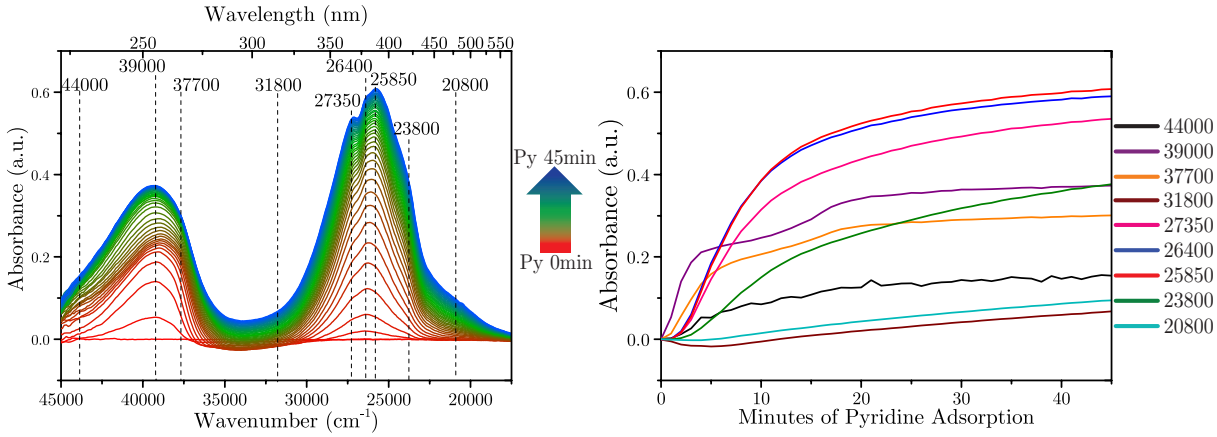

Figure 33: Pyridine UV-Vis spectra of 45 minutes of pyridine adsorption on FAlZ catalyst (left) and the evolution of the bands marked in the UV-Vis spectrum (right).

The difference between the catalyst with only alumina as binder (Figure 33) and silica as binder (Figure 34), is mainly visible in the intensity of the bands between 20000 and 30000 cm^{-1}. Although the current pyridine UV-Vis spectroscopy does not allow to set a standard distance between the probe and the sample, the distance was chosen at which the scope in ADC counts of the UV-Vis probe was comparable for all measurements. More pyridine adsorbs on weakly acidic surface sites on the catalyst with alumina as binder.

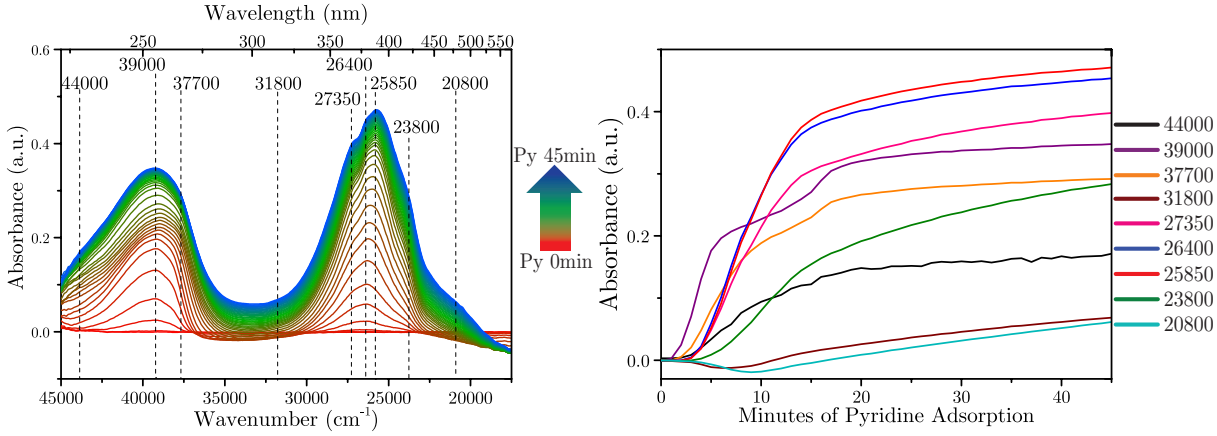

Figure 34: Pyridine UV-Vis spectra of 45 minutes of pyridine adsorption on FSiZ catalyst (left) and the evolution of the bands marked in the UV-Vis spectrum (right).

The TPD spectra of FAlZ (Appendix D Figure 53) and FSiZ (Appendix D Figure 54) show a small increase in absorbance due to the increase in temperature up to 75 ℃. After this increase, first the bands in the region between 20000 and 30000 cm^{-1} disappear. Subsequently pyridine desorbs from the Lewis and Brønsted acid sites and the bands around 39000 cm^{-1} disappear. At 600 ℃ a band at 27350 is visible for FAlZ and at 27500 cm^{-1} for FSiZ.

3.4 Steam treatment effect on FCC catalyst

The conditions within an FCC reactor are very extreme. The temperature is very high and the gases flow in a very high speed to the top of the riser. The products are removed from the catalyst in the stripper by steam at high temperatures. The catalyst is then exposed to even higher temperature when coke is burned off to regenerate the catalyst. Also during the regeneration a lot of steam is present. This steam can lead to dealumination of the catalyst.[56] The catalyst samples were subjected to steam treatment to study the effect of the steam on the acidity of the samples. To study the effect of the time of the steam treatment on the samples, samples were taken after 5, 10 and 20 hours. These samples can give an indication of the deactivation rate of the FCC catalysts. Although the catalyst is only in the riser for a couple of seconds, it is used for many cycles. The fresh catalysts without zeolite were also steam treated. Only one sample was taken, after 20 hours. In this part we will look at the effect of the steam treatment on the acidity of the catalyst.

Pyridine FT-Infrared Spectroscopy

Figure 35 shows the pyridine IR spectra of the FSiAlZ and the steam treated samples after 5, 10 and 20 hours. The spectra were taken after 30 minutes of pyridine adsorption.

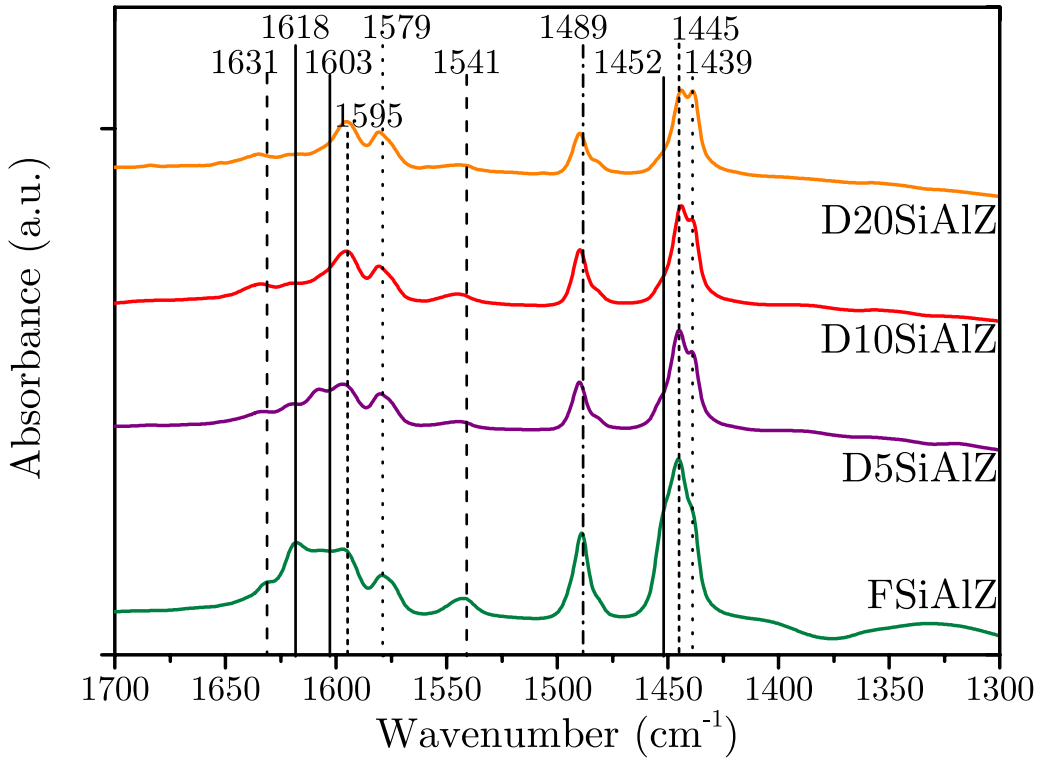

Figure 35: Pyridine FT-IR spectra of the FSiAlZ fresh catalyst and after 5, 10 and 20 hours of steam treatment. Spectra taken after 30 minutes op pyridine adsorption. All spectra are corrected for pellet weight. Plotted with y-offset for clarity.

The peak at 1445 cm^{-1}, attributed to pyridine adsorbed on surface hydroxyl groups and weak Lewis acid sites, decreases during the steam treatment. However the peak at 1595 cm^{-1} which is also contributed to pyridine adsorbed on surface hydroxyl groups,

seems to remain consistent. When looking at the Lewis acid peaks at 1452, 1603 and 1618 cm^{-1}, we see that the amount of pyridine adsorbed on these sites decreases during steam treatment. The decrease in intensity of the peak at 1445 cm^{-1} is therefore attributed to the decrease in Lewis acid sites and not the amount of surface hydroxyl groups. Also the amount of pyridine adsorbed in a physisorbed manner does not decrease a lot during the steam treatment process, as can be seen from the stable intensities of the peaks at 1439 and 1579 cm^{-1}. The peak at 1541 cm^{-1} which is attributed to the 19b vibration of pyridinium (see Table 1.2.1) also decreases in intensity during steam treatment. During steam treatment dealumination takes place, resulting in destruction of the Lewis acid sites in the zeolite.[12]

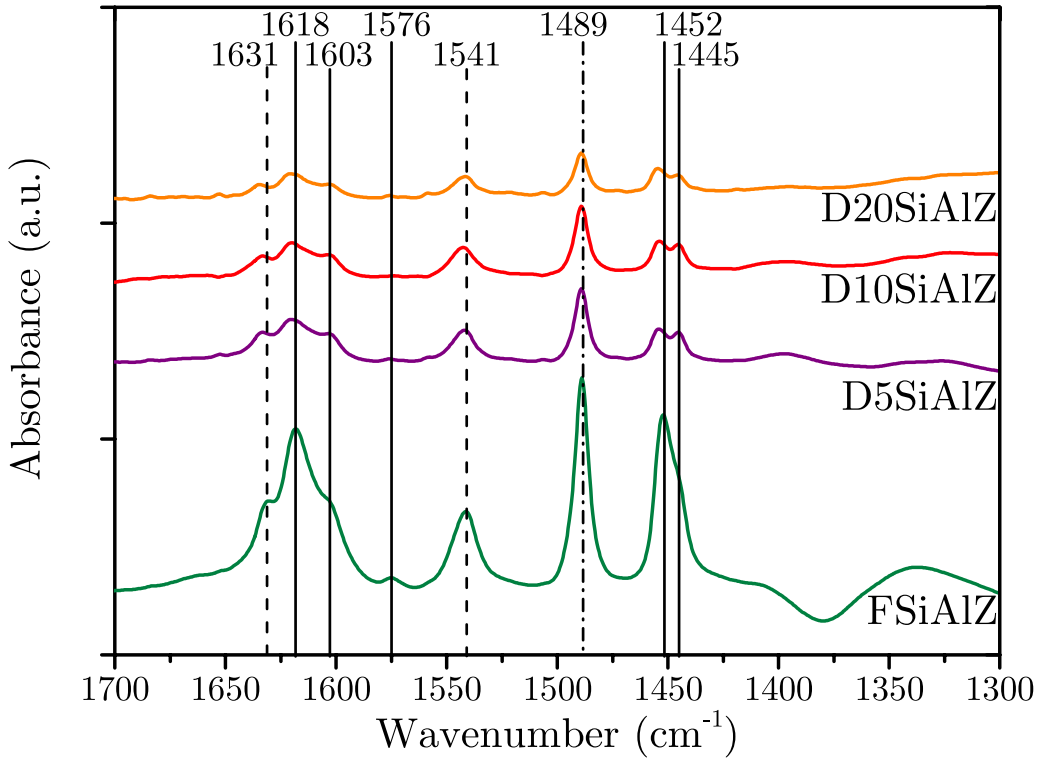

Figure 36: Pyridine FT-IR spectra of the FSiAlZ fresh catalyst and after 5, 10 and 20 hours of steam treatment. Spectra taken after 200 ℃ of TPD. All spectra are corrected for pellet weight. Plotted with y-offset for clarity.

Figure 36 shows the same samples after evacuation and 200 ℃ of temperature programmed desorption. The peak at 1438 cm^{-1} has completely disappeared for all the samples at 200 ℃. The maximum of the Lewis peak at 1618 cm^{-1} for FSiAlZ, has blue-shifted to 1620 cm^{-1} after 5 hours. This shift shows an increase in strength in the Lewis acidity. Also the Lewis acid peak at 1455 cm^{-1} shows a blue shift, thus increase in acidity. During the steam treatment dealumination takes place in the zeolite which results in the migration of Al^{3+} from framework alumina to extraframework alumina. This decreases the amount of Brønsted acid sites but creates strong Lewis acid sites in the extra-framework alumina.[12,13] The strength of the weaker Lewis acids with peaks at 1445 and 1603 cm^{-1} does not change during steam treatment. The amount of Brønsted acid sites also decrease, as is clearly visible from the decrease in intensity of the peaks at 1541 and 1631 cm^{-1}. The decrease in Brønsted acid sites due to steam was already reported before, for example in research by Buurmans *et al.*[10] The largest changes have already taken place

after 5 hours of steam treatment. The decrease in acid sites continues between 5 and 10 hours of steam treatment, but stabilizes after this.

In Figure 37, the spectra after 30 minutes of pyridine adsorption on the FAlZ catalyst and the FAlZ catalyst after 5, 10 and 20 hours are shown. The most notable change during the steam treatment is again the decrease in intensity of the peak at 1445 cm^{-1}. The peak at 1595 cm^{-1} stays relatively stable, but the peak at 1603 cm^{-1} contributed to weak Lewis acid sites decreases. Therefore, the peak decrease of the peak at 1445 cm^{-1} is mainly due to the decrease of weak Lewis acid sites. The decrease in intensity for the peaks at 1452 and 1618 cm^{-1} shows that also the amount of stronger Lewis acid sites decreases. Furthermore, we see again that the intensity of the peaks indicating physisorbed pyridine are not affected a lot by the steam treatment. As for the FSiAlZ catalyst, the FAlZ catalyst also shows a decrease of Brønsted acid sites during steam treatment.

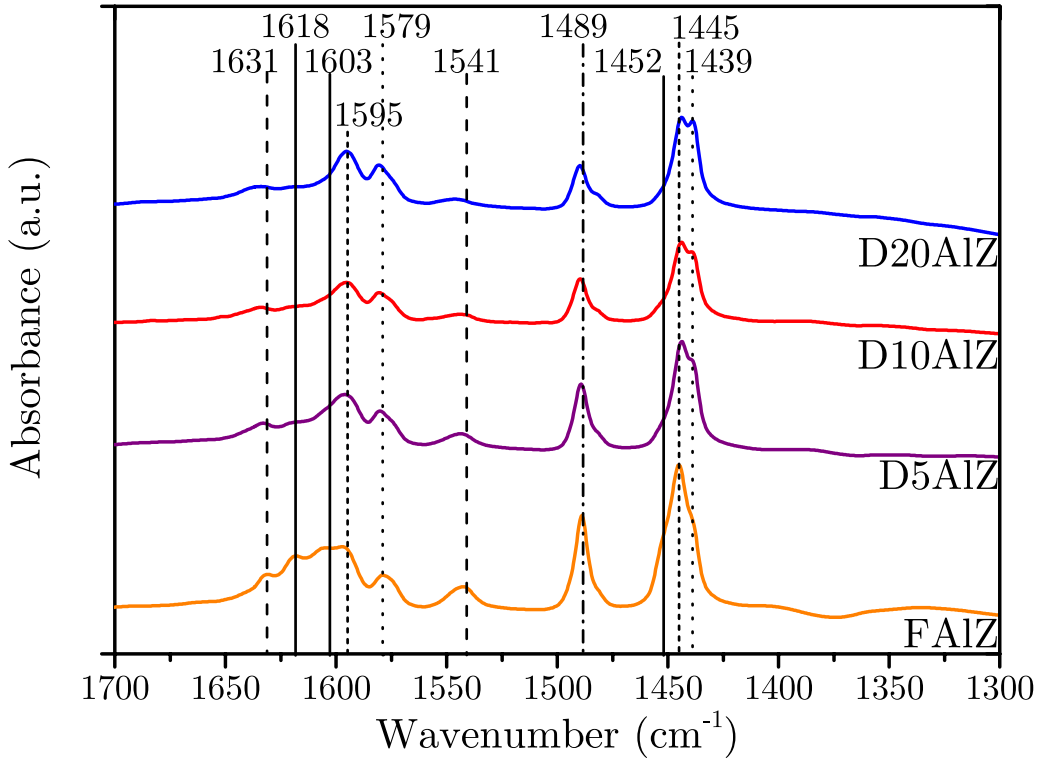

Figure 37: Pyridine FT-IR spectra of the FAlZ fresh catalyst and after 5, 10 and 20 hours of steam treatment. Spectra taken after 30 minutes op pyridine adsorption. All spectra are corrected for pellet weight. Plotted with y-offset for clarity.

In Figure 38 the spectra of FAlZ and the steam treated catalysts after evacuation and 200 ℃ of TPD are shown. The maxima of the peaks indicating strong Lewis acid sites show a blue shift from 1452 and 1618 cm^{-1} to 1454 and 1620 cm^{-1}. As discussed before, the amount of Lewis acid sites decrease. The largest changes have already taken place after 5 hours of steam treatment. The decrease in acid sites continues between 5 and 10 hours of steam treatment, but stabilizes after this. The strength of the weak Lewis acid sites (1445 and 1603 cm^{-1}) does not change. The amount of strong Lewis acid sites decrease more during steam treatment in relation to the amount of weak Lewis acid sites. This could be because part of these weaker LAS are from the alumina binder. The LAS in the alumina component are less strong than those in the zeolite. This would suggest that the framework of alumina is less destructed by the steam than the framework of the zeolite.

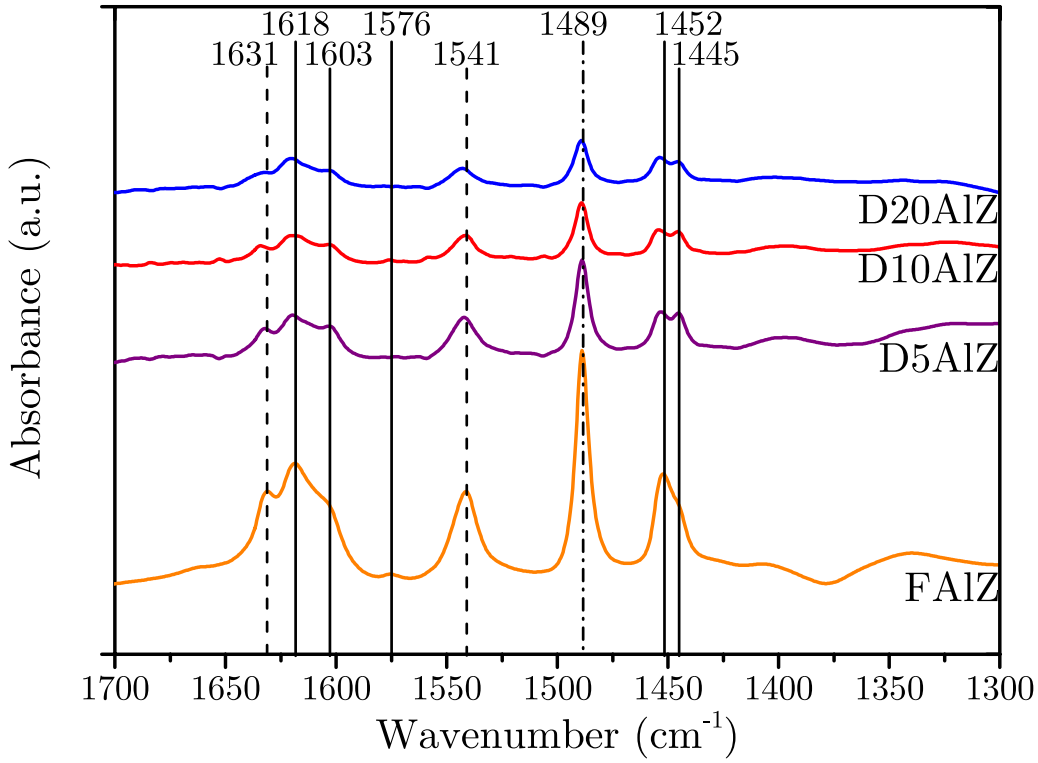

Figure 38: Pyridine FT-IR spectra of the FAlZ fresh catalyst and after 5, 10 and 20 hours of steam treatment. Spectra taken after 200 ℃ of TPD. All spectra are corrected for pellet weight. Plotted with y-offset for clarity.

Figure 39 shows the FT-IR spectra of the FSiZ catalyst fresh and after 5, 10 and 20 hours of steam treatment. The spectra were taken after 30 minutes of pyridine adsorption. The amount of strong and weak Lewis acid sites decrease during steam treatment. Due to the overlap in bands at the region between 1445 and 1455 cm^{-1} it is more reliable to look at the bands at 1603 and 1618 cm^{-1} for the weak and strong acid sites respectively. Although also for this region multiple band arise near each other and therefore influence the resulting bands, the peak maxima are farther apart than for the 1445 to 1455 cm^{-1} region. As for FSiAlZ and FAlZ, for FSiZ we see a decrease in Brønsted acid sites during steam treatment. The amount of physisorbed pyridine seems to decrease more during the steam treatment than for the other catalyst.

In Figure 40 the spectra of the FSiZ catalyst and the steam treated samples after evacuation and 200 degrees of steam treatment are shown. The strength of the strong Lewis acid sites increases during steam treatment. The peak at 1453 cm^{-1} moves to 1455 cm^{-1} during the steam treatment. Also the strength of the Brønsted acid site increase as can be seen by the blue shift of the peak at peak at 1541 to 1543 cm^{-1} and the blue shift of the peak at 1631 to 1633 cm^{-1}. The increase in the strength of the BAS is due to the formation of so-called superacidic Brønsted sites. The extra-framework alumina which is formed when the zeolite is dealuminated, contains LAS than can increase the strength of BAS in their vicinity.[65 17] The strength of the weaker Lewis acid sites are not influenced by the steam treatment. The largest changes have already taken place after 5 hours of steam treatment. The decrease in acid sites continues between 5 and 10 hours of steam treatment, but stabilizes after this.

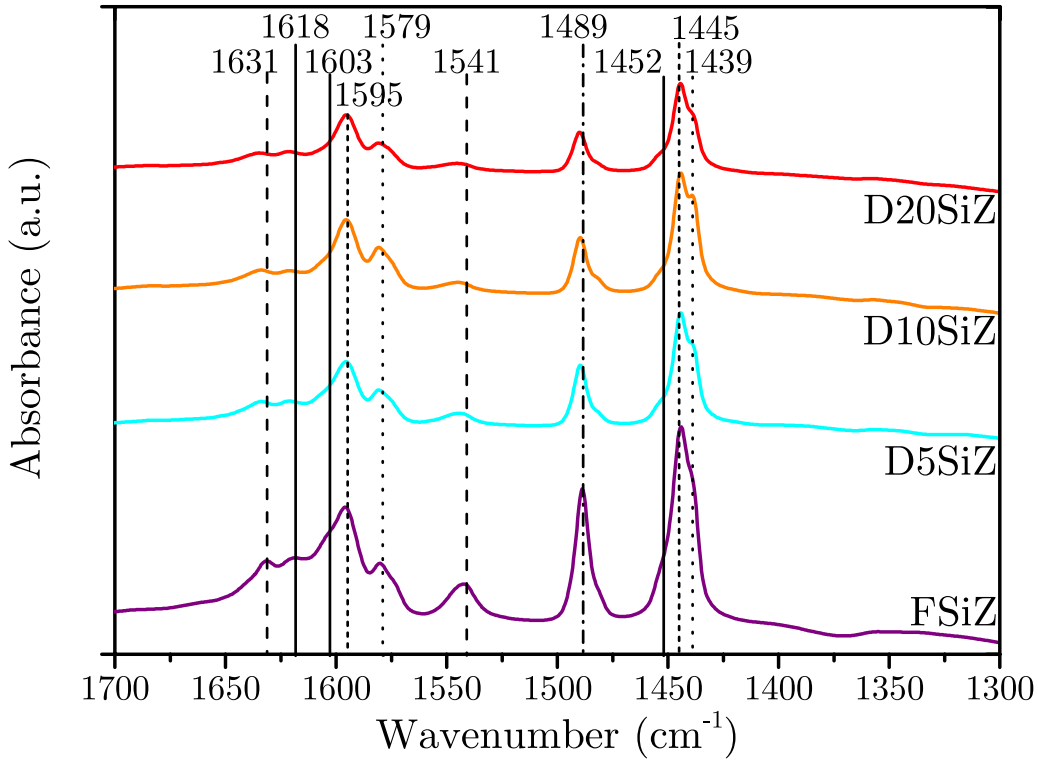

Figure 39: Pyridine FT-IR spectra of the FSiZ fresh catalyst and after 5, 10 and 20 hours of steam treatment. Spectra taken after 30 minutes op pyridine adsorption. All spectra are corrected for pellet weight. Plotted with y-offset for clarity.

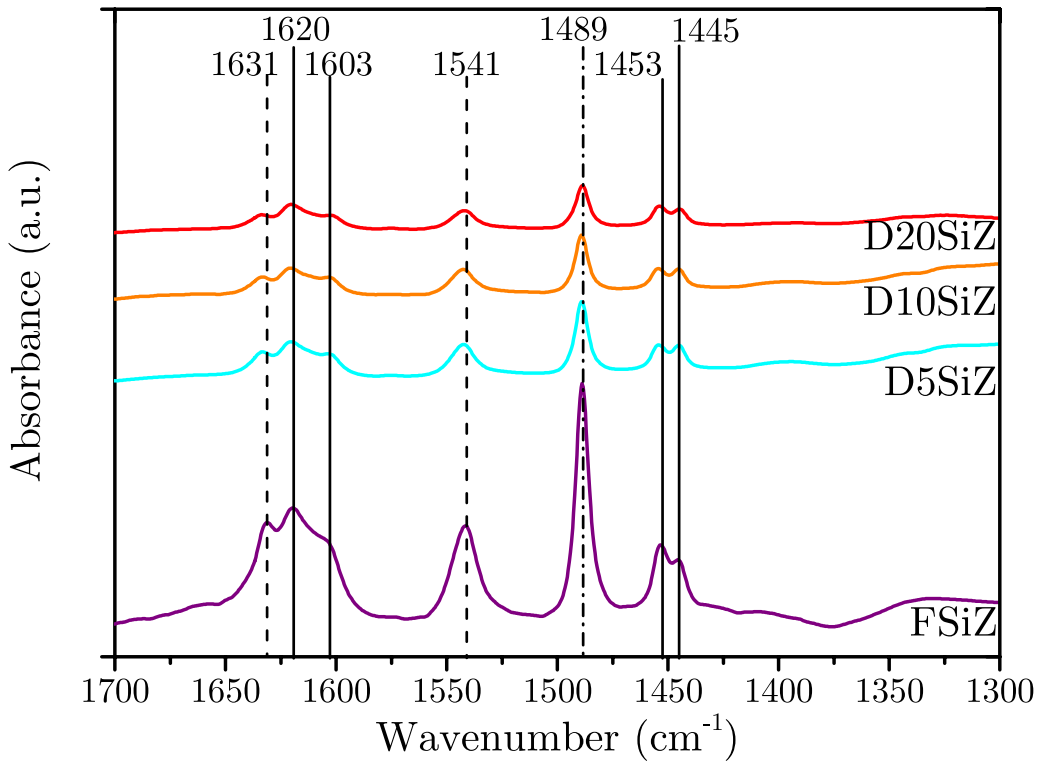

Figure 40: Pyridine FT-IR spectra of the FSiZ fresh catalyst and after 5, 10 and 20 hours of steam treatment. Spectra taken after 200 ℃ of TPD. All spectra are corrected for pellet weight. Plotted with y-offset for clarity.

In Figure 41 we see the spectra of the three different catalysts after 20 hours of steam treatment. These spectra were taken after 30 minutes of pyridine adsorption. By looking at the intensity of the band at 1580 cm^{-1}, we see that the catalyst with only silica as binder has adsorbed the least pyridine in a physisorbed way. In Figure 13 we also saw that silica adsorbs less pyridine in a physisorbed way than alumina, explaining the differences. However, the surface area of silica (162 m^2/g) is larger than that of alumina (123 m^2/g) (see Table 3.1.1). The (weakly) acidic surface sites of alumina seem to have a positive effect on the ability of the material to adsorb pyridine in a physisorbed manner.

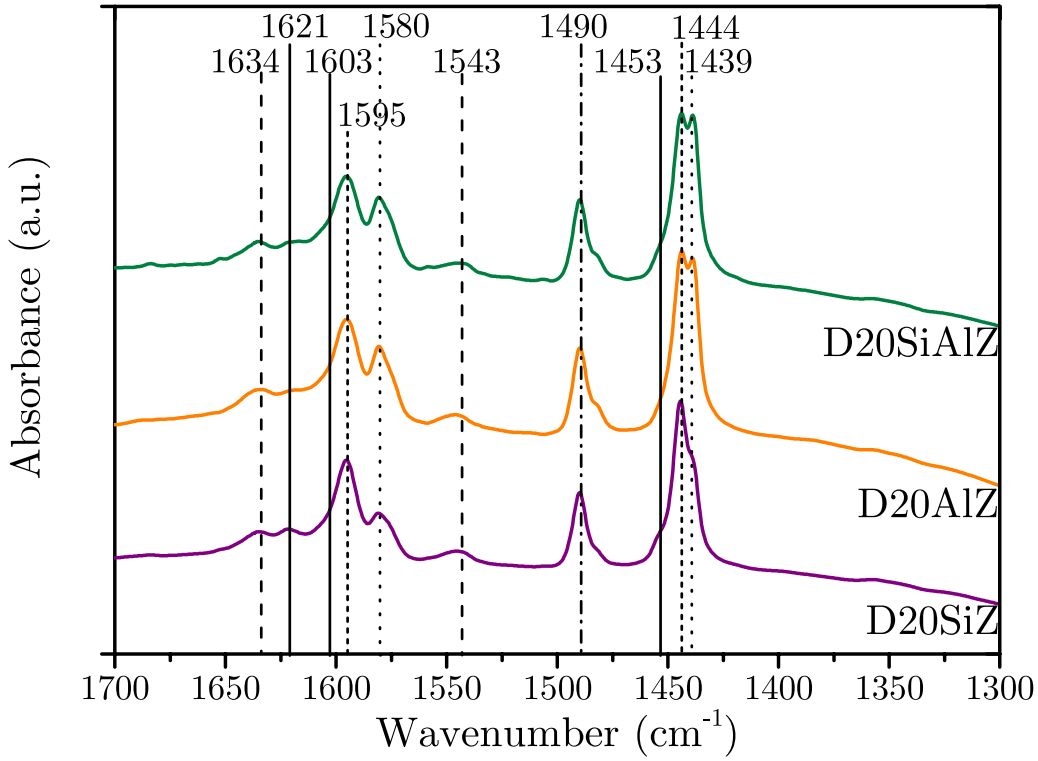

Figure 41: Pyridine FT-IR spectra of the FSiZ, FAlZ and FSiAlZ catalysts after 20 hours of steam treatment. Spectra taken after 30 minutes op pyridine adsorption. All spectra are corrected for pellet weight. Plotted with y-offset for clarity.

In Figure 52 (Appendix C) the spectra of the three different steamed catalysts after evacuation and 200 ℃ of temperature programmed desorption are shown. There are no significant differences in the strengths of the Lewis or Brønsted acid sites observed between the different catalysts. For all catalysts there are clearly two types of Lewis acid sites and one type of Brønsted acid sites present. The increase in strength of the LAS upon incorporation of silica is not seen anymore. This is probably because steam treatment has the same effect on the strength of LAS, and after 20 hours of steam treatment the effect of silica incorporation is negligible.

FT-IR Spectroscopy

Figure 42 shows the OH region of the FCC catalysts with SiAl as binder before steam treatment and after 5, 10 and 20 hours of steam treatment. The isolated silanol band at 3750 cm^{-1} becomes more distinct due to steam treatment. This is because dealumination takes place and more isolated silanols are created. The band around 3670 cm^{-1} indicating aluminol groups in extraframework species decreases. Dealumination causes an increase in LAS on extraframework alumina. These results would suggest that during this process, the surface hydroxyl groups decrease.
The intensity of the band at 3631 cm^{-1}, indicating Brønsted acid sites in a super cage structure, seems to decrease slightly. The intensity of the 3525 cm^{-1} band, indicating Brønsted acid in the sodalite cage does not change. The steam treatment seems to affect the supercages to a larger extent than the sodalite cages.

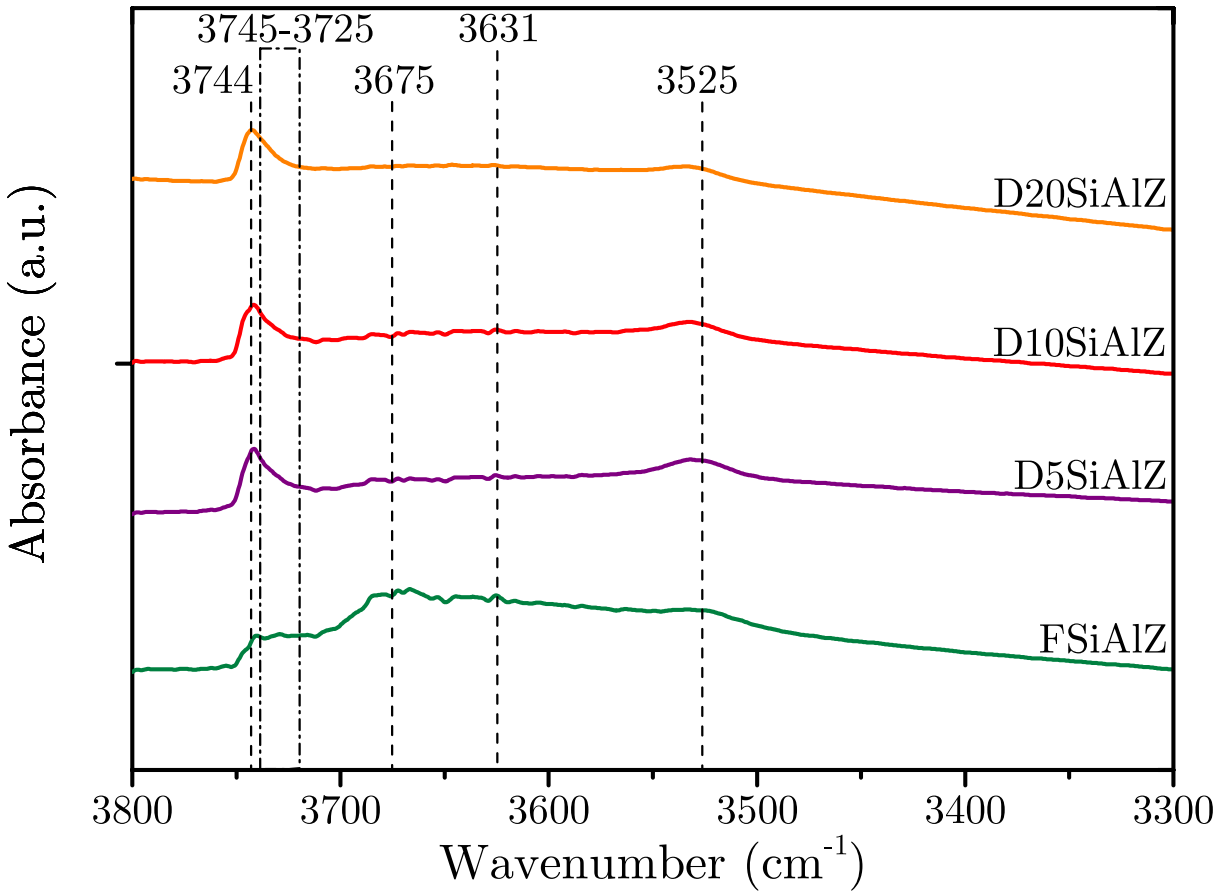

Figure 42: FT-IR spectrum of OH region of the FSiAlZ fresh catalyst and after 5, 10 and 20 hours of steam treatment. Spectra taken after drying procedure. All spectra are corrected for pellet weight. Plotted with y-offset for clarity. IR spectrum of the OH region of the FSiAlZ catalyst and this catalyst after 5, 10 and 20 hours of steam treatment.

Pyridine UV-Vis spectroscopy

Figure 43 shows the 45 minutes of pyridine adsorption on D5SiAlZ recorded with UV-Vis spectroscopy and the evolution of the indicated bands. The band around 39000 cm^{-1} arises within the first few minutes, indicating the presence of strong acidic sites. The band at 37700 cm^{-1} arises simultaneously with the band at 39000 cm^{-1}. The shape of

the absorbance evolution is again due to the presence of both micro and mesopores. After three minutes the bands between 23000 and 30000 cm^{-1} start arising. The band at 20800 cm^{-1} start arising about ten minutes after the pyridine introduction has started.

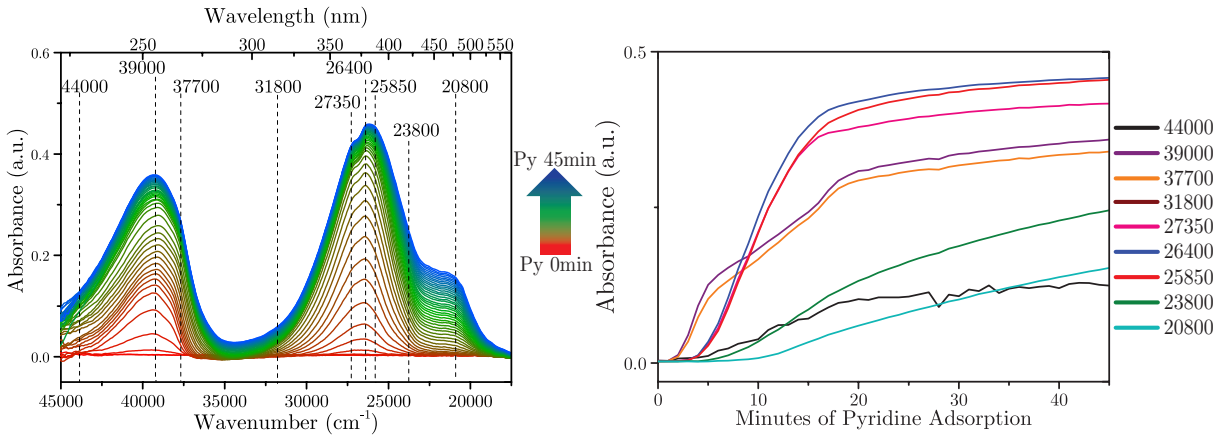

Figure 43: Pyridine UV-Vis spectra of 45 minutes of pyridine adsorption on D5SiAlZ catalyst (left) and the evolution of the bands marked in the UV-Vis spectrum (right).

Figure 44 shows the UV-Vis spectrum of the adsorption of pyridine on the D10SiAlZ sample. The evolution of the band at 39000 cm^{-1} is very similar to that of the D5SiAlZ catalyst. The band at 37700 cm^{-1}, which is assigned to the π to π^* excitation for Lewis acid sites, starts arising later than within the D5SiAlZ catalyst and the band arises slower. The evolution of the band does not have the typical shape for a species with micro and mesopores. It seems as if the Lewis acid sites in the micropores are being destroyed and the Lewis acid sites in mesopores are still present. This agrees with the migration of LAS to extraframework alumina (which has mesopores). The bands between 23000 and 30000 cm^{-1} arise similar to the D5SiAlZ sample. The band that is assigned to amorphous Si-(OH)-Al groups shows a slightly higher absorbance than for the D5SiAlZ catalyst, showing that more pyridine is adsorbed on this kind of weakly acidic surface sites.

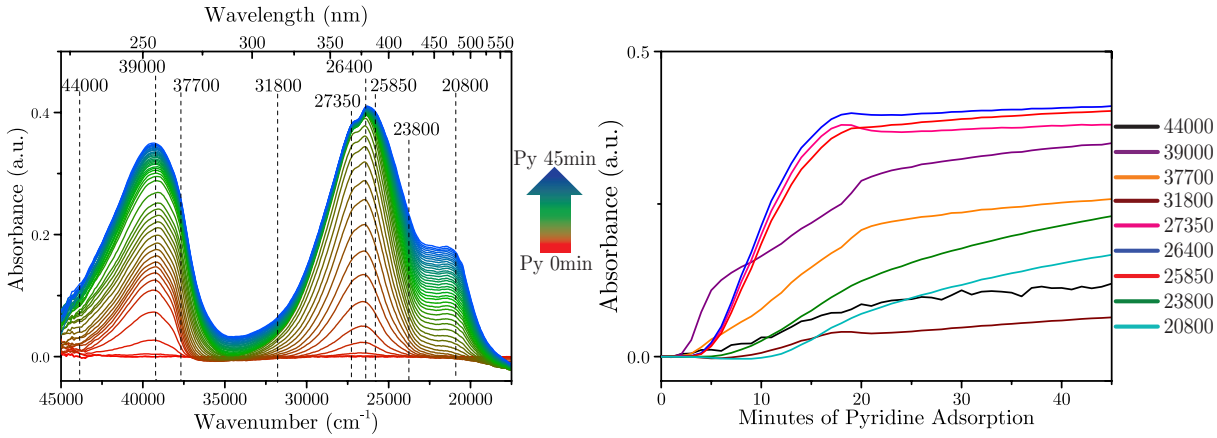

Figure 44: Pyridine UV-Vis spectra of 45 minutes of pyridine adsorption on D10SiAlZ catalyst (left) and the evolution of the bands marked in the UV-Vis spectrum (right).

Figure 45 shows the pyridine adsorption on the D20SiAlZ catalyst. In the evolution of the bands it can be seen that the band at 44000 cm^{-1}, which is assigned to Lewis acid

sites[48], arises from the beginning of pyridine adsorption. For the other samples this band did not start arising before a few minutes had passed. This band arises earlier as the strength of the Lewis sites has increased due to dealumination and the pyridine will be more prone to quickly adsorb on these sites. The pyridine also adsorbs more quickly on the other surface sites. As the steam destroys part of the structure of the FCC catalyst, the pyridine molecules have easier access to the (remaining) acid sites and the adsorption of pyridine takes place quicker.

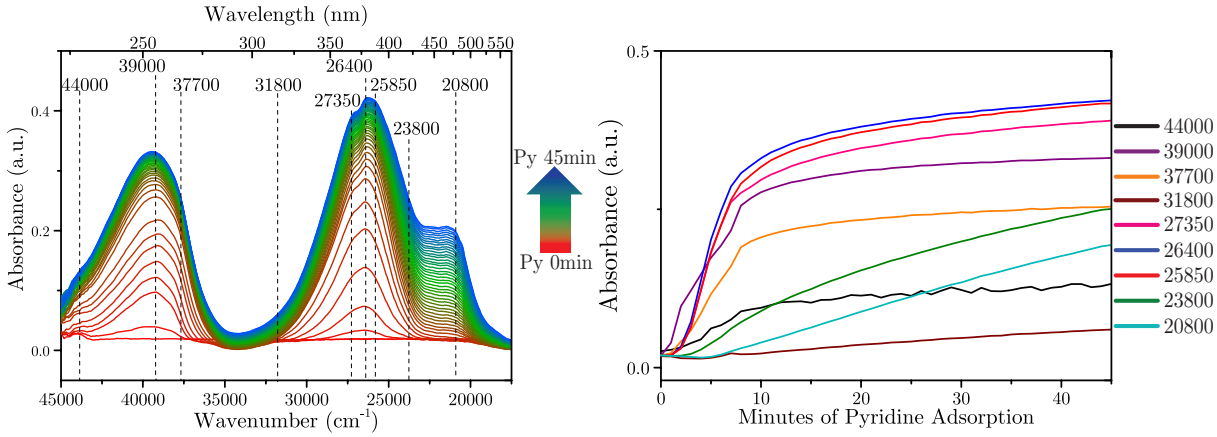

Figure 45: Pyridine UV-Vis spectra of 45 minutes of pyridine adsorption on D20SiAlZ catalyst (left) and the evolution of the bands marked in the UV-Vis spectrum (right).

Figure 46 shows the UV-Vis spectra of the steam treated samples of FSiAlZ after 5, 10 and 20 hours of steam treatment. One of the most clear difference is the strong increase of the band at 20800 cm^{-1} which is ascribed to amorphous Si-(OH)-Al groups.[48] This would suggest that these changes would be visible in the OH region of the steam treated samples (Figure 42). However, it is difficult to compare the tailed off part of the silanol peak at 3742 cm^{-1} as the band at 3686 cm^{-1} (aluminol[48]), which is present in the FSiAlZ catalyst, deforms the tail of the silanol peak.

The UV-Vis spectra of TPD at 200 ℃ of the steam treated catalysts are shown in Figure 47. Although the 39000 cm^{-1} band was relatively similar for the samples after 45 minutes of pyridine adsorption, after 200 ℃ of TPD these are very different. The band decreases in intensity after more hours of steam treatment. This shows that samples with less Brønsted acid sites show a faster decrease in the 39000 cm^{-1} band intensity than samples with more Brønsted acid sites, as would be expected. Due to the dealumination, the zeolite loses crystallinity and the BAS are transformed into amorphous Si-(OH)-Al groups. This explains the increase of the band at 20800 cm^{-1} during steam treatment (see Figure 46).

The UV-Vis spectra after 45 minutes of pyridine adsorption of the steamed FAlZ and FSiZ catalysts are shown in Appendix 55 and 56. For both catalyst the band at 20800 cm^{-1} increases as the bands around 25000-27500 cm^{-1} decrease in intensity.
To study the effect of steam treatment on the single components, the zeolite component was subjected to steam treatment. Only a XRD measurement and pyridine UV-Vis spectroscopy was performed on this sample. Due to the incompleteness, this experiment is not further discussed here. The methods and some results can be found in Appendix E.

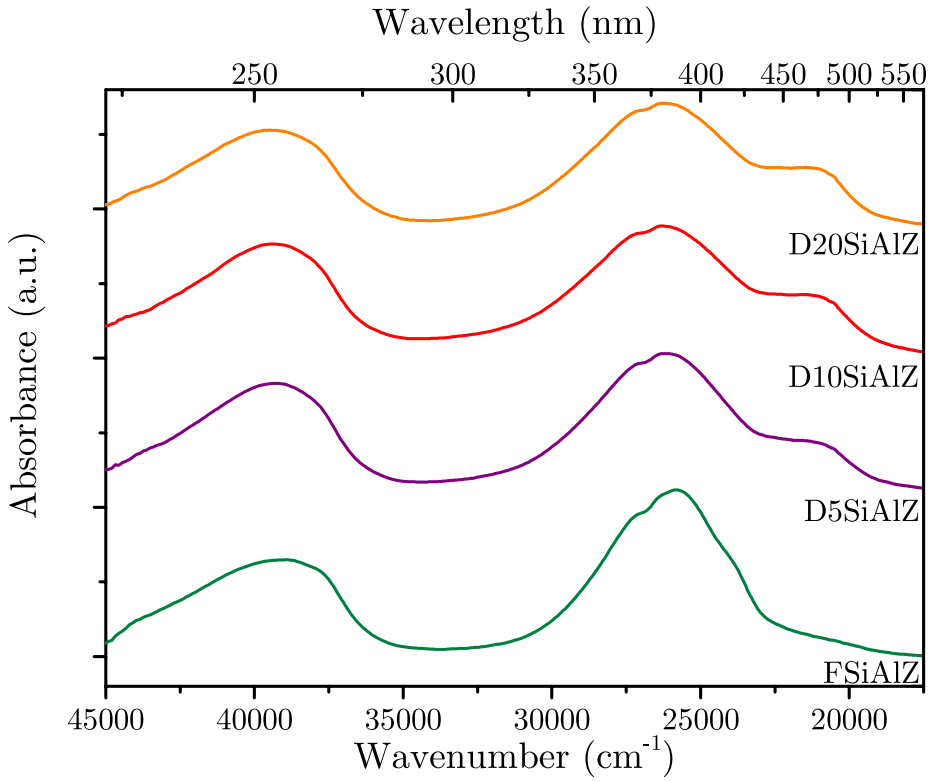

Figure 46: Pyridine UV-Vis spectra of the FSiAlZ fresh catalyst and after 5, 10 and 20 hours of steam treatment. Spectra taken after 45 minute of pyridine adsorption. Plotted with y-offset for clarity.

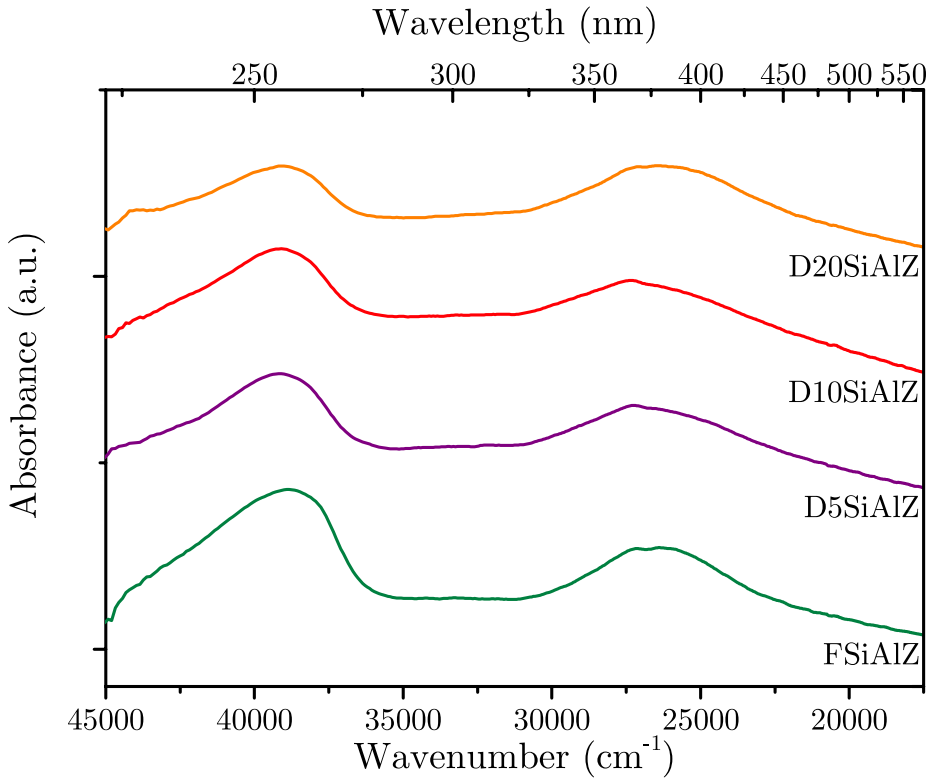

Figure 47: Pyridine UV-Vis spectra of the FSiAlZ fresh catalyst and after 5, 10 and 20 hours of steam treatment. Spectra taken after 200 ℃ of TPD. Plotted with y-offset for clarity.

3.5 Pyridine Adsorption at High Temperature

For the zeolite, two pyridine UV-Vis experiments were repeated as described in 2.2, but instead of cooling down the system to room temperature before introducing pyridine, the pyridine was introduced at higher temperatures. This was done because during the temperature programmed desorption of the zeolite, alumina and the catalysts, a new band arose. To further explore the nature of this band we were curious what would happen if the pyridine directly came into contact with a hot surface and atmosphere when introduced into the Linkam Cell. The temperatures that were chosen were 300 ℃ and 600 ℃. These temperatures where chosen because at these temperatures the pyridinium band at 39000 cm^{-1} was still intact and the new band had already come up.

Figure 48 shows the pyridine adsorption for 45 minutes on zeolite at 300 ℃ (left) and 600 ℃ (right). As during the measurement at 300 ℃ the band around 39000 cm^{-1} arose very quick, for the measurement at 600 ℃ a spectrum was taken every 20 seconds in stead of the standard 60 seconds.
The pyridine adsorption at 300 ℃ shows a very quick rise of the pyridinium band, which is already saturated after a few minutes. Apparently, the high temperature makes the pyridine very mobile and it can adsorb on all of the Brønsted acid sites very quickly. At room temperature the protonation reaction takes place less easily as it is an endothermic reaction. This explains the difference in saturation time of BAS at room temperature and elevated temperatures. The additional band that arises has a maximum at 31900 cm^{-1}.

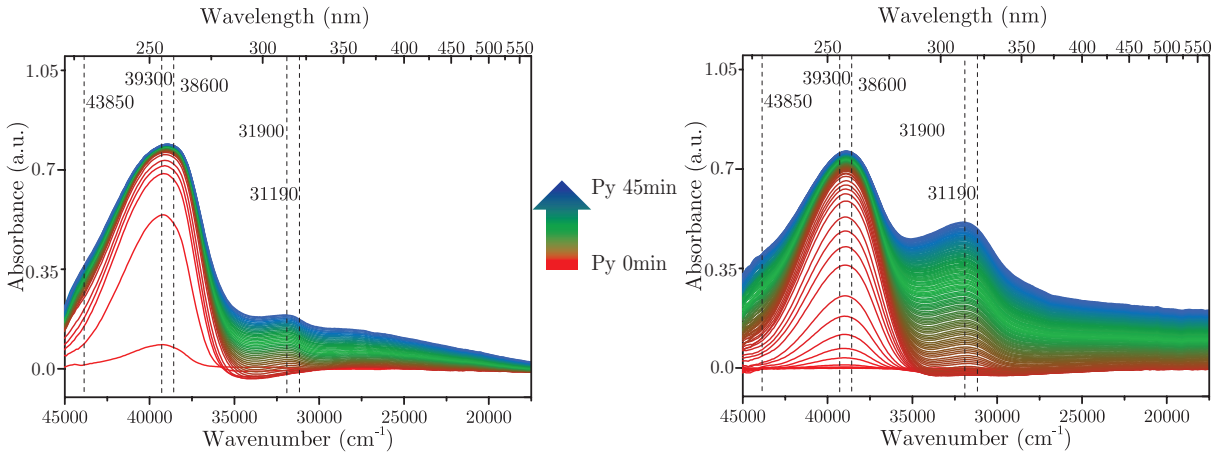

Figure 48: UV-Vis spectra of zeolite during 45 minutes of pyridine adsorption at 300 ℃ (left) with one spectrum taken every minute and 600 ℃ (right) with one spectrum taken every 20 seconds

The pyridine adsorption at 600 ℃ also shows an equally quick rise of the 39000 cm^{-1} band. The band at 31900 cm^{-1} start arising after 10 minutes. The band increases up to a much higher intensity than during the experiment at 300 ℃. The maximum of the new peak lies at 31900 cm^{-1}, which is higher than during the normal UV-Vis experiment on the zeolite (31190 cm^{-1}, see Figure 23). This band could indicate that a new molecule is formed due to a reaction with pyridine at an elevated temperature. One of the possibilities would be the formation of pyridone, the oxidized form of pyridine. This

oxidation of pyridine takes place on a Lewis acid site when an hydroxyl group is near, forming pyridone and hydrogen. Pyridone was observed to form during pyridine-IR TPD in other studies.[41] [33] At 600 ℃, pyridine has already desorbed from the Lewis acid sites (see Figure 24 for the UV-Vis desorption), and these Lewis acid sites are therefore free as reaction site to form pyridone. The formation of pyridone was probably not observed during the pyridine IR experiments because these were performed *in vacuo* and therefore pyridine is removed from the system before it can react.[48]

3.6 Performance Data

Table 3.6.1 and 3.6.2 show some of the average results of the activity tests performed by Albemarle. The activity test used that was used was the Fluid-bed simulation test and all tests were performed in duplicate. All results of all the tests can be found in Appendix G, Tables G.0.1 and G.0.2. The values of the tests done with the catalysts without zeolite had relative large variations. This is probably because the activity of these catalysts is much lower than the ones normally tested with this method and the test is not suited to fluidize catalysts without zeolite. It is not clear how reliable these results are. Only the catalysts that were subjected to a steam treatment of 20 hours were used in the performance tests as these are expected to be close to the FCC catalysts in the real conditions.

Table 3.6.1: Averaged results of performance tests of the three catalysts without zeolite, performed in duplicate. Testing: FST, Feed: KVGO

	D20_Al_NZ	D20_Si_NZ	D20_SiAl_NZ
<221 ℃ and Conversion wt% of crude oil	33.29	28.51	30.575
Coke wt% of crude oil	2.1885	1.3235	1.7035
Hydrogen wt% of conversion	0.1565	0.0915	0.1125
Propylene wt% of conversion	2.5505	2.4085	2.5165
Gasoline (C5-221 ℃) wt% of conversion	20.182	16.6305	17.981
343 ℃+ wt% of crude oil	51.055	59.7625	56.6405

Table 3.6.2: Averaged results of performance tests of the three catalysts with zeolite, performed in duplicate. Testing: FST, Feed: KVGO

	D20_Al_Z	D20_Si_Z	D20_SiAl_Z
<221 ℃ and Conversion wt% of crude oil	74.755	68.375	73.905
Coke wt% of crude oil	3.9865	3.857	4.3225
Hydrogen wt% of conversion	0.048	0.0565	0.0475
Propylene wt% of conversion	5.167	4.853	5.0085
Gasoline (C5-221 ℃) wt% of conversion	48.591	42.9055	47.754
343 ℃+ wt% of crude oil	9.3795	17.589	10.462

It is clear that the catalysts with zeolite show better conversion than the catalysts without zeolite. The catalysts without zeolite show a conversion for products with a boiling point of 221 ℃ or lower of about 30 % and the catalysts with zeolite of 70-75 %. For the catalysts without zeolite the D20AlNZ catalyst performs the best on propylene and

gasoline (gas form) conversion. Also for the catalysts with zeolite the D20AlZ performs best on these product conversions, although the differences with D20SiAlZ are smaller.

When looking at the formation of coke on the different catalysts, we see that the D20SiAlZ catalyst is the most affected. The catalysts without zeolite have a lot less coke formation as coke mainly adsorbs on surface acid sites.[66][67] This also explains why the catalysts containing only silica shows less coke formation than the catalysts containing alumina as binder, as alumina has Lewis acid sites.
As hydrogen is released when a cracking reaction takes place on a Lewis acid site, one would expect the amount of hydrogen formed to be the highest in the catalysts containing the most Lewis acid sites. For the catalysts without zeolite this is indeed the case, the hydrogen percentage is higher for D20AlNZ (0.1565 wt% of conversion) than for D20SiAlNZ (0.1125 wt% of conversion) and D20SiNZ (0.0915 wt% of conversion). However, for the catalysts with zeolite the D20SiZ shows the highest amount of hydrogen produced. When looking at the complete data sets in Appendix G.0.2, the small differences between the catalysts and the relatively larges differences between the tests of the same catalyst are seen. Either the role of the Lewis acid sites of the binder becomes less important when the zeolite is introduced into the catalyst, or the amount of hydrogen formed is not a good indicator of Lewis acid sites activity at this scale.

These performance data suggest that the for the highest gasoline and propylene conversion, the FCC catalyst should contain no silica. However, a matrix in which the alumina/silica ratio is increased has larger pore diameters and pore volumes. Although this could have a positive effect on the activity of a fresh catalyst, the catalyst will become more unstable when decreasing the silica percentage and the catalyst might deactivate sooner.[57]
The amount of surface hydroxyl groups was higher for the FCC catalysts containing alumina than for the catalyst only containing silica (Figure 33 and 34, Figure 41). The higher activity for the alumina containing catalysts would suggest that these weakly acidic surface sites also contribute to the activity of the catalyst.

3.7 XRD measurements

To study the effects of steam treatment on the crystal structure of the FCC catalyst, XRD measurements were performed. In Appendix F the diffractograms of XRD measurements of the FSiAlZ and the steam treated FSiAlZ showed that the catalysts have crystallinity. The catalyst without zeolite (FSiAlNZ) showed no crystallinity. This tells us that the crystallinity originates only from the zeolite and not from the other components. The steam treated samples showed that the crystallinity decreased during steam treatment and dealumination takes place. Because the peaks of TiO_2 are at the same position for all spectra, we know that the shift of the other peaks is not due to a lattice shift.

Chapter 4

Conclusions

To be able to rationally design the FCC catalyst used in the FCC process, the acidity in this catalyst was thoroughly investigated. Often only the zeolite is studied but in this work all single components were investigated. In this way we can further study the role of the clay, silica and alumina in the acidity of the catalyst.
Pyridine FT-IR measurements were used as an established technique to provide information on the acidity of the samples. A new technique to probe acidity is pyridine UV-Vis spectroscopy. This technique shows promising results for the identification of different weakly acidic surface hydroxyl groups, as well as stronger acid sites.
The zeolite is the component that has the most acidic sites. Pyridine FT-IR showed that it has Brønsted acid sites (BAS) and two types of Lewis acid sites (LAS). The zeolite also showed a lot of physisorbed pyridine and pyridine adsorbed on a variety of surface hydroxyl groups. Clay contained both types of acid sites but in very low quantity. Also the amount of pyridine adsorbed on weak acidic sites and in a physisorbed manner was low. Alumina contained one type of LAS and a variety of surface hydroxyl groups. Pyridine also adsorbed in a physisorbed manner of alumina. Silica only contained weak acidic hydroxyl groups.
The FSiAlZ catalyst showed the presence of BAS and two types of LAS. Also on the FCC catalyst a lot of physisorbed pyridine was observed. The FCC catalyst had a variety of surface hydroxyl groups.

Normally, the binder of the FCC catalyst consists of a mixture of silica and alumina. In this work, also catalysts with only silica or only alumina as binder were studied. Incorporation of silica in the FCC catalyst slightly increased the strength of the Lewis acid sites in the catalyst. The incorporation of alumina increased the amount of weakly acidic hydroxyl surface groups and surface sites on which pyridine adsorbed in a physisorbed manner.

In the FCC process the catalyst is exposed to steam in the stripper and the regenerator. To study the effect of this steam on the FCC catalysts, steam treatment was performed on the catalyst samples. Steam treatment caused dealumination of the catalyst. The amount of LAS and BAS decreased due to the steam treatment. The dealumination of the zeolite created LAS on extraframework alumina species. The LAS on these species were stronger than in the zeolite, as observed in pyridine FT-IR. Pyridine UV-Vis spectroscopy showed that the decrease of BAS is accompanied by an increase of weakly acidic amorphous Si-(OH)-Al surface groups. The change of the shape of the evolution of the

band assigned to LAS, indicated the migration of LAS from the zeolite to extraframework alumina species.
The biggest changes take place in the first 5 hours of steam treatment. The decrease in acid sites continues between 5 and 10 hours of steam treatment. Between 10 and 20 hours not a lot of changes are observed.

Pyridine UV-Vis spectroscopy showed bands in the region between 20000 and 30000 cm^{-1} that indicated the different weakly acidic hydroxyl groups on the solid acids. The presence of Brønsted acidity was observed by a steep increase of the band at 39000 cm^{-1} quickly after the pyridine was introduced. The integrity of this band after 200 ℃ of TPD provided information on the amount of BAS in the sample. The shape of the evolution of the bands in pyridine UV-Vis provided information on whether the acidic sites were present in a species with micro- and mesopores or with only one type of pores.

The new band that arose in the UV-Vis spectra during TPD, might be due to the formation of pyridone. Pyridone is the oxidized form of pyridine that forms on a LAS in the vicinity of an hydroxyl group.

Performance data showed that the catalyst with only alumina as binder performed the best in performance tests. A catalyst with a maximum amount of alumina and a minimum of silica would be suggested, however the stability of such a catalyst has to be tested. As the catalysts with alumina showed the presence of a lot of weakly acidic surface hydroxyl groups, it is suggested that these sites also contribute to the activity of the catalyst.

Chapter 5

Outlook

To further study the effect of the amount of silica on the stability of the FCC catalyst, it might be interesting to do performance tests with the catalysts after 5 and 10 hours of steam treatment. If the silica indeed has a positive effect on the stability of the catalyst one would expect a faster (relative) decrease in activity for the FAlZ and FSiAlZ than for the FSiZ catalyst.

Pyridine based molecules like lutidine and collidine can also be used as probe molecules for FT-IR spectroscopy. Lutidine is a more basic molecule and can therefore determine the strength of Brønsted acid sites with a higher precision. Due to sterical hindrance of the methyl groups, lutidine is not very suitable to probe Lewis acid sites.[5] Collidine can provide information on the accessibility of Brønsted acid sites as the large molecule is not able to enter all micropores of the zeolite.[13]

To study the effect of steam treatment on all components, the experiment in Appendix E should be performed with all components. These steamed samples should then be used for pyridine FT-IR and UV-Vis experiments.

CO is a very well-known probe molecule for FT-IR spectroscopy measurements.[31] Performing these measurements on the samples can provide additional information on *e.g.* the strength of the acidic sites and the amount of Brønsted acid sites.[52] For a CO FT-IR spectroscopy study on related samples, the master thesis by Iris Teune can be consulted.

To study the origin of the new band arising during TPD, the pyridine adsorption at high temperature experiments have to be performed on more samples. It would also be interesting to choose temperature between 300 ℃ and 600 ℃, to have a more precise evaluation of the arise of the band. Also pyridine FT-IR spectroscopy experiments at elevated temperatures should be performed. As there is already more knowledge on this technique, the origin of the new band should be easier to assign.

The biggest challenge for the future of pyridine UV-Vis spectroscopy as acidity probing technique is improvement of the setup. Within the current setup there were a few problems that can influence the results. The first problem was that the nitrogen flow exiting the system was not consistent over different days. This was solved by adjusting the flow until the exiting flow was found equal to previous measurements. As this was done by eye it would be much more reliable to create a fully closed system with a con-

sistent flow. Another suggestion would be to create a setup in which the sample can be brought under vacuum. This would create a more reliable comparison between the results of pyridine UV-Vis spectroscopy and of pyridine FT-IR.
Another problem was that the sample would sometimes move during the drying procedure. Due to the heat the sample would form a pellet and the flow would move it off the heating plate. This problem was solved by slightly lifting the Linkam Cell at one side as the sample always fell off at the same side. The distance of the UV-Vis probe to the sample was adjusted to have comparable signals for all experiments. It would be better to automatize this to be able to compare the intensities of the absorbance bands.

Chapter 6

Acknowledgments

First of all, I would like to thank Marjolein. You were a great supervisor and I've learned a lot from you in the last year and a half. Our Tuesday morning meetings were very helpful to discuss my results and to make sure I kept thinking of other and better ways to display and explain my data. You did not only help me with my project but also with other things like planning a future as scientist and writing motivation letters for internships. You were patient and made sure I would always first try to figure things out myself before giving your own thoughts. I am grateful to have had you as my supervisor and I hope we stay in touch in the future.

Bert, thank you for the opportunity to do my master thesis at your group. Our meetings made sure I kept thinking of what the next steps in my research would be and what my work will contribute to the science community. Thank you also for the opportunity to be part of the visit of the delegation of the Ministry of Science and Education. This day inspired me a lot and you showed the importance of our science for the whole society.

Iris, I really enjoyed working alongside each other as Marjolein's master students. I admire your passion for (in)organic research and it was great to be a small part of your project via the Tuesday morning meetings. I also want to thank you for your ideas on my project.
I would like to thank Oscar, Ramon, Fouad, Petra, Paul, Özgun, Ana , Anne-Eva, Marjan and Zoran for helping me with setups, instruments and measurements during my project.
Thomas, Nienke, Laura, David, Sophie, Iris and Lucas, I really enjoyed doing our master projects at the same time. Not only did it make the lunch breaks more enjoyable, we also had useful discussions about each others projects and helped each other prepare presentations.
Last but not least, I would like to thank the rest of the ICC group for making me feel welcome and for the great time.

Bibliography

[1] BP; *BP Energy Outlook 2018 Edition*; Tech. Rep.; 2018.

[2] Zakzeski, J.; Bruijnincx, P. C. A.; Jongerius, A. L.; Weckhuysen, B. M. *Chem. Rev.* **2010**, *110*, 3552–3599.

[3] Mangu, R.; Prayaga, K.; Nadimpally, B.; Nicaise, S. In *IEEE Green Technol. Conf.*

[4] Vermeiren, W.; Gilson, J. P. *Top. Catal.* **2009**, *52*, 1131–1161.

[5] Vogt, E. T. C.; Weckhuysen, B. M. *Chem. Soc. Rev.* **2015**, *44*, 7342–7370.

[6] Letzsch, W. In *Handb. Pet. Process.*, 2nd ed.; Treese, S. A.; Pujadó, P. R.; Jones, D. S. J., Eds.; Springer International Publishing, 2015; Vol. 1, pp 261–312.

[7] Reichle, A. D. *Chem. Eng. Prog.* **1990**, *22*, 70–74.

[8] Kalirai, S.; Ph.D. thesis; Utrecht University; 2016.

[9] Sadeghbeigi, R. *Fluid Catalytic Cracking Handbook*, third edit ed.; Butterworth-Heinemann: Waltham, MA, USA, 2012.

[10] Buurmans, I. L. C.; Ruiz-Martínez, J.; Knowles, W. V.; van der Beek, D.; Bergwerff, J. a.; Vogt, E. T. C.; Weckhuysen, B. M. *Nat. Chem.* **2011**, *3*, 862–867.

[11] Rawlence, D.; Gosling, K. *Appl. Catal.* **1988**, *43*, 213–237.

[12] Cerqueira, H.; Caeiro, G.; Costa, L.; Ramôa Ribeiro, F. *J. Mol. Catal. A Chem.* **2008**, *292*, 1–13.

[13] Bordiga, S.; Lamberti, C.; Bonino, F.; Travert, A.; Thibault-Starzyk, F. *Chem. Soc. Rev.* **2015**, *44*, 7262–7341.

[14] Robinson, P. R.; Hsu, C. S. In *Handb. Ind. Chem. Biotechnol.*, 2017; Chapter Petroleum, pp 13–106.

[15] Buurmans, I. L. C. *Catalyst Particles for Fluid Catalytic Cracking Visualized at the Individual Particle Level by*, 2011.

[16] Cronstedt, A. F. *Akad. Handl. Stock.* **1756**, *18*, 120–123.

[17] Hunger, M. In *Zeolites Catal. Synth. React. Appl.*, 2010; pp 493–546.

[18] Damjanović, L.; Auroux, A. *Zeolite Characterization and Catalysis*; Chester, A. W.; Derouane, E., Eds.; Springer Netherlands: Dordrecht, 2009.

[19] Watanabe, Y.; Habgood, H. W. *J. Phys. Chem.* **1968**, *72*, 3066–3069.

[20] McCusker, L. B.; Baerlocher, C. In *Introd. to Zeolite Sci. Pract.*; Jacobs, P. A.; Flanigen, E. M.; Jansen, J. C.; van Bekkum, H., Eds.; Studies in Surface Science and Catalysis; Elsevier Science, 2001; pp 37–45.

[21] Igarashi, M.; Nakano, T.; Thi, P. T.; Nozue, Y.; Goto, A.; Hashi, K.; Ohki, S.; Shimizu, T.; Krajnc, A.; Jeglic, P.; Arcon, D. *Phys. Rev. B* **2013**, *87*.

[22] Bronsted, J. *Recl. DES Trav. Chim. DES PAYS-BAS* **1923**, *42*, 718–728.

[23] Brönsted, J. *Chem. Rev.* **1927**, *5*, 231–338.

[24] Lewis, G. N. *Chem. Cat. Co.* **1923**, 142.

[25] Olah, G. A. *Nobel Lect.* **1994**, *Dec 8*.

[26] Bolton, A. P.; Lanewala, M. A. *J. Catal.* **1970**, *18*, 1–11.

[27] Coster, D.; Blumenfeld, A.; Fripiat, J. J. *J. Phys. Chem* **1994**, *98*, 6201–6211.

[28] Derouane, E.; Védrine, J.; Ramos Pinto, R.; Borges, P.; Costa, L.; Lemos, M.; Lemos, F.; Ramoa Ribeiro, F. *Catal. Rev.* **2013**, *55*, 454–515.

[29] Phung, T. K.; Busca, G. *Appl. Catal. A Gen.* **2015**, *504*, 151–157.

[30] Rothenberg, G. *Catalysis: Concepts and Green Applications*; Wiley-VCH Verlag GmbH & Co. KGaA: Weinheim, Germany, 2008.

[31] Hadjiivanov, K. I.; Vayssilov, G. N. *Adv. Catal.* **2002**, *47*, 305–511.

[32] Trunschke, A. *Max Planck Soc.* **2014**.

[33] Vimont, A. *Spectro Cat* **2016**.

[34] Corma, A.; Fornes, V.; Forni, L.; Marquez, F.; Martinez-Triguero, J.; Moscotti, D. *J. Catal.* **1998**, *179*, 451–458.

[35] Khabtou, S.; Chevreau, T.; Lavalley, J. C. *Microporous Mater.* **1994**, *3*, 133–148.

[36] Ryczkowski, J. *Catal. Today* **2001**, *68*, 263–381.

[37] Beale, A. M.; Hofmann, J. P.; Sankar, M.; van Schrojenstein Lantman, E. M.; Weckhuysen, B. M. *Heterog. Catal. Clean Technol. Spectrosc. Des. Monit.* **2013**, 365–411.

[38] Beale, A. M. In *Vib. Spectrosc.*, 2013.

[39] Thibault-Starzyk, F.; Maugé, F. In *Charact. Solid Mater. Heterog. Catal.*; Wiley-VCH Verlag GmbH & Co. KGaA: Weinheim, Germany, 2012; pp 3–48.

[40] Parry, E. *J. Catal.* **1963**, *2*, 371–379.

[41] Morterra, C.; Magnacca, G. *Catal. Today* **1996**, *27*, 497–532.

[42] Kline, C. H.; Turkevich, J. *J. Chem. Phys.* **1944**, *12*, 300–309.

[43] Barzetti, T.; Selli, E.; Moscotti, D.; Forni, L. *J. Chem. Soc. Faraday Trans.* **1996**, *92*, 1401–1407.

[44] Jentoft, F. C. In *Charact. Solid Mater. Heterog. Catal.*; Wiley-VCH Verlag GmbH & Co. KGaA: Weinheim, Germany, 2012; Vol. 1, pp 89–147.

[45] Bruice, P. Y. *Organic Chemistry*; Jaworski, A., Ed., 2014.

[46] McMurry, J. *Organic Chemistry*, seventh ed ed.; Brooks/Cole Cengage Learning, 2008.

[47] Clayden, J.; Greeves, N.; Warren, S. *Organic Chemistry*; Oxford University Press Inc.: New York, 2012.

[48] Velthoen, M. E. Z.; Nab, S.; Weckhuysen, B. M. *Submiss.* **2018**.

[49] Kaljurand, I.; Rodima, T.; Leito, I.; Koppel, I. A.; Schwesinger, R. *J. Org. Chem.* **2000**, *65*, 6202–6208.

[50] Stavitski, E.; Kox, M. H. F.; Weckhuysen, B. M. *Chem. Eur. J.* **2007**, *13*, 7057–7065.

[51] Whiting, G. T.; Meirer, F.; Valencia, D.; Mertens, M. M.; Bons, A.-J.; Weiss, B. M.; Stevens, P. A.; de Smit, E.; Weckhuysen, B. M. *Phys. Chem. Chem. Phys.* **2014**, *16*, 21531–42.

[52] Hadjiivanov, K. In *Adv. Catal.*, 2014; Vol. 57, pp 99–318.

[53] Corma, A.; Planelles, J.; Sánchez-Marín, J.; Tomás, F. *J. Catal.* **1985**, *93*, 30–37.

[54] Quinones, A.; Keyworth, D.; Imhof, P. *Fluid-bed Simulation Test (FST)*, 1997.

[55] *FCC catalyst additive and binder (WO 2017015597 A1).*

[56] Rautiainen, E.; Pimenta, R.; Ludvig, M.; Pouwels, C. *Catal. Today* **2009**, *140*, 179–186.

[57] Scherzer, J. *Appl. Catal.* **1991**, *75*, 1–32.

[58] Góra-Marek, K.; Derewiński, M.; Sarv, P.; Datka, J. *Catal. Today* **2005**, *101*, 131–138.

[59] Crépeau, G.; Montouillout, V.; Vimont, A.; Mariey, L.; Cseri, T.; Mauge, F. *J. Phys. Chem. B* **2006**, *110*, 15172–15185.

[60] Farmer, V. C. *Clay Miner.* **1998**, *33*, 601–604.

[61] Llewellyn, P. L.; Bloch, E.; Bourrelly, S. In *Charact. Solid Mater. Heterog. Catal. From Struct. to Surf. React. Vol. 1&2*, 2012; Vol. 2, pp 853–879.

[62] Hammond, K. D.; Conner, W. C. In *Adv. Catal.*, 2013; Vol. 56, pp 1–101.

[63] Emeis, C. *J. Catal.* **1993**, *141*, 347–354.

[64] Hensen, E. J. M.; Poduval, D. G.; Degirmenci, V.; Ligthart, D. A. J. M.; Chen, W.; Rigutto, M. S.; Veen, J. A. R. V. *J. Phys. Chem. C* **2012**, *116*, 21416–21429.

[65] Shigeishi, R. A.; Chiche, B. H.; Fajula, F. *Microporous Mesoporous Mater.* **2001**, *43*, 211–226.

[66] Hopkins, P. D.; Miller, J. T.; Meyers, B. L.; Ray, G. J.; Roginski, R. T.; Kuehne, M. A.; Kung, H. H. *Appl. Catal. A Gen.* **1996**, *136*, 29–48.

[67] Qian, K.; Tomczak, D. C.; Rakiewicz, E. F.; Harding, R. H.; Yaluris, G.; Cheng, W.-c.; Zhao, X.; Peters, A. W. *Energy & Fuels* **1997**, *11*, 596–601.

[68] Aramburo, L. R.; Karwacki, L.; Cubillas, P.; Asahina, S.; De Winter, D. A.; Drury, M. R.; Buurmans, I. L.; Stavitski, E.; Mores, D.; Daturi, M.; Bazin, P.; Dumas, P.; Thibault-Starzyk, F.; Post, J. A.; Anderson, M. W.; Terasaki, O.; Weckhuysen, B. M. *Chem. - A Eur. J.* **2011**, *17*, 13773–13781.

Appendices

Appendix A

Experimental Methods

A.1 Temperature Calibration Linkam cell

A temperature calibration was performed to measure the temperature on the heating plate in the Linkam cell used for pyridine UV-Vis measurements. The actual temperature of the heating plate turned out to be lower than the indicated temperature on the temperature controller. In the thesis the temperature on the temperature controller is used. Figure 49 shows how this can be corrected for the real temperature.

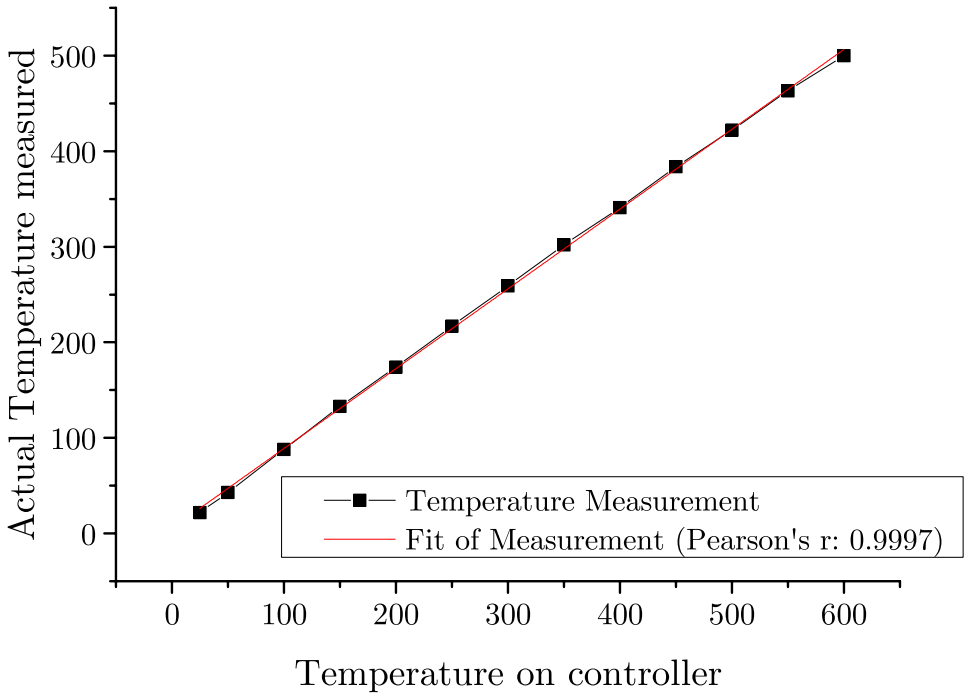

Figure 49: Temperature calibration of the Linkam Cell heating plate. In black the temperature measurement and in red the fit of the graph.

Appendix B

Characterization Data

B.1 Dry Weight Composition

All of these percentages are the dry weights before calcination.

Table B.1.1: Overview of composition of the calcined fresh catalysts in dry weight percentage

Sample	Zeolite	Alumina	Silica	Clay
F_Al_NZ	0	24	0	76
F_Al_Z New	30	24	0	46
F_Si_NZ	0	0	24	76
F_Si_Z	30	0	24	46
F_SiAl_NZ	0	12	12	76
F_SiAl_Z	30	12	12	46

Table B.1.2: Overview of composition of the calcined fresh catalysts in dry weight percentage

Sample	Zeolite	Alumina	Silica	Clay
D20_Al_NZ	0	24	0	76
D5_Al_Z New	30	24	0	46
D10_Al_Z New	30	24	0	46
D20_Al_Z New	30	24	0	46
D20_Si_NZ	0	0	24	76
D5_Si_Z	30	0	24	46
D10_Si_Z	30	0	24	46
D20_Si_Z	30	0	24	46
D20_SiAl_NZ	0	12	12	76
D5_SiAl_Z	30	12	12	46
D10_SiAl_Z	30	12	12	46
D20_SiAl_Z	30	12	12	46

B.2 Chemical Composition by XRF spectroscopy

Table B.2.1: Overview of the chemical compositions of the single components as determined with XRF spectroscopy

Sample	Al_2O_3	SiO_2	REO	TiO_2
Clay	43.8	52.15	0.03	2.944
Silica	0.23	99.71	0.01	0.006
Zeolite	21.317	65.93	12.35	0.021
Alumina	99.69	0.16	0.01	0

Table B.2.2: Overview of the chemical compositions of the calcined fresh catalysts as determined with XRF spectroscopy

Sample	Al_2O_3	SiO_2	REO	TiO_2
F_Al_NZ	55.9	40.87	0.04	2.312
F_Al_Z New	50.32	43.84	3.63	1.41
F_Si_NZ	33.76	63.1	0.05	2.294
F_Si_Z	26.78	67.46	3.68	1.394
F_SiAl_NZ	44.84	52.02	0.08	2.235
F_SiAl_Z	38.25	55.86	3.82	1.375

Table B.2.3: Overview of the chemical compositions of the steamed catalysts as determined with XRF spectroscopy

Sample	Al_2O_3	SiO_2	REO	TiO_2
D20_Al_NZ	55.9	40.87	0.04	2.312
D5_Al_Z New	50.32	43.84	3.63	1.41
D10_Al_Z New	50.32	43.84	3.63	1.41
D20_Al_Z New	50.32	43.84	3.63	1.41
D20_Si_NZ	33.76	63.1	0.05	2.294
D5_Si_Z	26.78	67.46	3.68	1.394
D10_Si_Z	26.78	67.46	3.68	1.394
D20_Si_Z	26.78	67.46	3.68	1.394
D20_SiAl_NZ	44.84	52.02	0.08	2.235
D5_SiAl_Z	38.25	55.86	3.82	1.375
D10_SiAl_Z	38.25	55.86	3.82	1.375
D20_SiAl_Z	38.25	55.86	3.82	1.375

Appendix C

Additional FT-IR spectra

C.1 Pyridine IR spectra

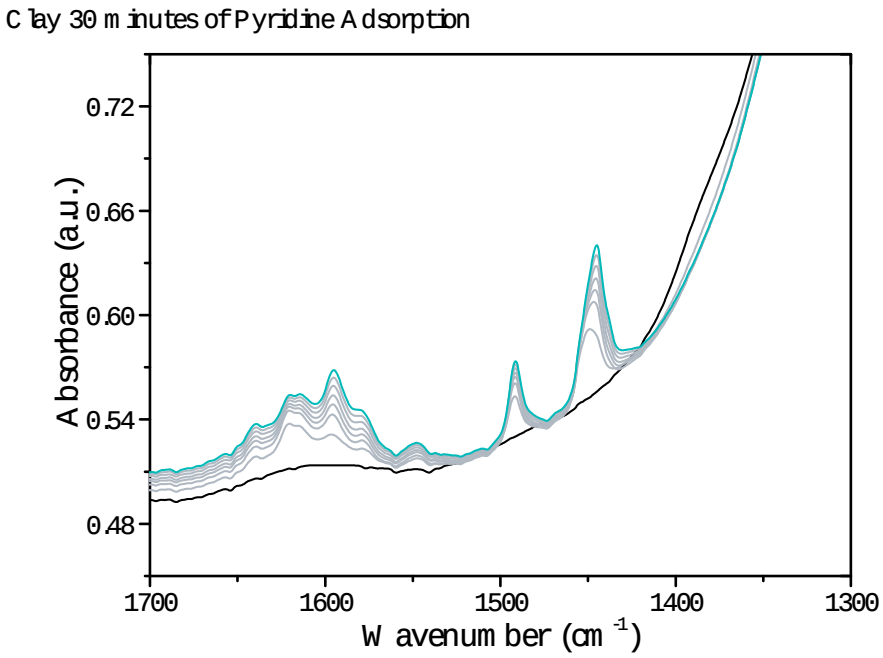

Figure 50: Pyridine FT-IR spectrum of 30 minutes of pyridine adsorption on the clay component. Spectra are taken every 5 minutes.

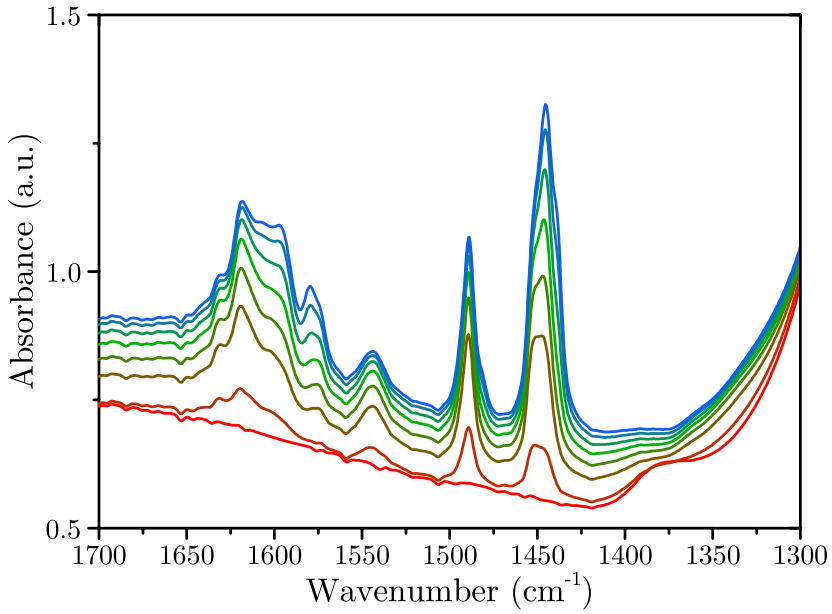

Figure 51: Pyridine FT-IR spectrum of 30 minutes of pyridine adsorption on the FSiAlZ catalyst. Spectra are taken every 5 minutes.

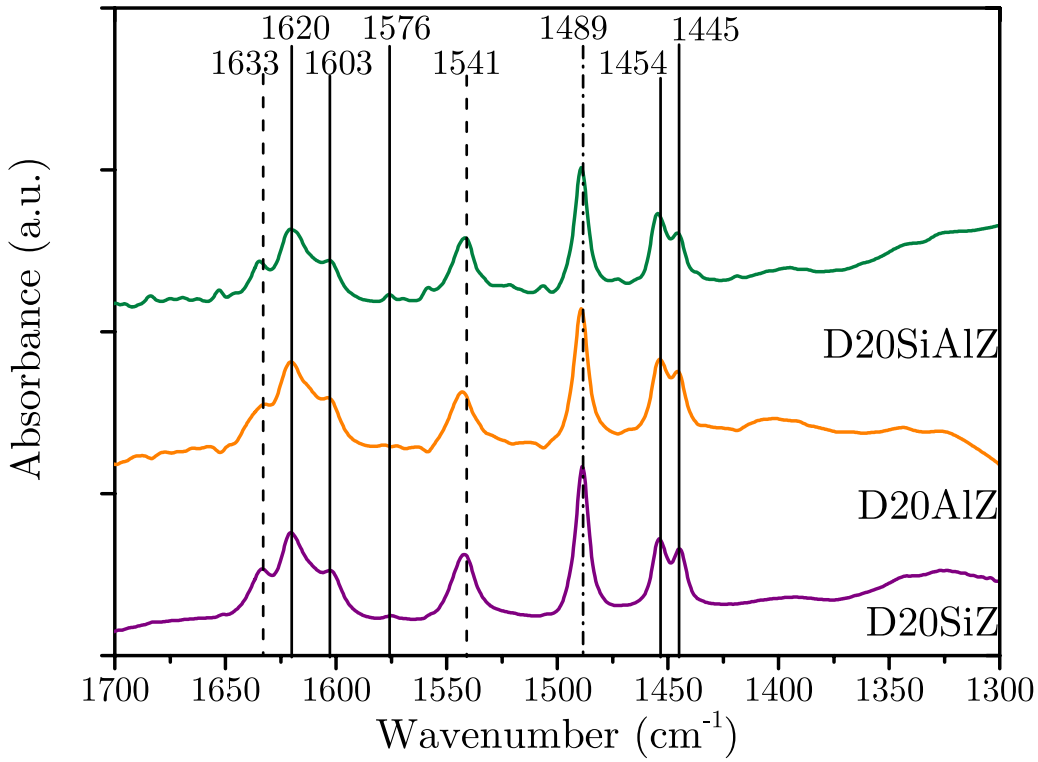

Figure 52: FT-IR spectrum D20 TPD 200

Appendix D

Additional UV-Vis spectra

D.1 Desorption

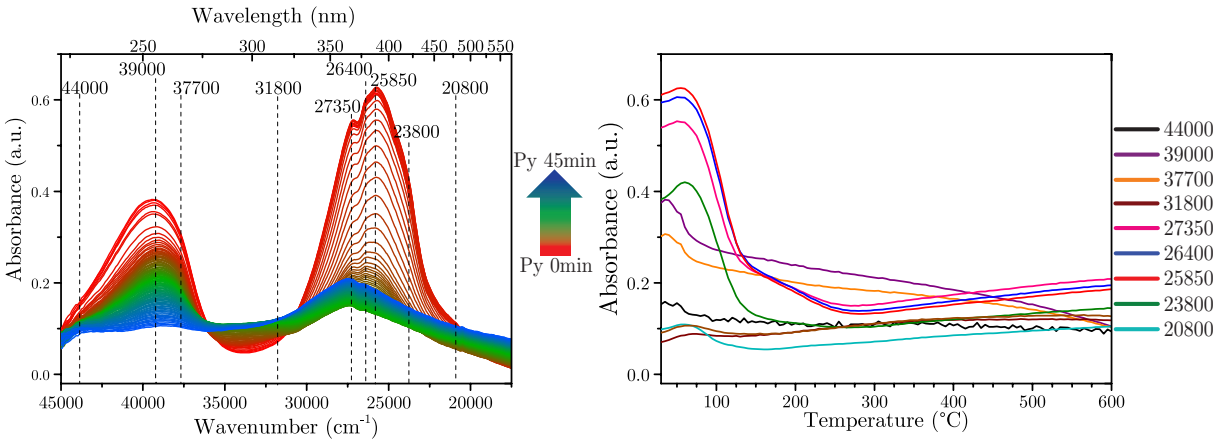

Figure 53: UV-Vis spectra of FAlZ during pyridine desorption

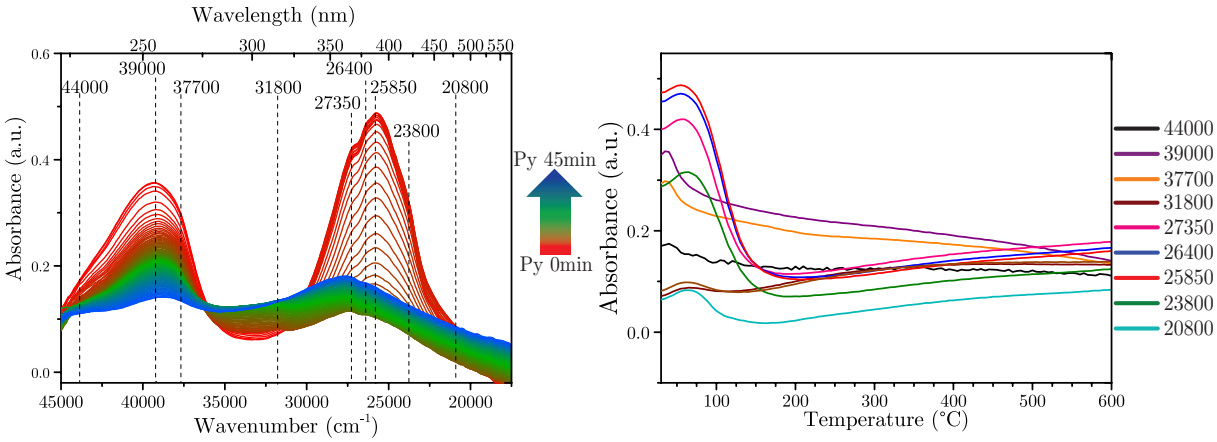

Figure 54: UV-Vis spectrum of TPD FSiZ

D.2 Steam-treated catalysts

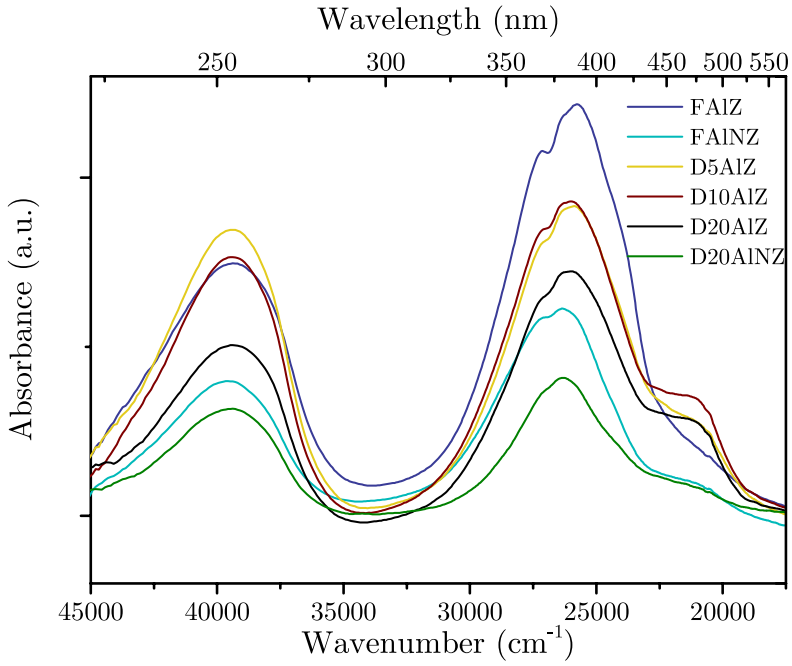

Figure 55: UV-Vis spectrum of FAlZ steam treated samples after 45 minutes of pyridine adsorption

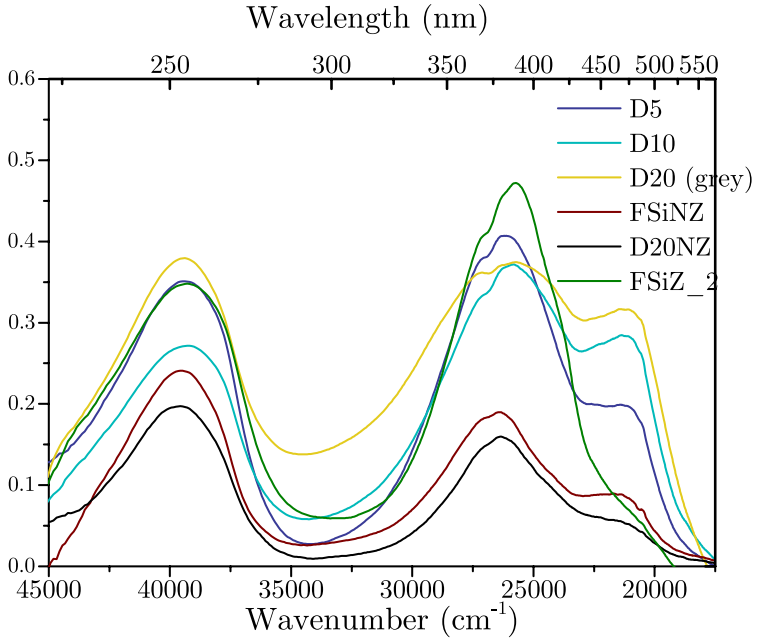

Figure 56: UV-Vis spectrum of FSiZ steam treated samples after 45 minutes of pyridine adsorption

D.3 Fityk

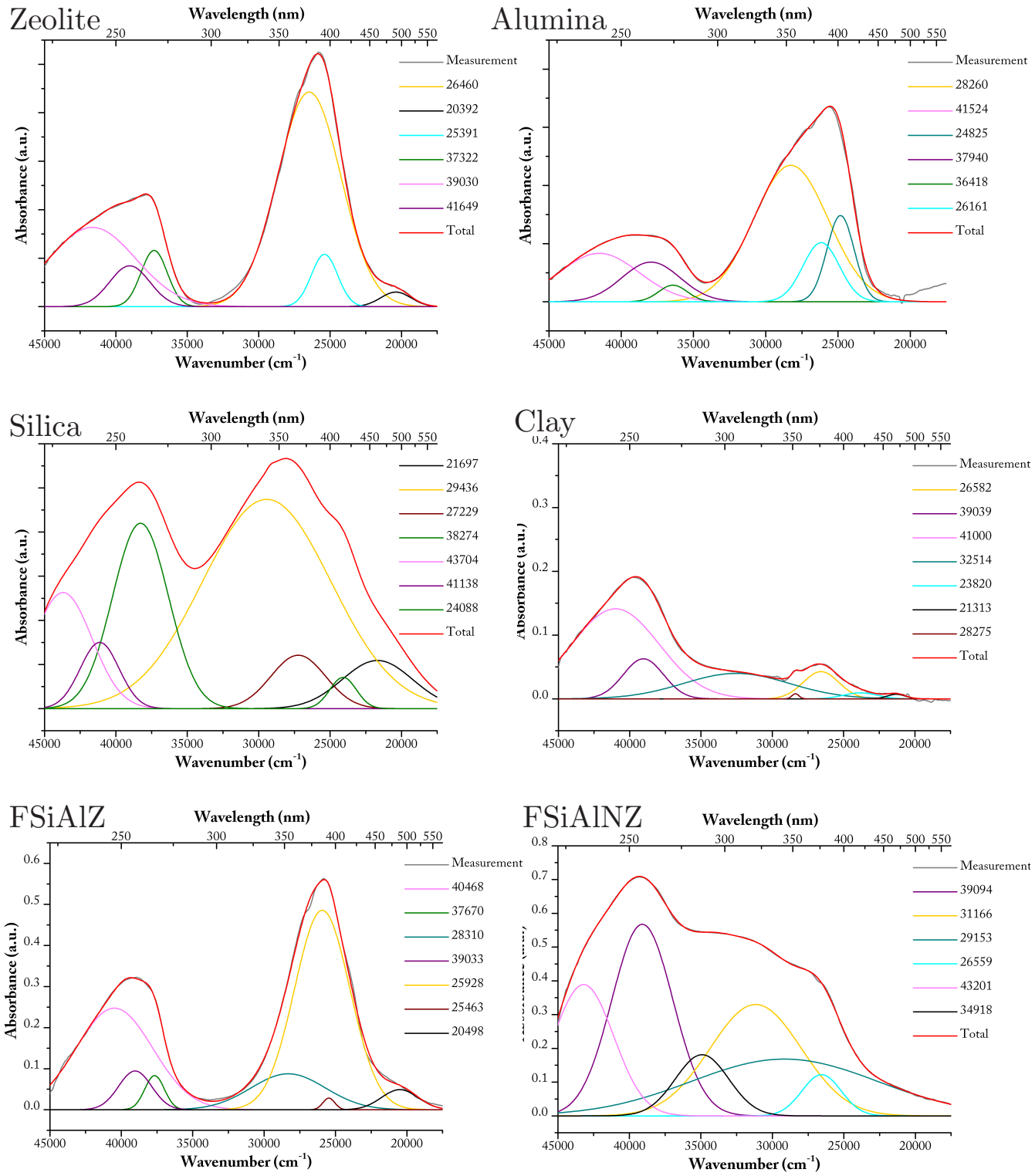

Figure 57: Deconvolution of UV-Vis spectrum after 45 minutes of pyridine adsorption. For some of the samples the measurements were repeated, therefore not all spectra are similar to the ones in the thesis.

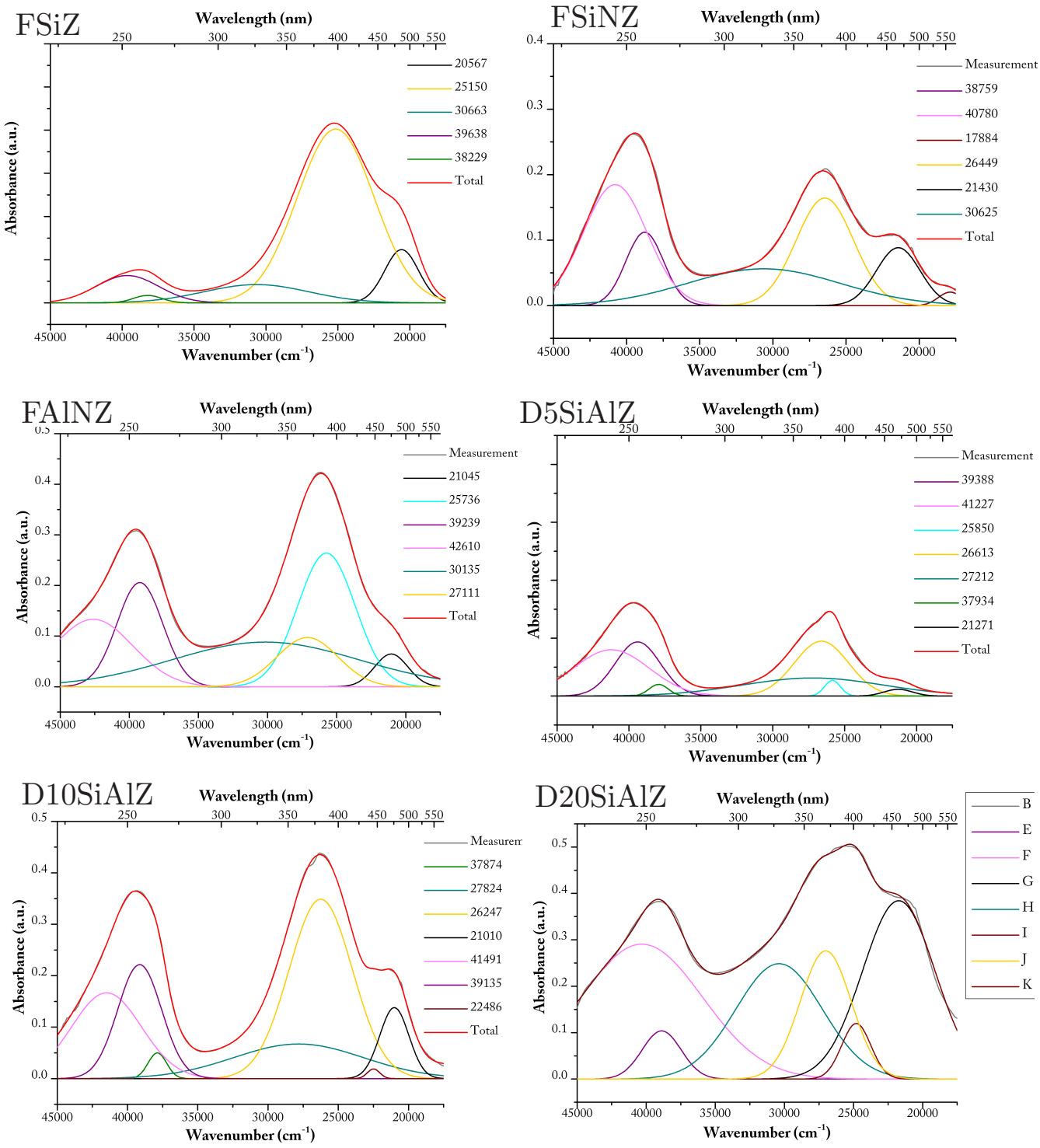

Figure 58: Deconvolution of UV-Vis spectrum after 45 minutes of pyridine adsorption. For some of the samples the measurements were repeated, therefore not all spectra are similar to the ones in the thesis. The FAlZ catalyst was replaced and the spectrum of the old sample is not reported.

Appendix E

Steam treatment on zeolite

To further study the effect of steam treatment on the components, the zeolite was steamed. The zeolite was put in a crucible and inserted into a clean quartz tubular oven (Thermoline 79300). The zeolite was preheated at 120 ℃ for 30 minutes with a rate of 2 ℃/min. The temperature was the further increased to 788 ℃ with a rate of 10 ℃/min. Steam treatment was performed at this temperature for 5 hours using a water (100℃) saturated N_2 flow (140 ml/min). After the steam treatment, the zeolite crystals were calcined at 550 ℃ (5 ℃/min, 6 hours).[68] An XRD diffractogram of the steamed zeolite was made, see Appendix F Figure 66, confirming that the zeolite was affected by the steam treatment. Pyridine UV-Vis measurements were done on the steamed zeolite, see Figure 59 for the pyridine adsorption and Figure 60 for the desorption up to 175 ℃(power cut stopped the TPD).

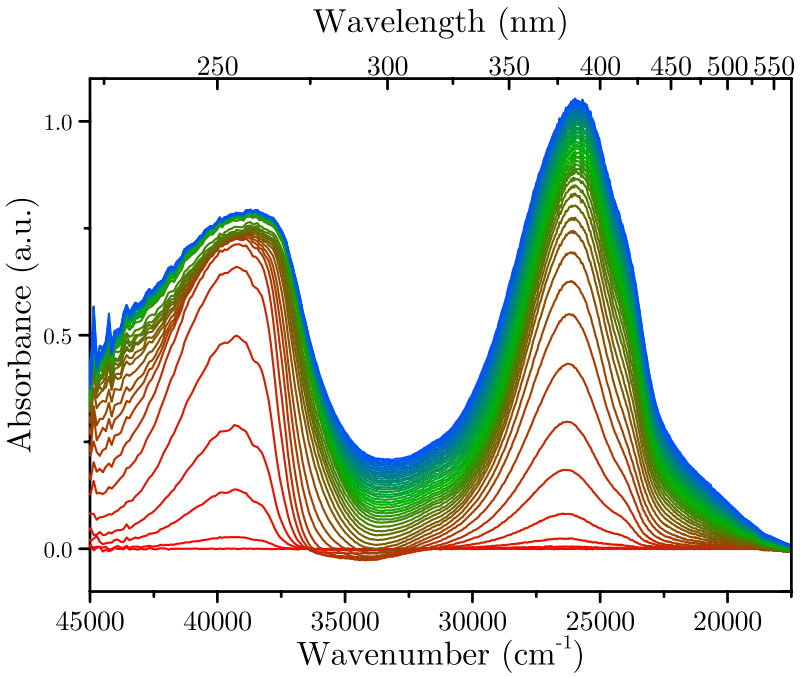

Figure 59: UV-Vis spectra of the steamed zeolite during 45 minutes of pyridine adsorption.

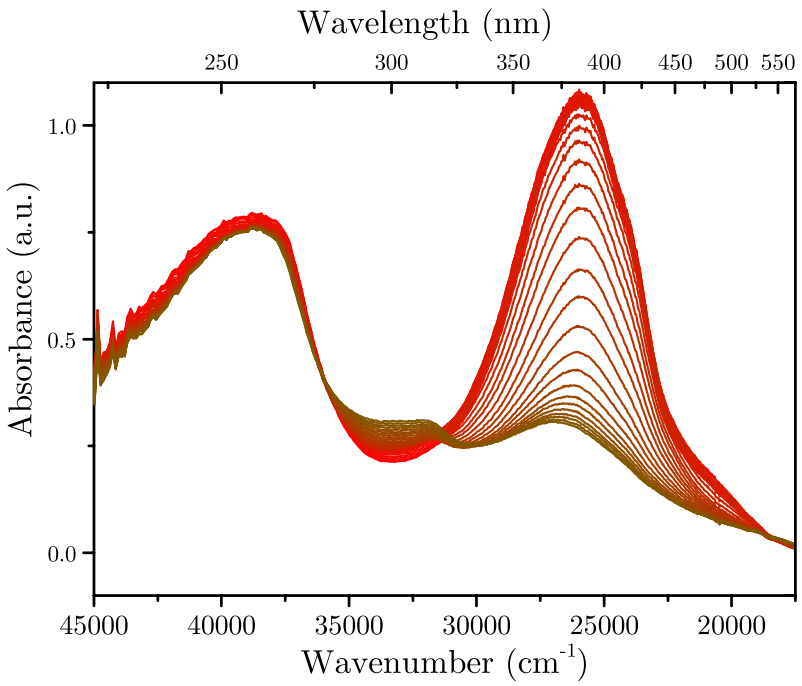

Figure 60: UV-Vis spectra of the steamed zeolite during TPD up to 175 ℃.

Appendix F

XRD measurements

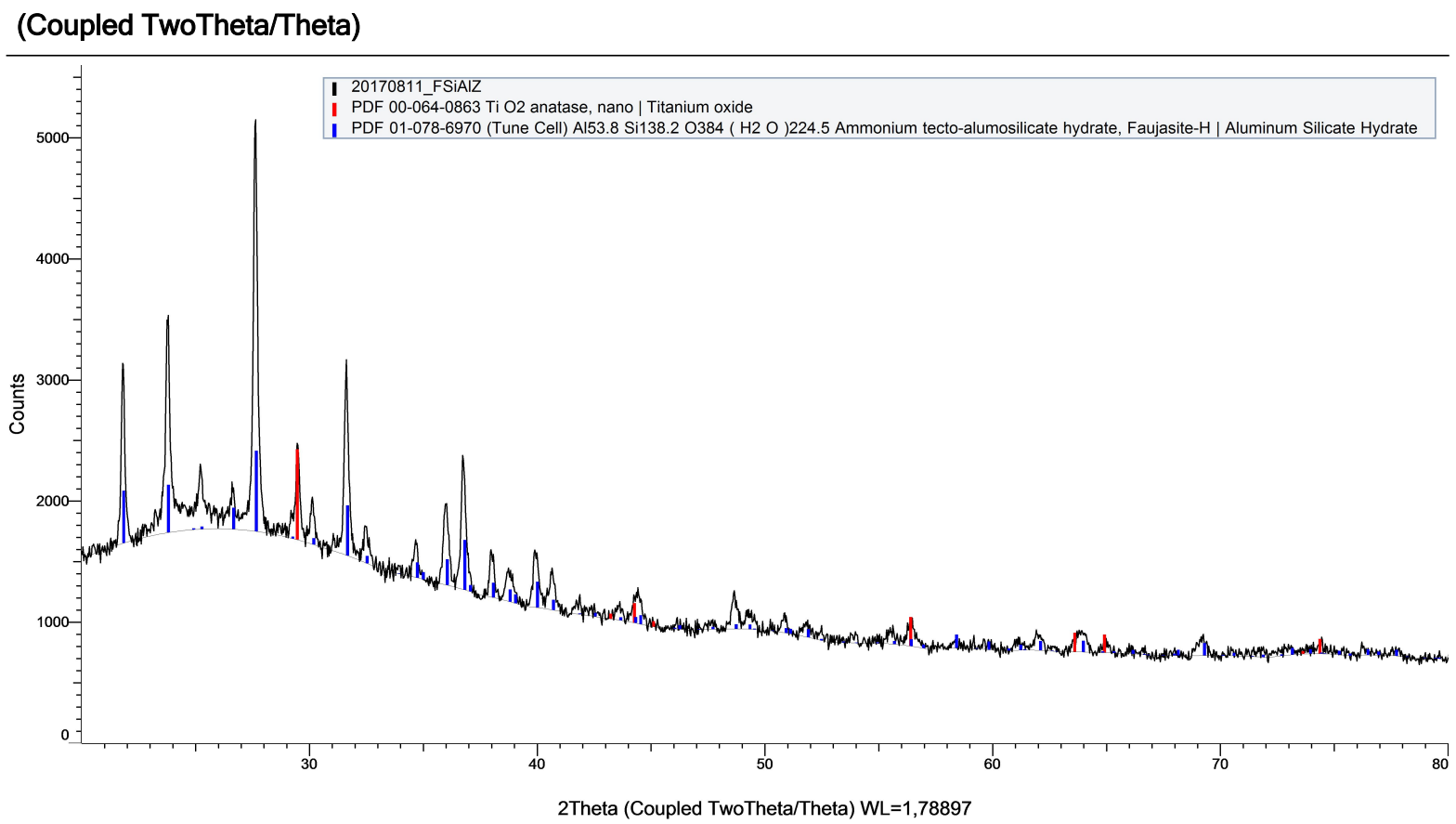

Figure 61: XRD of FSiAlZ

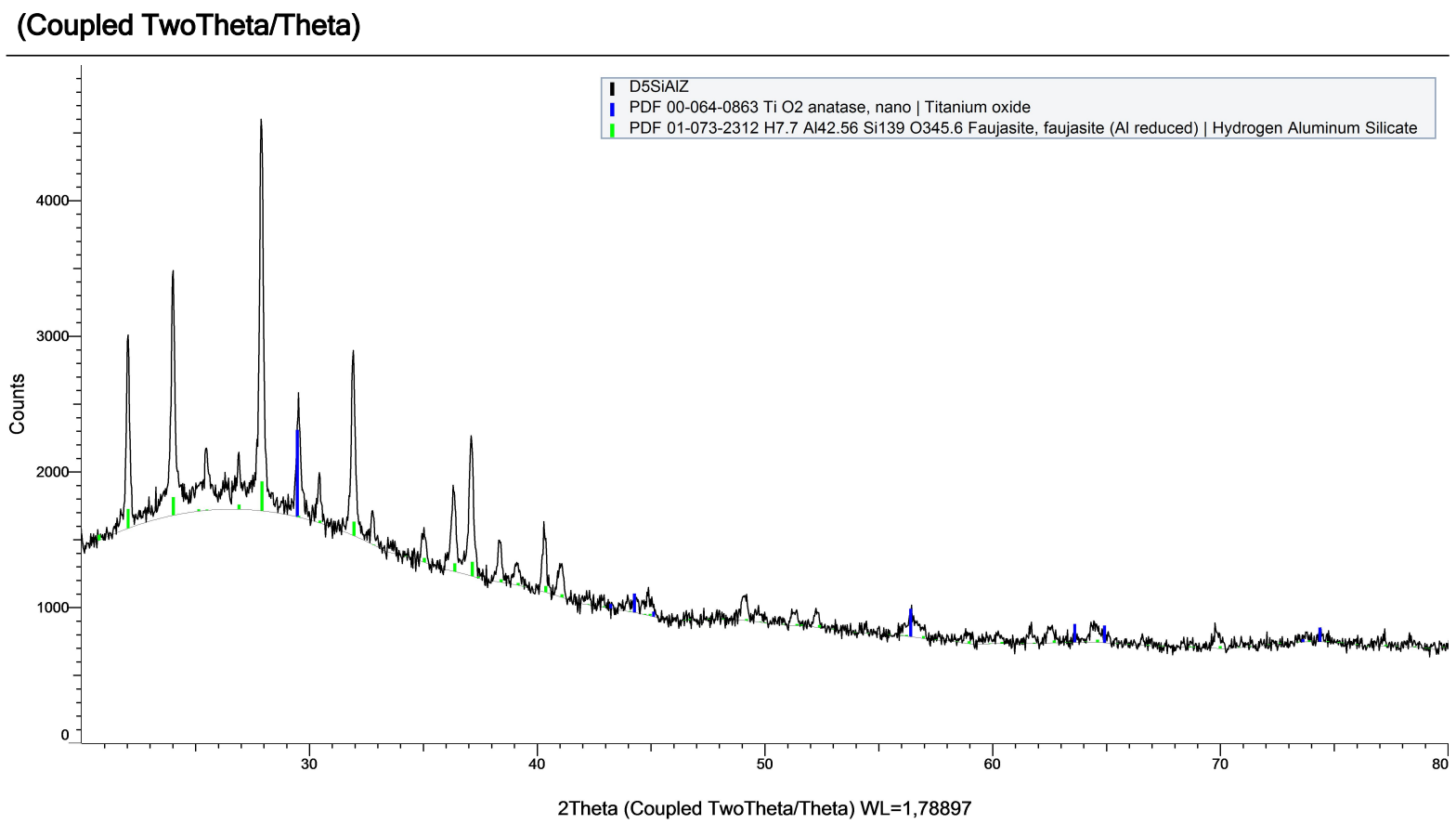

Figure 62: XRD of D5SiAlZ, FSiAlZ catalyst after 5 hours of steam treatment

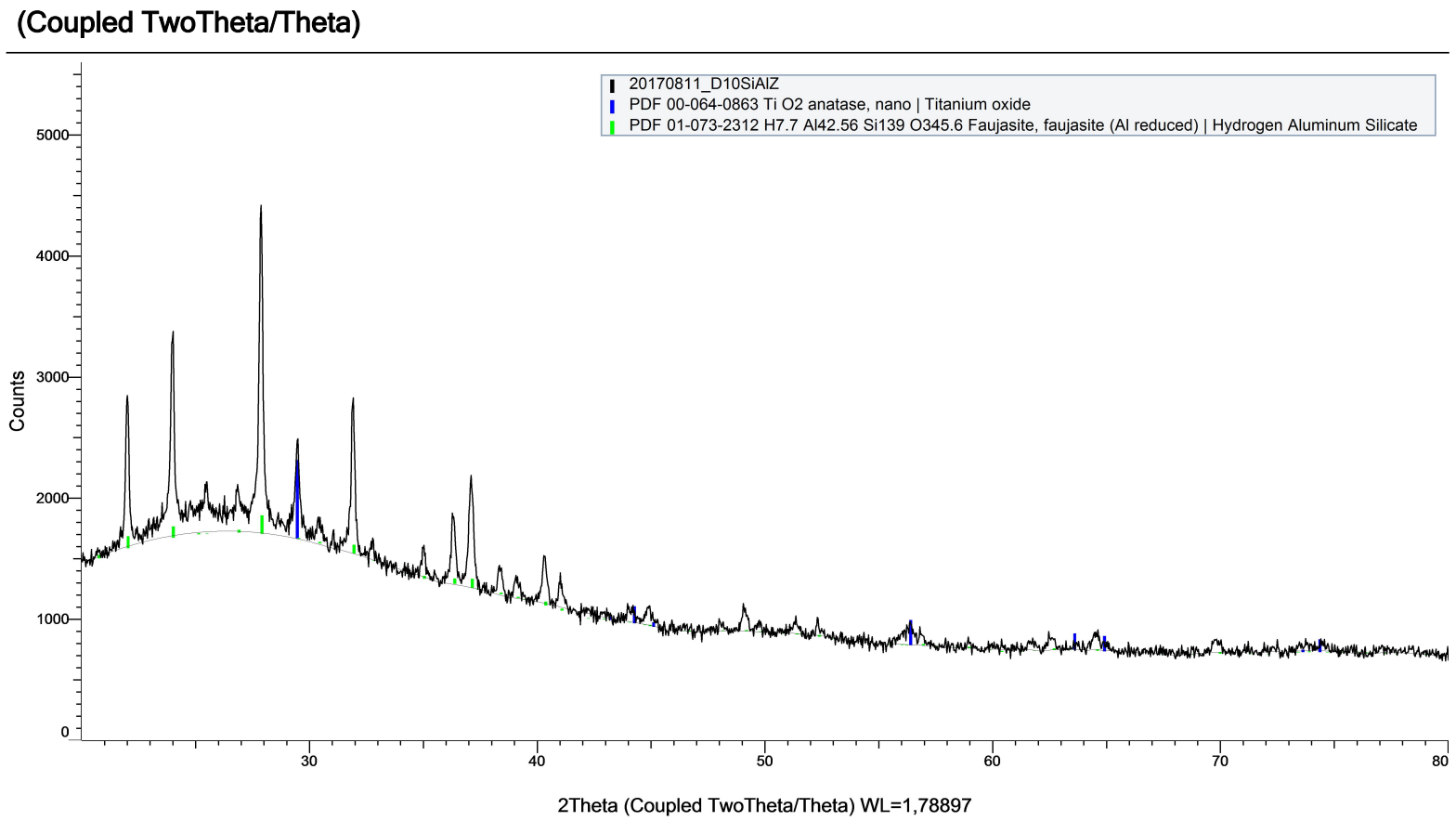

Figure 63: XRD of D10SiAlZ

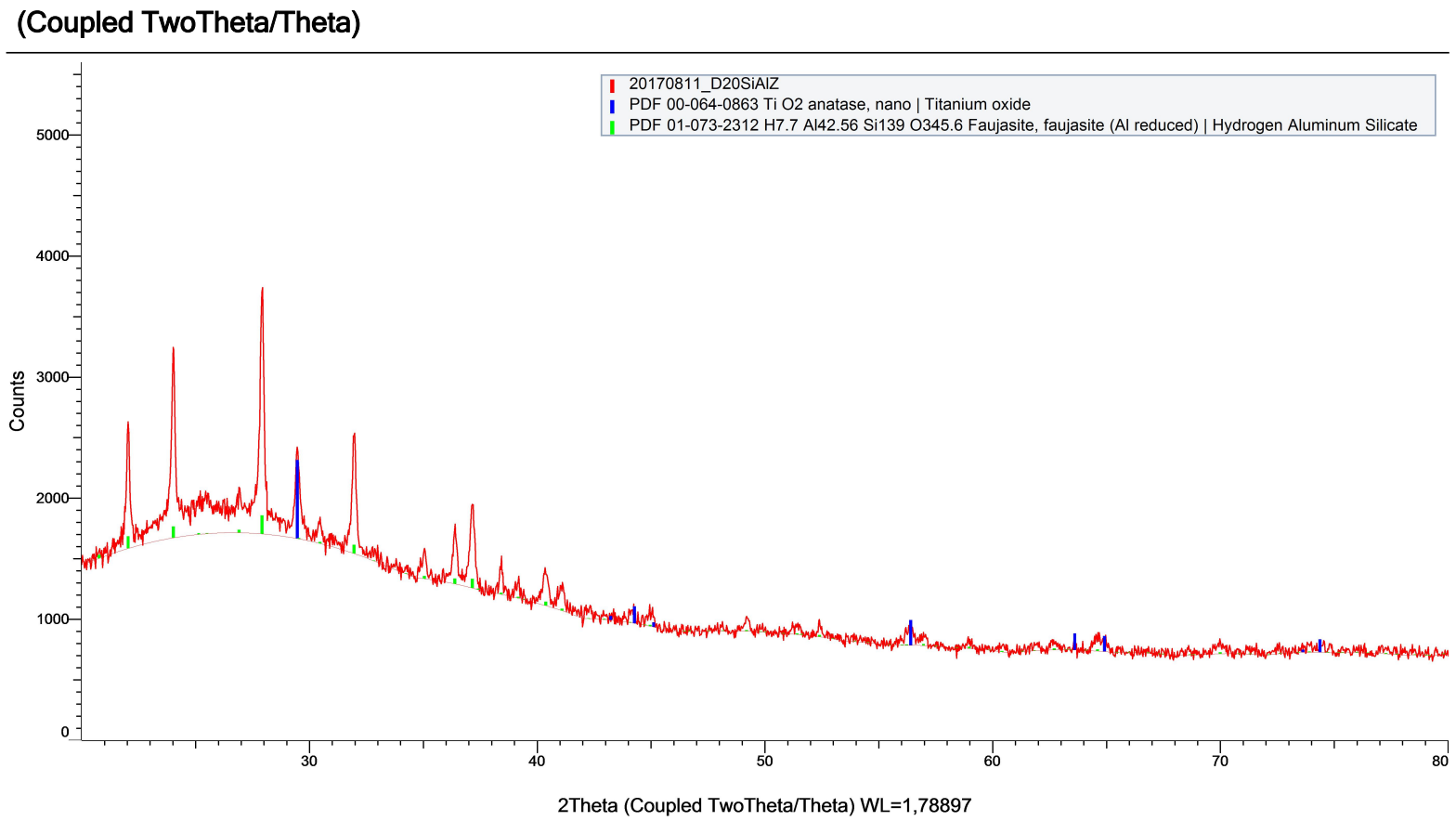

Figure 64: XRD of D20SiAlZ

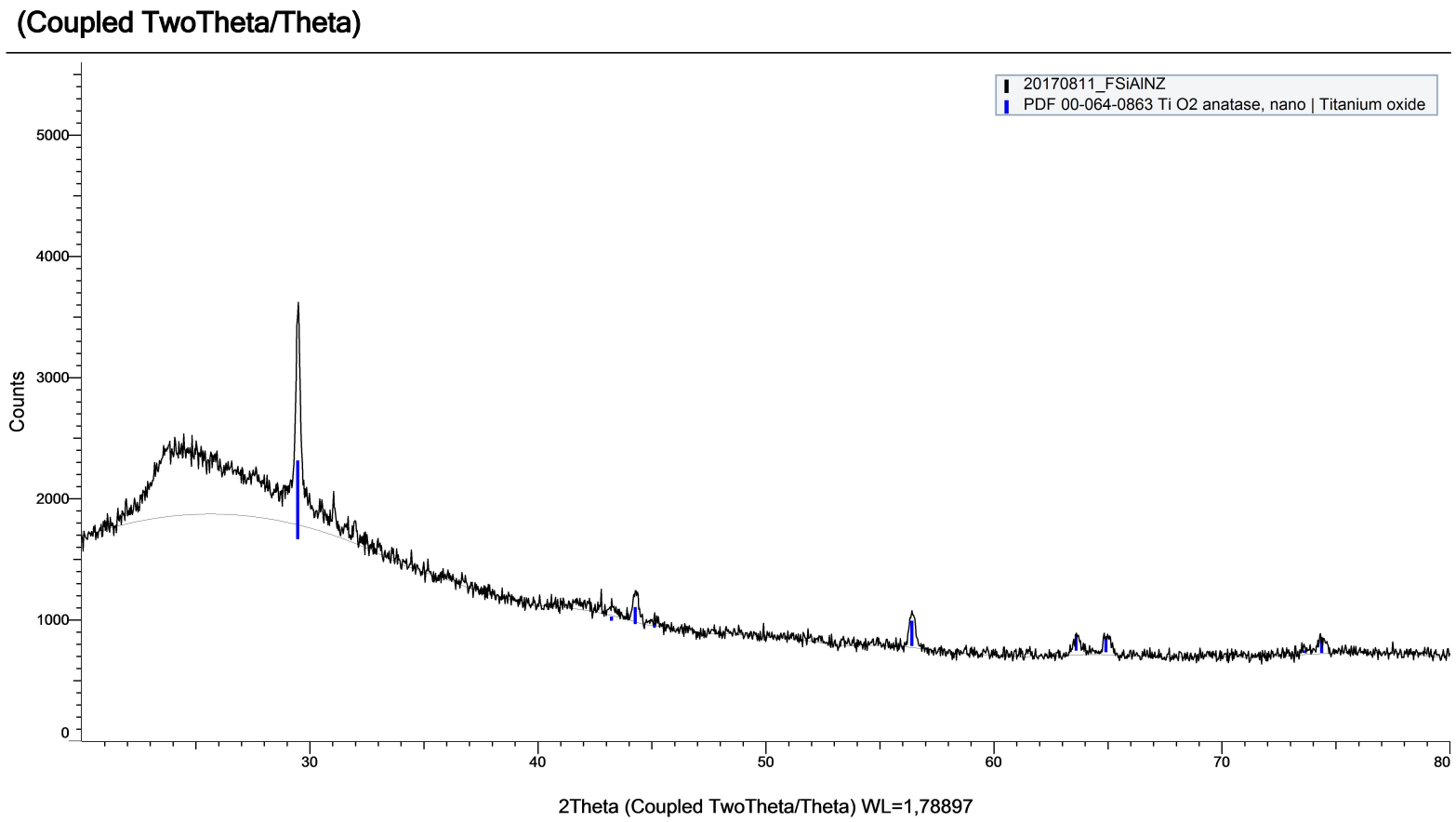

Figure 65: XRD of FSiAlNZ

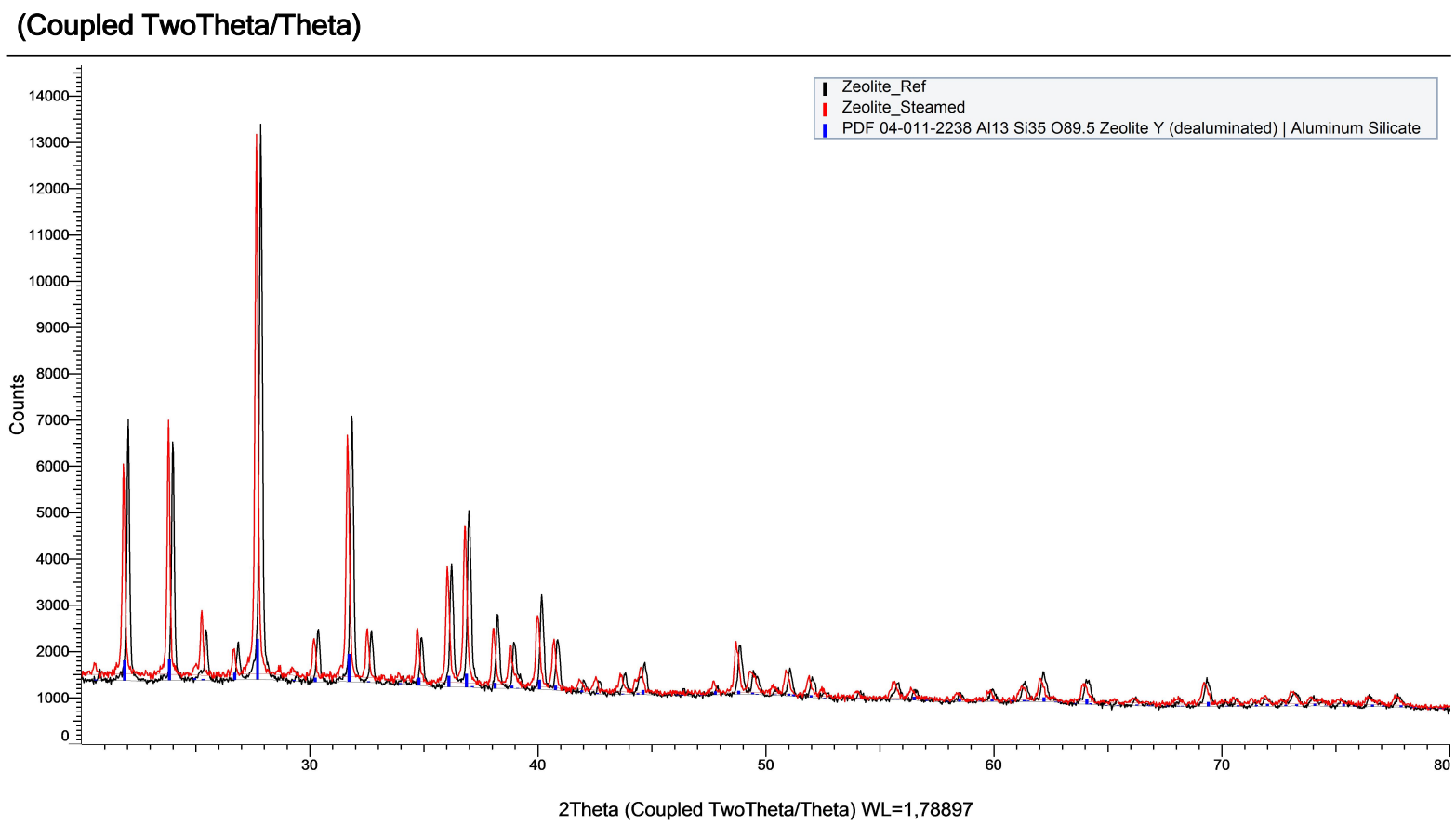

Figure 66: XRD of the zeolite and the steamed zeolite

Appendix G

Performance Data

	D20_Al_NZ	D20_Al_NZ	D20_Si_NZ	D20_Si_NZ	D20_SiAl_NZ	D20_SiAl_NZ
221 °C+ Conversion, wt%	35.4	31.2	32.1	24.9	30.0	31.2
Catalyst-to-Oil, wt/wt	4.00	4.00	4.00	4.00	4.00	4.00
Coke	2.2	2.2	1.3	1.4	1.8	1.6
Hydrogen	0.17	0.15	0.10	0.09	0.13	0.10
Dry Gas	4.38	4.32	4.31	4.32	4.53	4.31
Propylene	2.58	2.52	2.42	2.40	2.45	2.58
C4 Olefins	2.98	2.92	2.80	2.79	2.72	2.95
Gasoline (C5-221 °C)	22.1	18.2	20.2	13.1	17.5	18.5
LCO	16.92	14.39	14.79	8.67	12.14	13.43
343 °C+	47.71	54.40	53.13	66.39	57.87	55.42
LPG	6.67	6.47	6.30	6.19	6.21	6.73
C3=/C3s	0.82	0.83	0.82	0.82	0.82	0.83
C4=/C4s	0.84	0.85	0.84	0.85	0.85	0.82
C4=/C3=	1.15	1.16	1.16	1.16	1.11	1.14
LCO/bottoms	0.35	0.26	0.28	0.13	0.21	0.24

Table G.0.1: Results of catalytic tests performed in dual. In this Table the values are shown with two decimals. For calculating the average in the thesis, all decimals provided were used. Testing: FST, Feed: KVGO

	D20_Al_Z	D20_Al_Z	D20_Si_Z	D20_Si_Z	D20_SiAl_Z	D20_SiAl_Z
221 °C+ Conversion, wt%	74.7	74.8	68.0	68.8	73.7	74.1
Catalyst-to-Oil, wt/wt	4.00	4.00	4.00	4.00	4.00	4.00
Coke	3.9	4.0	3.9	3.8	4.4	4.3
Hydrogen	0.04	0.05	0.06	0.05	0.06	0.04
Dry Gas	3.92	3.96	4.06	4.13	3.93	3.96
Propylene	5.13	5.21	4.70	5.01	4.97	5.05
C4 Olefins	6.09	6.25	5.23	5.64	5.79	5.80
Gasoline (C5-221 °C)	48.8	48.4	43.1	42.7	47.7	47.8
LCO	15.84	15.89	14.17	13.90	15.71	15.56
343 °C+	9.42	9.34	17.82	17.35	10.55	10.38
LPG	18.09	18.39	16.95	18.09	17.72	18.05
C3=/C3s	0.78	0.78	0.76	0.76	0.77	0.77
C4=/C4s	0.53	0.53	0.49	0.49	0.51	0.51
C4=/C3=	1.19	1.20	1.11	1.13	1.17	1.15
LCO/bottoms	1.68	1.70	0.80	0.80	1.49	1.50

Table G.0.2: Results of catalytic tests performed in dual. In this Table the values are shown with two decimals. For calculating the average in the thesis, all decimals provided were used. Testing: FST, Feed: KVGO

Utrecht University